Cell

Gut microbiota promotes immune tolerance at the maternal-fetal interface

Graphical abstract

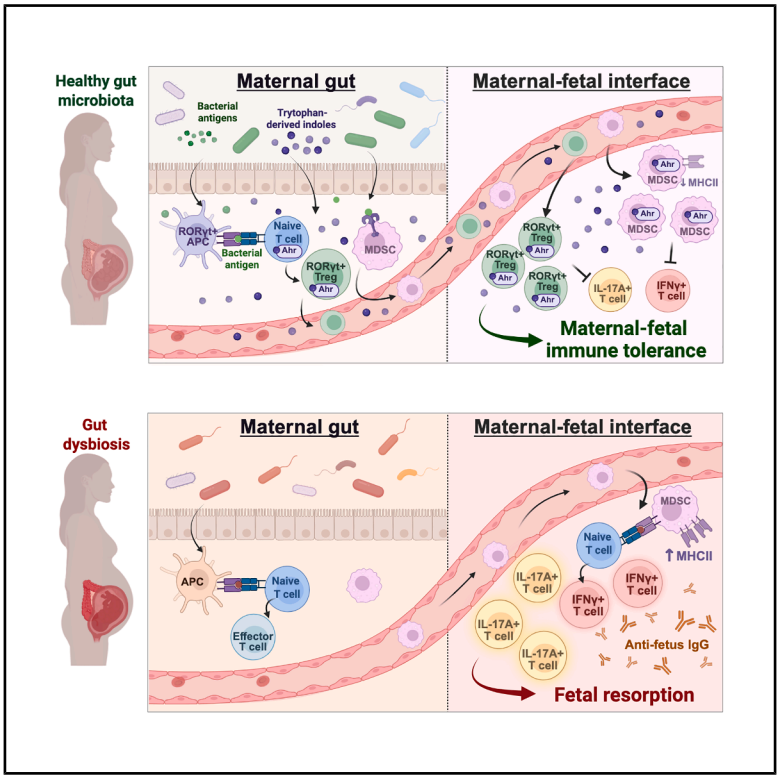

Authors

Julia A. Brown, Mohammed Amir, Shui Yu, ..., Gregory F. Sonnenberg, Virginia Pascual, Melody Y. Zeng

Correspondence

myz4001@med.cornell.edu

In brief

Microbiota-dependent tryptophan-derived indole deficiency is linked to mouse fetal resorption and human recurrent miscarriage. Tryptophan-derived indoles prime MDSCs and RORγt+ Tregs to suppress IFN-γ+ or IL-17A+ T cells at the maternal-fetal interface, respectively, thereby promoting maternal-fetal immune tolerance.

Highlights

- Microbiota disruption leads to loss of maternal-fetal immune tolerance
- Microbiota primes MDSCs to suppress IFN-γ+ T cell-driven fetal resorption
- Gut-derived RORγt+ Tregs restrain Th17 cells in the uterus
- Microbiota-derived indoles promote maternal-fetal tolerance via MDSCs and RORγt+ Tregs

Brown et al., 2026, Cell *189*, 196–214
January 8, 2026
https://doi.org/10.1016/j.cell.2025.11.022

CellPress

CellPress

Cell

Article

Gut microbiota promotes immune tolerance at the maternal-fetal interface

Julia A. Brown,[1,2,12] Mohammed Amir,[1,2,12] Shui Yu,[1,2] Daniel S.H. Wong,[1,2,3] Jinghua Gu,[1,2] Uthra Balaji,[1,2] Christopher N. Parkhurst,[4] Seunghee Hong,[5] Lucy R. Hart,[1,2] Hannah C. Carrow,[1,2,3] Mamadou A. Bah,[3,6] Aparna Ananthanarayanan,[1,2] Katherine Z. Sanidad,[1,2] Mengze Lyu,[4,7] Anisa Siddikova,[1] Marina Lima Silva Santos,[1,2] Inna Serganova,[6,8] Gretchen E. Diehl,[3,9] Josef Anrather,[10] Naohiro Inohara,[11] Gregory F. Sonnenberg,[3,4,6,7] Virginia Pascual,[1,2,3] and Melody Y. Zeng[1,2,3,6,13,*]

[1]Gale and Ira Drukier Institute for Children's Health, Weill Cornell Medicine, New York, NY 10065, USA
[2]Department of Pediatrics, Weill Cornell Medicine, New York, NY 10065, USA
[3]Immunology and Microbial Pathogenesis Program, Weill Cornell Graduate School, New York, NY 10065, USA
[4]Jill Roberts Institute for Research in Inflammatory Bowel Disease, Weill Cornell Medicine, New York, NY 10065, USA
[5]Department of Biochemistry, College of Life Science and Biotechnology, Yonsei University, Seoul 03722, Republic of Korea
[6]Meyer Cancer Center, Weill Cornell Medicine, New York, NY 10065, USA
[7]Department of Medicine, Division of Gastroenterology and Hepatology, Weill Cornell Medicine, New York, NY 10065, USA
[8]Department of Medicine, Division of Hematology & Medical Oncology, Weill Cornell Medicine, New York, NY 10065, USA
[9]Immunology Program of the Sloan Kettering Institute, Memorial Sloan Kettering Cancer Center, New York, NY 10065, USA
[10]The Feil Family Brain and Mind Research Institute, Weill Cornell Medicine, New York, NY 10065, USA
[11]Rogel Cancer Center, University of Michigan, Ann Arbor, MI 48109, USA
[12]These authors contributed equally
[13]Lead contact
*Correspondence: myz4001@med.cornell.edu
https://doi.org/10.1016/j.cell.2025.11.022

SUMMARY

Immune tolerance at the maternal-fetal interface (MFI) is required for fetal development. Excessive maternal interferon-gamma (IFN-γ) and interleukin-17 (IL-17) are linked to pregnancy complications, but the regulation of maternal IFN-γ and IL-17 at the MFI is poorly understood. Here, we demonstrate a gut-placenta immune axis in pregnant mice in which the absence or perturbation of gut microbiota dysregulates maternal IFN-γ and IL-17 responses at the MFI, resulting in fetal resorption. Microbiota-dependent tryptophan derivatives suppress IFN-γ+ and IL-17+ T cells at the MFI by priming myeloid-derived suppressor cells (MDSCs) and gut-derived RORγt+ regulatory T cells (Tregs), respectively. The tryptophan derivative indole-3-carbinol, or tryptophan-metabolizing *Lactobacillus murinus*, rebalances the T cell response at the MFI and reduces fetal resorption in germ-free mice. Furthermore, MDSCs, RORγt+ Tregs, and microbiota-dependent tryptophan derivatives are dysregulated at the MFI in human recurrent miscarriage cases. Together, our findings identify microbiota-dependent immune tolerance mechanisms that promote fetal development.

INTRODUCTION

The gut microbiota, an essential regulator of the immune system and host metabolism,[1,2] significantly changes during pregnancy.[3–5] The gut microbiota influences maternal metabolic rewiring during pregnancy[5] and contributes to placental vascularization.[6] Maternal dysbiosis and gastrointestinal disease are associated with pregnancy complications,[3,7,8] including miscarriage, preterm birth, low birth weight, and preeclampsia. Pregnancy is associated with drastic changes to the immune system to facilitate tolerance of the semi-allogenic fetus,[9–12] mediated in part by the development of maternal regulatory T cells (Tregs) that dampen immune activation against fetal antigens.[13] Disruption of maternal-fetal tolerance is associated with pregnancy complications, including miscarriage and preterm birth.[10,14–18] However, the role of the microbiota in regulating maternal-fetal immune tolerance remains undefined. The gut microbiota is heavily influenced by a variety of maternal factors, including antibiotic (Abx) use and diet. It remains poorly understood whether/how the maternal immune response to the developing fetus is influenced by the gut microbiota.

Type I and II interferons (IFNs) contribute to uterine spiral artery remodeling for placentation, as well as protecting mother and fetus from pathogens.[19] However, excessive IFN responses and activation of IFN-stimulating genes (ISGs) may provoke anti-fetus T cell responses and lead to fetal resorption[20,21]; this may underlie the increased risk of poor pregnancy outcomes in women with autoimmune systemic lupus erythematosus (SLE)

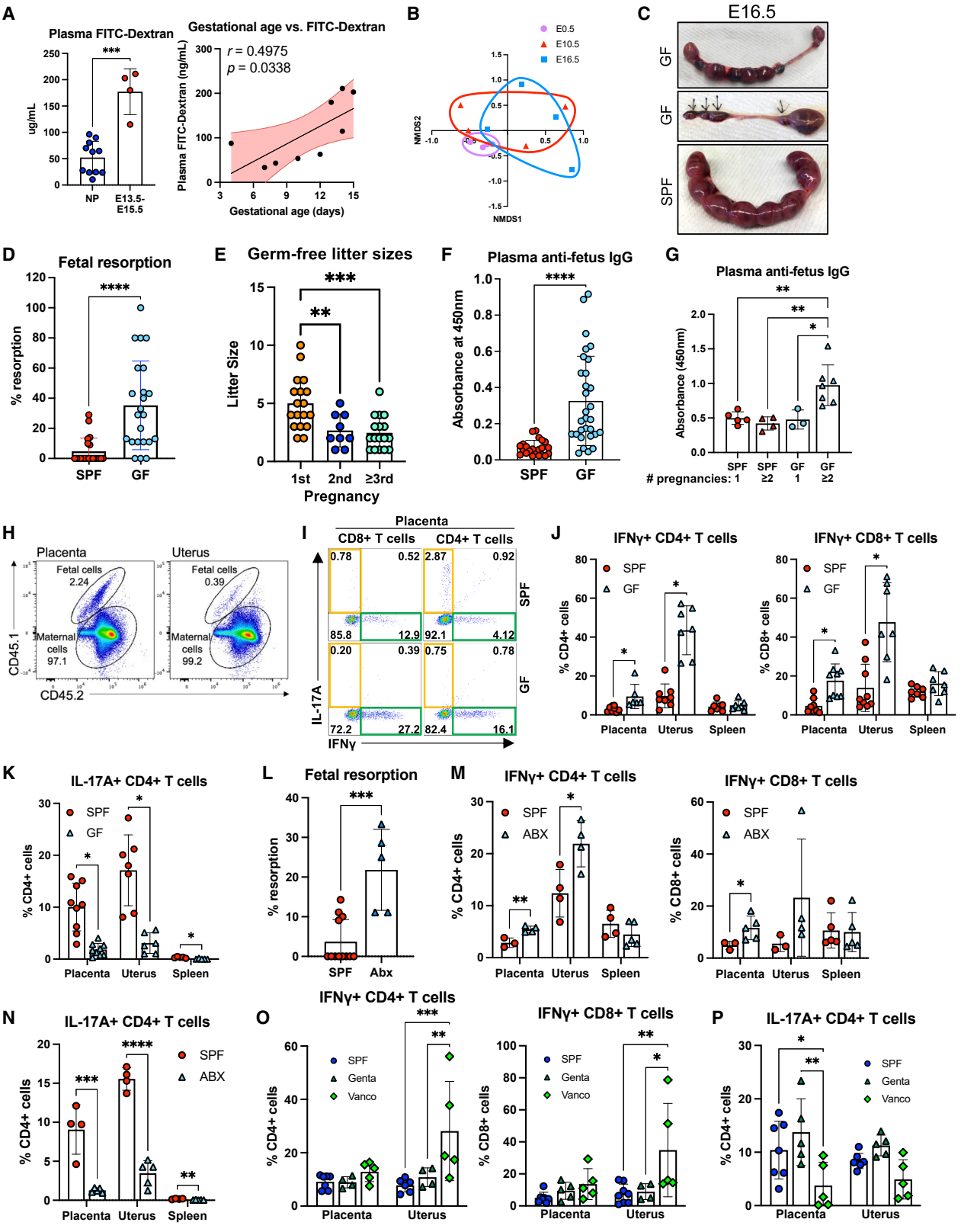

(legend on next page)

or antiphospholipid syndrome (APS), including premature delivery and fetal loss.[22,23] Futhermore, overexpression of IFN-gamma (IFN-γ) is associated with abnormal cerebellar development in mice.[24,25] Likewise, excessive maternal interleukin (IL)-17 production due to maternal immune activation (MIA), as in the case of maternal infection, has been suggested to disrupt fetal brain development and also imprint fetal intestinal stem cells to increase susceptibility to autoimmunity in later life.[26–28] However, it remains unclear how the maternal IL-17 response is regulated at the maternal-fetal interface (MFI) under homeostatic conditions. A better understanding of the regulation of maternal IFN and IL-17 responses during pregnancy would inform approaches to keep these two major immune pathways in check and thus improve pregnancy outcomes. In this study, we identify a critical role for maternal microbiota-derived tryptophan derivatives in the emergence of myeloid-derived suppressor cells (MDSCs) and RORγt+ Tregs in pregnant mice to maintain a balanced IFN-γ vs. IL-17 response at the MFI to promote maternal-fetal immune tolerance. We further demonstrate that both of these cell types are present at the human MFI and are dysregulated in cases of recurrent miscarriage (RM), highlighting these pathways as potential avenues to improve pregnancy outcomes in humans.

RESULTS

Gut microbiota is required for maternal tolerance during pregnancy

In this study, we explored a possible gut-placenta immune axis during pregnancy. We found increased gut permeability in pregnant wild-type C57BL/6 mice (hereafter referred to as WT), indicated by increased fluorescein isothiocyanate (FITC)-dextran leakiness, compared with age-matched nonpregnant females, which notably increased with gestational age (Figure 1A). To examine how pregnancy changes the gut microbiota, we performed 16S rRNA sequencing on fecal pellets from 8-week-old WT female C57BL/6 mice at embryonic day 0.5 (E0.5, defined as the day the copulation plug was detected), E10.5, and E16.5. The gut microbiota changed significantly between pregnant and nonpregnant (E0.5) mice (Figures 1B and S1A); pregnancy was associated with reduced bacterial diversity and expansion of *Porphyromonadaceae* and *Clostridiales* (Figure S1A). E16.5 dams showed significant elevation of Tregs and IL-17A+ T cells in the small intestine relative to age-matched nonpregnant mice, although not in the mesenteric lymph node (mLN) or colon (Figures S1B–S1F), suggesting dynamic changes in gut immune cells during pregnancy.

Further highlighting the importance of the microbiota in pregnancy, we found significantly higher rates of fetal resorption at E16.5 in WT germ-free (GF) dams compared with WT-specific pathogen-free (SPF) dams (Figures 1C and 1D), with a female bias in surviving pups from GF dams (Figure S1G). In GF dams, the rate of fetal death significantly increased after the first pregnancy (Figure 1E), suggesting a possible contribution from immunologic memory. Plasma from GF mice showed a significantly higher level of fetus-specific immunoglobulin G (IgG) than in SPF mice (Figure 1F); fetus-specific IgG was significantly increased after the first pregnancy in GF dams but not SPF dams (Figure 1G). Likewise, B cells isolated from the placenta and uterus of E16.5 GF mice produced significantly more IgG when co-cultured with fetal antigens than did B cells isolated from SPF mice (Figure S1H), suggesting a breakdown of maternal tolerance in the absence of the gut microbiota. Despite the female bias in surviving GF pups, we did not observe a difference in plasma IgG reactivity to fetal skin and liver antigens derived from male vs. female fetuses in either SPF or GF dams (Figure S1I).

To better understand how the lack of microbiota affects maternal immune cells at the MFI, we isolated immune cells from the mouse uterus (combining the uterus and decidua) and fetal side of the placenta after removing the decidua (hereafter referred to as the placenta). By mating a SPF WT CD45.2+ female (on the C57BL/6 background) with a SPF WT CD45.1+ syngenic male, we found that only 0.4% of immune cells in the uterus and 2.2% in the placenta were of fetal origin (CD45.1+ CD45.2+) (Figure 1H). The maternal immune cells from the placenta likely were maternal blood circulating cells. Furthermore, flow cytometry analysis showed significant increases in IFN-γ+ T cells in the placenta and uterus of GF mice at E16.5, as well as a significant reduction in IL-17A+ CD4+ T cells

Figure 1. The maternal gut microbiota changes dynamically during pregnancy and shapes immune responses at the MFI

(A) Intestinal permeability in SPF WT pregnant mice and age-matched nonpregnant females. Pearson's coefficient (r) correlation was calculated between gestational age and plasma FITC-dextran concentration. Data from individual mice as well as a simple linear regression with 95% confidence intervals are shown.

(B) Non-metric multidimensional scaling (NMDS) analysis of fecal microbial diversity at E0.5, E10.5, and E16.5.

(C and D) Representative photographs (C) and quantification (D) of fetal death in SPF and GF mice at E16.5.

(E) Litter size in GF mice in their first, second, and third or higher pregnancy.

(F) Anti-fetal IgG in the serum of E16.5 SPF and GF pregnant mice.

(G) Anti-fetal IgG in the serum of E16.5 SPF and GF pregnant mice during their first or later pregnancy.

(H) Representative flow plots of maternal cells (CD45.2+CD45.1−) and fetal cells (CD45.2+CD45.1+) in the placenta and uterus of CD45.2 females mated with CD45.1 males, gated on live CD45.2+ cells.

(I) Representative flow plots of placental CD4+ and CD8+ T cells from SPF and GF mice at E16.5.

(J and K) Frequency of IFN-γ+ (J) and IL-17A+ (K) T cells from placenta, uterus, and spleen of E16.5 SPF and GF mice.

(L–N) Resorption rates (L) and the frequency of IFN-γ+ T cells (M) and IL-17A+ CD4+ T cells (N) in the placenta, uterus, and spleen of SPF mice treated with PBS or broad-spectrum Abx.

(O and P) Abundance of IFN-γ+ T cells (O) and IL-17A+ CD4+ T cells (P) in the placenta and uterus of SPF mice treated with PBS, gentamicin, or vancomycin. For (A), (B), (F)–(K), and (L)–(O), each dot represents one dam; for (D), (E), and (K), each dot represents one litter. Error bars indicate one standard deviation. $^{*}p < 0.05$, $^{**}p < 0.01$, $^{***}p < 0.001$, $^{****}p < 0.0001$. SPF, specific pathogen-free; GF, germ-free; Abx, broad-spectrum antibiotics.

See also Figures S1 and S2.

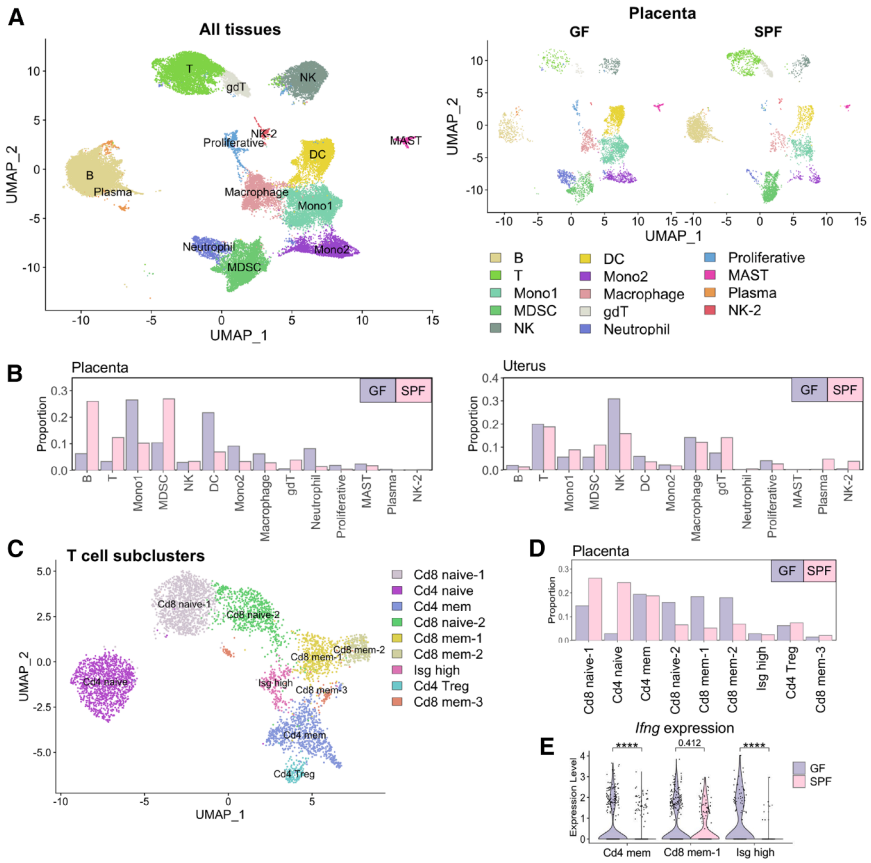

Figure 2. Altered immune cell landscape at the MFI in female mice lacking microbiota

(A and B) scRNA-seq on CD45+ cells from the blood, placenta, and uterus of pregnant SPF and GF mice (3 dams per group, 5 placentas pooled from each dam). (A) Fourteen clusters were defined by gene signature. Uniform manifold approximation and projection (UMAP) representations are shown for all samples combined (a total of 43,682 cells are depicted) as well as for placenta. (B) Relative abundance of each cluster, shown as the fraction of all cells from the indicated tissue.

(C–E) Within the T cell cluster (6,159 cells total), nine sub-clusters were defined. (C) UMAP representation of T cell sub-clusters. (D) Relative abundance of each cluster within the placenta, shown as the fraction of all placental T cells. (E) Relative expression of *Ifng* within selected T cell sub-clusters. ****$p < 0.0001$.

See also Figure S2.

(Figures 1I–1K and S1J); these cells likely mostly represented maternal cells. Consistently, by using LegendPlex ELISA, higher levels of IFN-γ were found in placenta and uterus homogenates as well as amniotic fluid (AF) from GF dams at E16.5 (Figure S1K), with a similar reduction in IL-17A concentration in placenta and uterus homogenates (Figure S1L), although IL-17A was not detectable in AF. Similar phenotypes were observed between mid-gestation and late-gestation dams (Figures S1M–S1O), and no significant differences were found in *Tgfb* mRNA expression (Figure S1P) or in IL-4+, IL-22+, or tumor necrosis factor (TNF)-α+ T cells (Figures S1Q and S1R).

GF mice exhibit significant developmental issues,[29–31] in addition to immune dysregulation, which may contribute to pregnancy complications; to further demonstrate the effect of microbiota perturbation during pregnancy, we treated WT SPF dams with broad-spectrum Abx from E7.5 to E16.5 and observed higher levels of fetal resorption than untreated dams (Figure 1L), as well as increased IFN-γ production and reduced IL-17A production in placental and uterine T cells (Figures 1M and 1N). Increased plasma levels of anti-fetus IgG1 and IgG3 were detected in E16.5 Abx-treated dams (Figure S1S). Interestingly, treatment of SPF dams with vancomycin, but not gentamicin, caused similar increases in fetal resorption (Figure S2A) and IFN-γ+ T cells (Figure 1O) and reduced IL-17A+ T cells (Figure 1P). Vancomycin primarily kills Gram-positive bacteria, whereas gentamicin is effective primarily against Gram-negative bacteria and some Gram-positive bacteria[32]; in a previous study by our lab,[33] we found that vancomycin treatment altered the microbiota to a much greater degree than gentamicin, including a near-complete loss of Bacteroidales and an expansion of Verrucomicrrobiales (Figure S2B). Collectively, these findings suggest that the absence or perturbation of the gut microbiota in mice, likely the loss of vancomycin-susceptible bacteria, provokes an excessive IFN-γ-biased T cell response at the MFI.

Maternal microbiota shapes immune responses at the MFI

To better define how the immune landscape of the MFI is dependent on the gut microbiota, we performed single-cell RNA sequencing (scRNA-seq) on CD45+ cells from the placenta, uterus, and blood of SPF and GF mice at E16.5. We identified 14 clusters based on gene signature (Figures 2A, S2C, and S2D); the abundance of several of these clusters, including T cells and MDSCs, was altered in GF mice (Figures 2B and S2E). Within the T cell cluster, nine sub-clusters were identified (Figure 2C, S2F, and S2G). The placentas of GF mice had significantly fewer naive CD4+ T cells and significantly more CD8+ memory T cells (Figure 2D); the CD4+ and CD8+ memory T cell clusters, as well as the ISG-high cluster, all exhibited higher expression of *Ifng* in the GF placenta (Figure 2E), which is consistent with our flow cytometry analyses (Figures 1I and 1J).

To further demonstrate that gut microbiota perturbation changes the anti-fetus T cell response, we mated 8-week-old WT females with ovalbumin-expressing (OVA) males and administered Abx to the females starting at E7.5. As expected, fetal resorption was enhanced in the Abx-treated OVA-mated dams, especially in the second pregnancy (Figure 3A). At E16.5, the placentas of Abx-treated mice showed a higher level of OVA-specific CD4+ and CD8+ T cells, indicating elevated

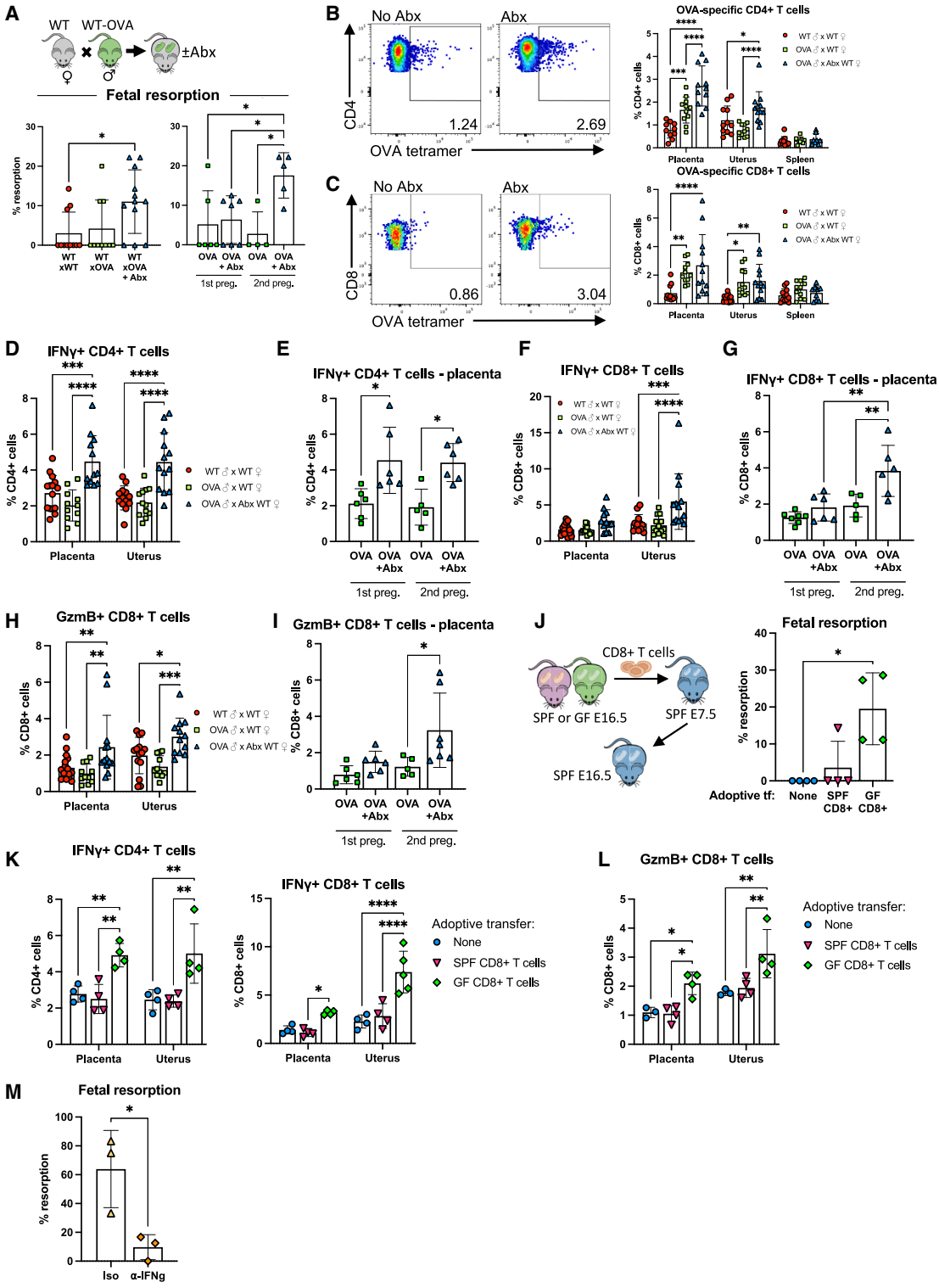

Figure 3. Microbiota perturbation exacerbates anti-fetus T cell responses

(A–I) WT SPF females were mated with OVA-expressing males and treated with PBS or broad-spectrum Abx from E7.5 to E16.5. Some mice were allowed to give birth, then euthanized during their 2nd pregnancy. (A) Fetal resorption rates, shown in aggregate and separated into 1st and 2nd pregnancy. (B and C) Abundance of OVA-reactive CD4+ (B) and CD8+ (C) T cells in the placenta, uterus, and spleen at E16.5. (D) Abundance of IFN-γ+ CD4+ T cells in the placenta and uterus. (E) Abundance of placental IFN-γ+ CD4+ T cells during the 1st and 2nd pregnancy. (F) Abundance of IFN-γ+ CD8+ T cells in the placenta and uterus. (G) Abundance of

(legend continued on next page)

maternal T cell responses against a fetal antigen following maternal gut microbiota perturbation (Figures 3B and 3C). IFN-γ+ CD4+ T cells were likewise elevated in the Abx-treated dams during both the first and second pregnancy (Figures 3D, 3E, and S3A), while IFN-γ+ and GzmB+ CD8+ T cells did not significantly increase until the second pregnancy (Figures 3F–3I, S3B, and S3C). Similarly to the Abx-treated WT dams, Abx-treated OVA-mated dams had reduced IL-17a-producing CD4+ T cells (Figure S3D). We also observed higher OVA-specific IgG in the AF of Abx-treated OVA-mated dams, exclusively during the second pregnancy (Figure S3E). The increase in OVA-specific CD8+ T cells in Abx-treated dams during second pregnancies correlated with increased fetal resorption; this may be consistent with a previous study by Perchellet et al.[34] showing a greater increase in fetal resorption in OT-I dams than in OT-II dams, following mating to OVA-expressing males, suggesting that the OT-I+ CD8+ T cells, lacking the restraint by CD4+ T cells (including Tregs), might play a more significant role in immune rejection against the OVA-expressing fetus.

In addition, to determine if CD8+ T cells contribute to fetal resorption in GF dams, we isolated CD8+ T cells from the placenta and uterus of E16.5 WT SPF and GF dams and adoptively transferred them into E7.5 WT SPF dams, which resulted in elevated fetal resorption and higher levels of IFN-γ+ and GzmB+ T cells in the recipients of GF CD8+ T cells at E16.5 (Figures 3J–3L), while IL-17A-producing T cells were not affected (Figure S3F). Finally, we treated GF dams with anti-IFN-γ or isotope control antibody from E7.5 until E16.5 and found that the anti-IFN-γ-treated dams had less fetal resorption than the control dams (Figure 3M). Together, these data suggest that excessive IFN-γ at the MFI, likely produced by fetal-reactive T cells, contributes to fetal resorption in GF mice. Of note, we found increased T helper 17 (Th17) cells in the placenta and uterus of SPF dams, following anti-IFN-γ treatment (Figures S3G and S3H), suggesting an inhibitory effect of IFN-γ on Th17 cells at the MFI. In support of this, we found that Th17 cells at the MFI express high levels of *Ifngr*, which was further elevated in GF dams (Figure S3I), suggesting that Th17 cells at the MFI are highly responsive to IFN-γ.

Microbiota-dependent placental MDSCs dampen maternal T cell IFN-γ response

Our scRNA-seq data demonstrated a reduction in MDSCs in the placenta and uterus of GF mice (Figures 2A and 2B). This was validated by flow cytometry, showing a reduction of CD11b+Ly6G+ polymorphonuclear cells (PMNs, which includes both neutrophils and MDSCs) in the placenta, decidua, and uterus of GF mice at E16.5 (Figure 4A); both MDSCs (Ly-6G^{mid}) and neutrophils (Ly-6G^{hi}) were reduced in GF mice (Figure S3J). PMN-deficient *Mcl-1$^{fl/fl}$Mrp8-cre+* mice reproduce with extreme difficulty,[35] but in pregnant *Mcl-1$^{fl/wt}$Mrp8-cre+* mice, which exhibit only a partial reduction in PMNs, we observed higher levels of plasma anti-fetus IgG relative to *Mcl-1$^{wt/wt}$Mrp8-cre+* littermates (Figure 4B), highlighting the importance of these cells in controlling anti-fetus immunity. To confirm the role of PMN-mediated maternal tolerance, we depleted PMNs in pregnant mice by administering anti-Ly6G antibody or isotype from E7.5 to E16.5 (Figure S3K), which resulted in higher fetal resorption (Figure 4C). PMN-depleted mice had an elevated level of plasma anti-fetus IgG (Figure 4D) and more IFN-γ+ T cells in the placenta, uterus, and spleen (Figure 4E), similarly to GF and Abx-treated mice. Interestingly, there was no significant change in IL-17A+ CD4+ T cells or IL-17A+γδ T cells in the uterus or spleen of anti-Ly6G-treated mice, and only a minor increase in the placenta (Figure S3L). These findings suggest an essential role for placental PMNs in dampening the T cell IFN-γ response.

We examined the MDSC and neutrophil clusters in our scRNA-seq dataset and found that several pattern-recognition receptors are highly expressed in both cell types in the placenta and uterus, including *Tlr2*, *Tlr4*, *Tlr6*, *Tlr13*, *Nlrp3*, *Nlrp12*, and *Nlrp1a* (Figure S3M).

We selectively deleted MyD88, an important microbial sensing adaptor protein, in PMNs and found higher IFN-γ expression in placental CD8+ T cells in E16.5 *Myd88$^{fl/fl}$Mrp8-cre* mice, compared with Cre− littermates, despite no significant change in the number of PMNs (Figure 4F). PMN-specific knockout of MyD88 also increased anti-fetus IgG (Figure S4A) but did not affect the abundance of IL-17A+ T cells in the placenta (Figure S4B). Interestingly, this effect was limited to the placenta and mLN; no changes were observed in the uterus, spleen, or colon (Figures 4F and S4C–S4E). These data suggest that microbial sensing is required for placental PMNs to suppress maternal IFN-γ responses to the fetus.

Analysis of differentially expressed genes (DEGs) in the MDSC cluster showed that the expression of *Il1b*, *Cd84*, *Wfdc17*, *Clec4e*, and *Arg2*, all of which are critical for MDSC function,[36–39] were all significantly reduced in MDSCs from GF placentas (and, to a lesser extent, the blood and uterus) relative to SPF MDSCs (Figure S4F). Of note, analysis of publicly available bulk RNA-seq data[40] from human PBMCs collected from healthy pregnant patients showed that expression of *Il1b*, *Arg2*, and *Cd84* increased from the second to the third trimester (Figure S4G). Pathway analysis of DEGs in the MDSC transcriptome showed that genes associated with neutrophil activation, prostaglandin biosynthesis, glycolysis, and gluconeogenesis were downregulated in GF MDSCs, while genes associated with antigen presentation, endothelial cell activation, and regulation of B cell function were upregulated (Figure S4H). Furthermore, while most genes associated with antigen presentation were downregulated in

placental IFN-γ+ CD8+ T cells during the 1st and 2nd pregnancy. (H) Abundance of GzmB+ CD8+ T cells in the placenta and uterus. (I) Abundance of placental GzmB+ CD8+ T cells during the 1st and 2nd pregnancy.

(J–L) CD8+ T cells were isolated from the placenta and uterus of E16.5 SPF or GF mice and adoptively transferred into E7.5 SPF dams. (J) Fetal resorption at E16.5; (K) IFN-γ+ T cells at E16.5; (L) GzmB+ CD8+ T cells at E16.5.

(M) Fetal resorption in GF dams given anti-IFN-γ or isotype control antibody. For (B)–(I), (K), and (L), each dot represents one dam. For (A), (J), and (M), each dot represents one litter. Error bars represent one standard deviation. *$p < 0.05$, **$p < 0.01$, ***$p < 0.001$, ****$p < 0.0001$.

See also Figure S3.

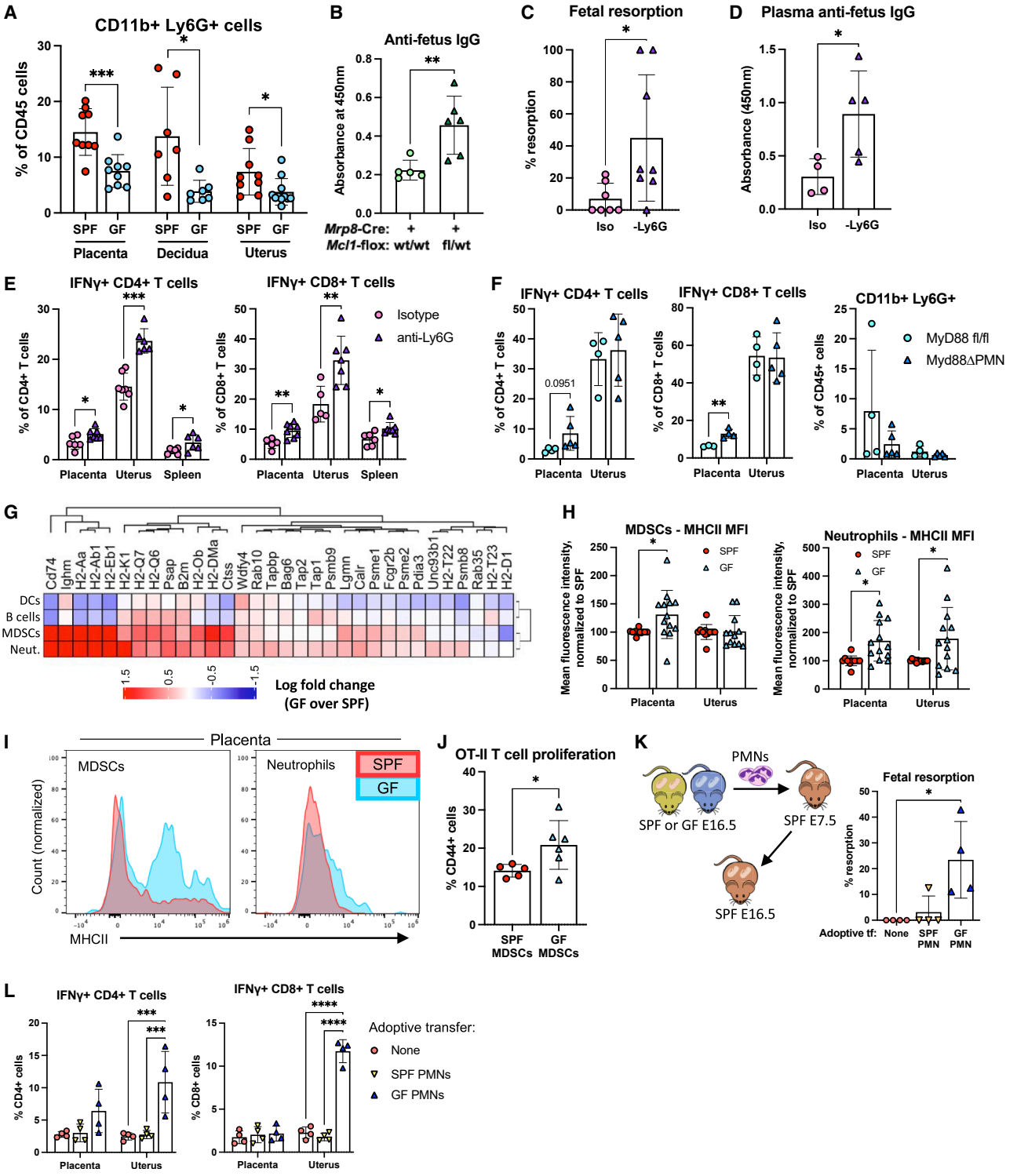

Figure 4. MDSCs are recruited to the MFI in a gut microbiota-dependent manner and restrict T cell IFN responses against the fetus

(A) Frequency of PMNs (CD11b+Ly6G+) in placenta, decidua, and uterus of E16.5 SPF and GF mice.

(B) Plasma anti-fetus IgG in *Mrp8-Cre+ Mcl1*$^{fl/wt}$ and littermate *Mrp8-Cre+ Mcl1*$^{wt/wt}$ dams.

(C–E) Fetal resorption (C), plasma anti-fetus IgG (D), and IFN-γ+ T cells (E) in SPF dams given anti-Ly6G or isotype control.

(F) Frequencies of IFN-γ+ T cells and PMNs in pregnant MyD88ΔPMN mice and Cre− littermate controls at E16.5.

(G) Fold change in expression of genes associated with antigen presentation within the indicated cell clusters, measured by scRNA-seq.

(legend continued on next page)

GF B cells and dendritic cells (DCs) relative to SPF, many were upregulated in GF neutrophils and MDSCs (Figures 4G and S4I). Consistently, flow cytometry analysis showed more major histocompatibility complex class II (MHC-II)-expressing MDSCs and neutrophils in the placenta and uterus of GF dams relative to SPF dams at E16.5 (Figures 4H and 4I). Strikingly, MDSCs expressed higher levels of both MHC-I and MHC-II than neutrophils, by either flow cytometry (Figure S4J) or qPCR (Figure S4K).

To investigate whether MDSCs from GF mice are functionally altered, we co-cultured carboxyfluorescein succinimidyl ester (CFSE)-labeled OT-II T cells with OVA-pulsed CD11b+Ly6G+ cells (PMNs) isolated from the placentas of E16.5 SPF and GF mice, and we found greater proliferation when T cells were co-cultured with PMNs from GF mice than PMNs from SPF mice (Figures 4J and S4L). We also co-cultured SPF and GF placental PMNs with WT T cells that were stimulated with α-CD3 and α-CD28 antibodies, and we found that T cell proliferation was reduced to a greater extent when co-cultured with PMNs from SPF mice than with PMNs from GF mice (Figure S4M). Furthermore, when CD11b+Ly6G+ cells from the placenta and uterus of E16.5 GF dams were adoptively transferred into E7.5 SPF dams, fetal resorption and uterine IFN-γ+ T cells were increased in the recipient dams at E16.5 (Figures 4K and 4L). Together, these data suggest that appropriate microbial signals are required to promote placental MDSCs, which dampen T cell IFN-γ responses at the MFI for the maintenance of maternal-fetal immune tolerance.

Gut-derived RORγt+ Tregs restrain Th17 responses at the MFI

The excessive IFN-γ+ T cells at the GF MFI might also be attributed to impairments in Tregs, which are crucial for maintaining maternal-fetal tolerance.[41,42] While we found no difference in the abundance of Tregs at the MFI between SPF and either GF or Abx-treated mice (Figures 5A and S4N), there was a significant reduction in RORγt+Tregs at the MFI of both GF and Abx-treated mice at E16.5 (Figures 5B, 5C, and S4N); consistent with previous studies,[43–45] RORγt+Tregs were also virtually absent from the intestines and mLNs of GF mice (Figure S5A). RORγt+Tregs increased dramatically with gestation in SPF, but not GF, mice (Figure 5D). Peripheral RORγt+Tregs represent a subset of Tregs with enhanced immunosuppressive ability, which is primarily associated with the intestine.[46,47] However, the regulation and function of RORγt+Tregs at the MFI are unknown. Our scRNA-seq data confirmed the presence of *Rorc*-expressing Tregs at the MFI (Figure S5B). Analysis of DEGs between *Rorc*+ and *Rorc*− Tregs showed altered expression of genes related to T cell trafficking, sphingolipid signaling, mitochondrial function, and hormone signaling (Figures S5C–S5F), suggesting differential functions between RORγt+ and RORγt−Tregs at the MFI.

RORγt+Tregs are induced by RORγt+ antigen-presenting cells (APCs) in an MHC-II-dependent manner.[48–52] We found a small population of lineage-negative RORγt+ cells (CD3−CD4−CD8−RORγt+) in the uterus, which increased in abundance with gestation in SPF but not GF mice (Figure S5G), suggesting that these cells may promote fetal tolerance via RORγt+Tregs. To test this, we selectively deleted MHC-II in RORγt-expressing cells by crossing *H2-Ab1*-flox mice with *Rorc*-Cre mice, a model originally employed to define the essential role of RORγt+APCs in driving intestinal immune tolerance.[53,54] E16.5 MHCIIΔRorc dams had fewer RORγt+Tregs in the uterus, compared with littermate controls (Figure 5E), while conventional Tregs remained unchanged (Figure S5H), suggesting a similar RORγt+APC-dependent mechanism for the emergence of RORγt+Tregs in the uterus. Importantly, IL-17A+ CD4+ T cells were increased in both the uterus and colon of pregnant E16.5 MHCIIΔRorc mice (Figure 5F), while the numbers of IFN-γ+ T cells and IL-17A+ γδ T cells remained unchanged (Figures 5F, S5I, and S5J), suggesting that RORγt+Tregs in the uterus function in part by dampening IL-17A+ T cells, reminiscent of their established role in the colon.[49,50] We did not observe any impact on CD11b+Ly6G+ cells (Figure S5K), and disruption of PMNs by either anti-Ly6G or MyD88 knockout likewise had no impact on Tregs (Figures S5L and S5M), suggesting that uterine RORγt+Tregs are regulated independently of PMNs/MDSCs. We also observed elevated levels of plasma anti-fetus IgG in pregnant MHCIIΔRorc mice (Figure 5G), and MHCIIΔRorc dams had significantly smaller litters than their Cre-negative littermates (Figure 5H), further underscoring a critical role for RORγt+APCs and RORγt+Tregs in the establishment of maternal tolerance. These findings collectively suggest a microbiota-dependent emergence of RORγt+Tregs at the MFI, which may require RORγt+APCs for induction and specifically inhibit uterine Th17 cells.

RORγt+Tregs have recently been reported to traffic from the intestine to distal sites and to contribute to tissue regeneration.[55] To investigate the origin of the RORγt+Tregs at the MFI, we utilized KikGR mice,[56] which express a photoconvertible green fluorescent protein (KikGR) that converts to red fluorescence (KikR) when exposed to 405 nm light.[57] We photoconverted the small intestine and colon of adult nonpregnant KikGR females via laparotomy, and we analyzed the uterus 24 h later. We found that 2%–5% of uterine CD45+ cells were KikR+ (Figure 5I), including PMNs, T cells, B cells, and dendritic cells (Figure S5N). Importantly, a significant proportion of uterine RORγt+Foxp3+ cells were KikR+ (Figures 5J and S6A), indicating an intestinal origin. Together, our data suggest that gut-derived RORγt+Tregs can traffic to the MFI, further suggesting a potential gut-placenta/uterus-immune axis that may influence maternal immune responses against the fetus.

(H and I) MHC-II expression level was measured by flow cytometry in MDSCs and neutrophils from E16.5 SPF and GF mice. Quantifications (H) and representative histograms (I) are shown.

(J) Proliferation of OT-II T cells co-cultured with OVA-pulsed MDSCs isolated from placentas of E16.5 SPF or GF mice.

(K and L) Fetal resorption (K) and IFN-γ+ T cells (L) in E16.5 SPF females 9 days after adoptive transfer of CD11b+Ly6G+ cells from the uterus and placenta of E16.5 SPF or GF females. For (A), (B), (D)–(F), (H)–(J), and (L), each dot represents one dam; for (C) and (K), each dot represents one litter. Error bars represent one standard deviation. $^{*}p < 0.05$, $^{**}p < 0.01$, $^{***}p < 0.001$.

See also Figures S3 and S4.

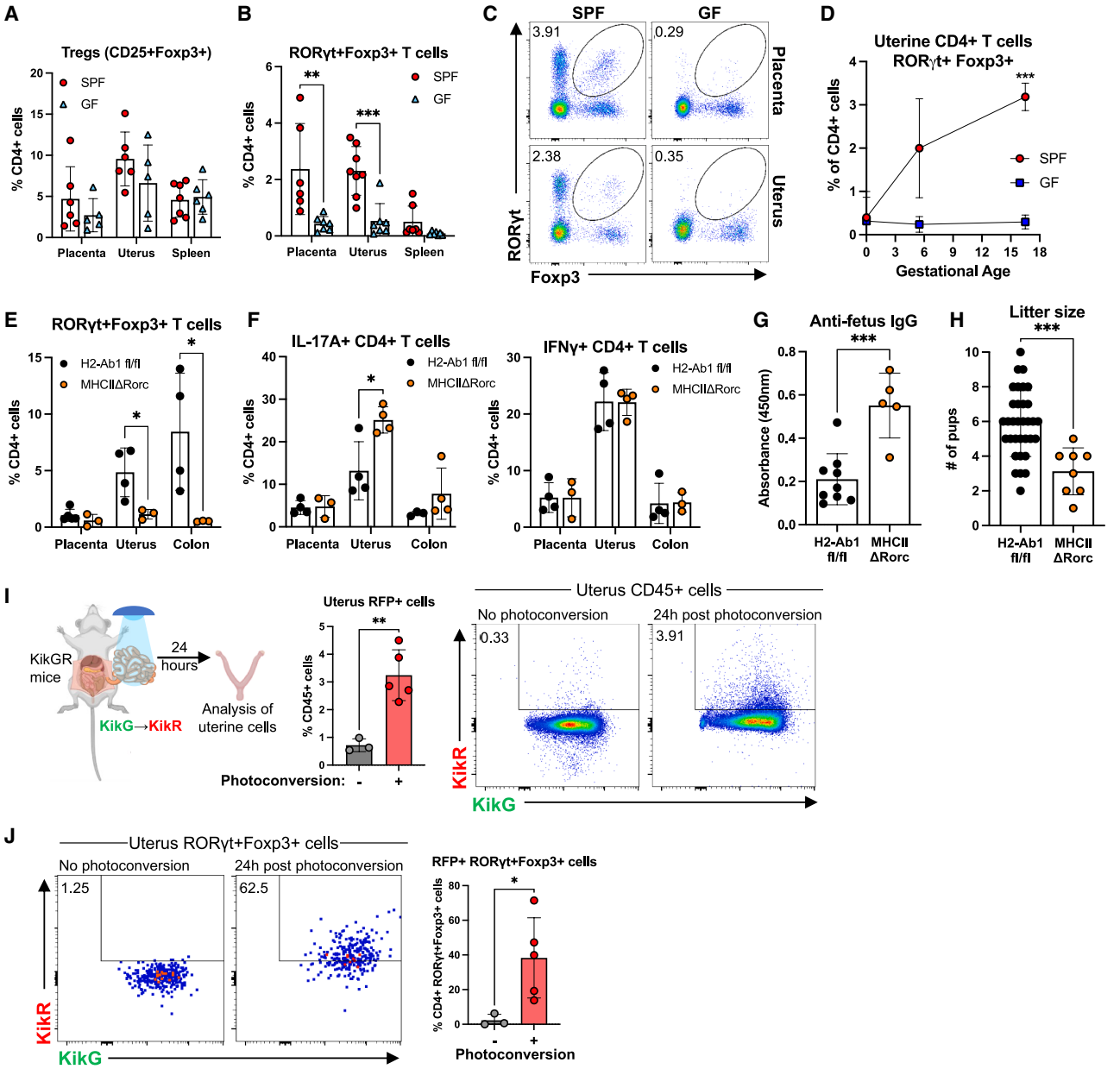

Figure 5. Uterine RORγt+FoxP3+ cells require microbiota-dependent RORγt+ APCs and restrict uterine IL-17A+CD4+ T cells

(A) Frequency of conventional CD25+Foxp3+ Tregs in the placenta, uterus, and spleen of E16.5 SPF and GF mice.

(B and C) Frequency (B) and representative flow plots (C; gated on live CD4+ T cells) of RORγt+Foxp3+ T cells in E16.5 SPF and GF mice.

(D) Abundance of uterine RORγt+Foxp3+ T cells in SPF and GF mice at E0.0 (n = 3 per group), E5.5 (n = 5 SPF and 6 GF), and E16.5 (n = 4 SPF and 3 GF).

(E–H) Analysis of E16.5 pregnant MHCIIΔRorc mice and littermate control *H2-Ab1*$^{fl/fl}$ mice. (E) Percentage of RORγt+Foxp3+ T cells in the placenta, uterus, and colon; (F) abundance of IL-17A+ or IFN-γ+ CD4+ T cells in the placenta, uterus, and colon; (G) plasma anti-fetus IgG; (H) litter sizes.

(I and J) Analysis of KikGR mice 24 h after photoconversion of intestines. (I) Abundance of KikR+ cells in the uterus; (J) proportion of KikR+ RORγt+Foxp3+ T cells in the uterus (gating strategy shown in Figure S6A). For (A), (B), (E)–(G), (I), and (J), each dot represents one dam; for (H), each dot represents one litter. Error bars represent one standard deviation. $^{*}p < 0.05$, $^{**}p < 0.01$, $^{***}p < 0.001$.

See also Figures S4–S6.

Tryptophan metabolites restore a balanced T cell response at the MFI

In order to identify potential mediators of gut-placenta crosstalk, we profiled the metabolomes of plasma and AF from SPF and GF mice at E16.5. Notably, tryptophan, as well as several members of tryptophan metabolic pathways, was significantly reduced in the plasma and AF of GF mice (Figure 6A; Tables S1 and S2). There are three major pathways by which tryptophan is

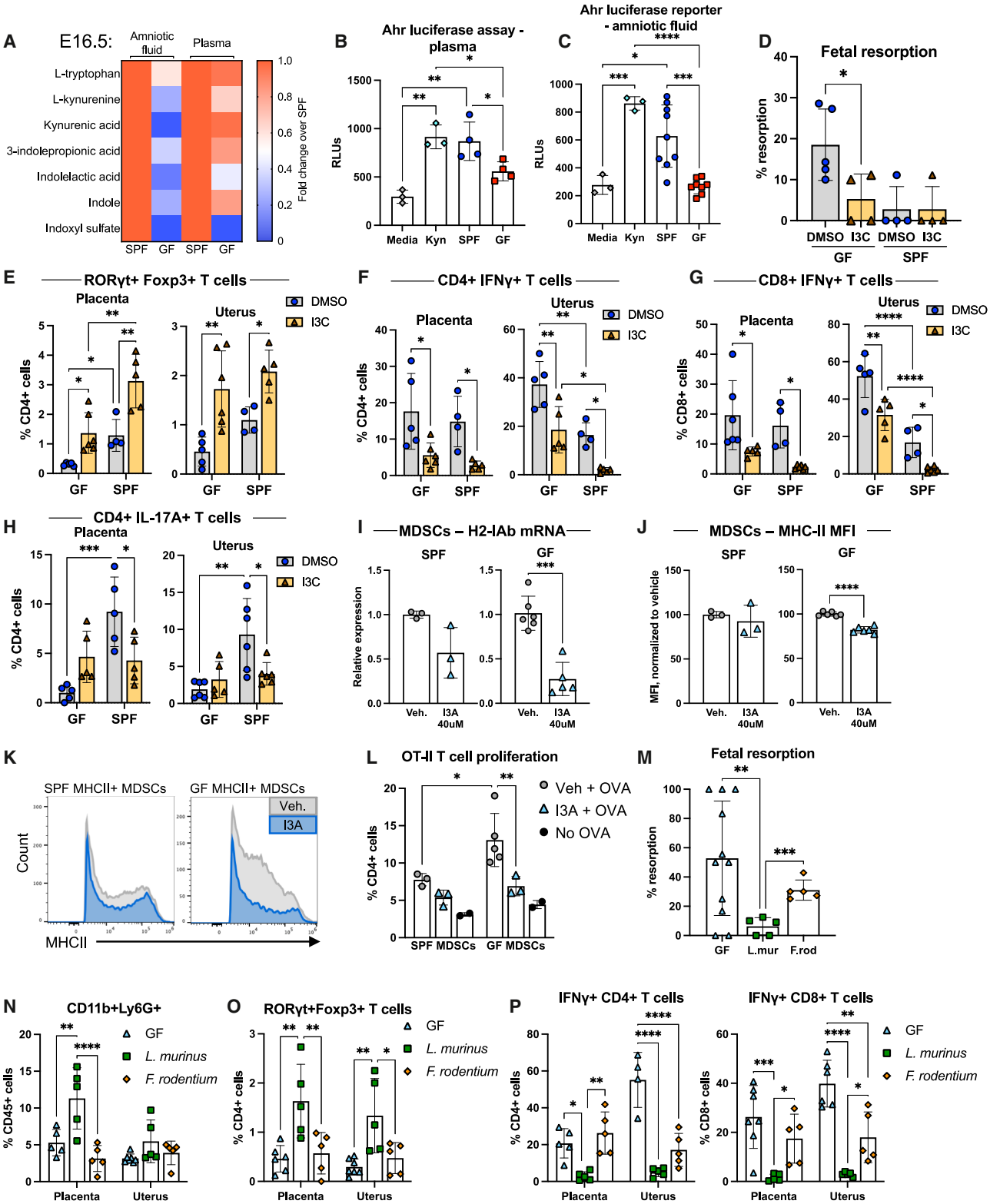

Figure 6. Tryptophan metabolites restore a balanced T cell response at the MFI

(A) Heatmap depicting the relative abundance of metabolites in the AF and plasma of E16.5 SPF and GF mice (n = 3 mice per group).

(B and C) Endpoint luminescence of AhR reporter cells cultured with plasma (B) or AF (C) from E16.5 SPF or GF dams. Media alone or 10 μM L-kynurenine (Kyn) was used as control.

(legend continued on next page)

metabolized: the serotonin pathway, via tryptophan hydroxylase (Tph); the kynurenine pathway, via tryptophan 2,3-dioxygenase (TPO) and indoleamine-2,3-dioxygenase (IDO); and the indole pathway, via aromatic amino acid aminotransferase (ArAT), tryptophan-2-monooxygenase (TMO), and tryptophan decarboxylase (TrD)[58] (Figure S6B). The products of the latter two pathways promote Treg development via signaling by the aryl hydrocarbon receptor (AhR).[59] We used an AhR cell line to analyze plasma and AF from SPF, GF, and Abx-treated dams; plasma and AF from GF mice induced significantly less luciferase expression than that of SPF mice (Figures 6B and 6C), indicating a lower level of AhR-activating ligands. Plasma and AF from dams treated with vancomycin, but not gentamicin, likewise demonstrated a reduction in AhR ligands (Figures S6C and S6D); this was consistent with the elevated placental/uterine IFN-γ+ T cells and increased fetal resorption we observed in vancomycin-treated dams (Figures 1O, 1P, and S2A).

An AhR-dependent metabolic pathway was recently shown to promote the development of RORγt+Tregs in the small intestine,[60] suggesting that RORγt+Tregs could be modulated by tryptophan metabolites. We therefore administered the AhR agonist indole-3-carbinol (I3C) orally to female SPF and GF mice, which reduced GF fetal resorption rates to the level of SPF dams (Figure 6D). Although the abundance of PMNs was not altered (Figure S6E), we observed a significant increase in RORγt+Tregs and a reduction in IFN-γ+ T cells in both the placenta and uterus in I3C-treated mice (Figures 6E–6G and S6F–S6H). I3C treatment did not significantly affect the levels of IL-17A+ T cells in GF dams, likely caused by the inherent diminishment of IL-17A+ T cells in GF mice due to the lack of microbial stimulation[31,61,62]; however, a reduction in IL-17A+ T cells was observed in I3C-treated SPF dams (Figure 6H). Of note, administering I3C intraperitoneally had no effect on the abundance of RORγt+ Tregs, IFN-γ+ T cells, or IL-17A+ T cells across all tissues examined (Figures S6I–S6M). This further suggests that I3C restores immune balance at the MFI via a gut-placenta axis in part by local modulation of immune cells in the gut.

The drastic reduction in placental and uterine IFN-γ+ T cells in I3C-treated GF or SPF dams suggests that I3C may also modulate the MDSC-IFN-γ+ T cell pathway. Oral I3C treatment *in vivo* did not appreciably alter PMN abundance (Figure S6E), but the potential for functional changes in these cells was unclear. We therefore examined the effect of tryptophan-derived indoles on PMNs/MDSCs *in vitro*. We found that *in vitro* treatment with the AhR agonist indole-3-acetaldehyde (I3A; selected for *in vitro* assays because I3C is not water-soluble) significantly reduced MHC-II expression at both the mRNA level (Figure 6I) and the protein level (Figures 6J and 6K) in MDSCs, but it had little to no effect on neutrophils (Figures S7A and S7B). We further found that OT-II T cell proliferation was reduced when co-cultured with I3A-treated OVA-pulsed MDSCs from GF mice, relative to vehicle-treated GF MDSCs, although the effect on SPF MDSCs was less pronounced, and T cells co-cultured with neutrophils did not proliferate irrespective of origin or I3A treatment (Figures 6L, S7C, and S7D). Together, these data suggest that in addition to their role in potentiating Tregs, AhR-activating tryptophan metabolites may also influence MDSC function by limiting their MHC expression and activation of T cells at the MFI.

Finally, to determine whether tryptophan-metabolizing gut bacteria could improve maternal tolerance and pregnancy outcomes, we monocolonized GF females with *Lactobacillus murinus*, which is abundant in our mouse colony (Figure S7E) and has been shown to metabolize tryptophan and produce AhR ligands,[63,64] or the non-tryptophan-metabolizing *Faecalibaculum rodentium*.[65] *L. murinus*-colonized dams had higher levels of AhR ligands in the AF than either GF dams or *F. rodentium*-colonized dams (Figure S7F). Like I3C-treated dams, *L. murinus*-colonized dams had less fetal resorption than GF or *F. rodentium*-colonized dams (Figure 6M), higher levels of PMNs and RORγt+Tregs, and lower levels of IFN-γ+ T cells at the MFI (Figures 6N–6P), although conventional Tregs were not significantly altered (Figure S7G). The colons of *L. murinus*-colonized mice exhibited a similar increase in RORγt+ Tregs (Figure S7H), as well as an increase in IL-17A+ CD4+ T cells (Figure S7I), while both *L. murinus* and *F. rodentium* reduced the abundance of IFN-γ+ T cells in the small intestine (Figure S7J); the abundance of PMNs and conventional Tregs was not significantly altered in the intestine (Figures S7K and S7L). Together, these data suggest that the gut microbiota promotes maternal tolerance in part via the AhR pathway, which may be a promising target to improve fetal tolerance following microbiota disruption.

Dysregulation of MDSCs, RORγt+Tregs, and microbiota-dependent tryptophan derivatives in human reccurent miscarriage

In order to confirm the relevance of our findings in the context of human pregnancy, we leveraged a publicly available scRNA-seq dataset[66] (GEO: GSE214607), in which scRNA-seq was

(D–H) Analysis of SPF or GF dams treated orally with I3C or vehicle (DMSO). (D) Fetal resorption rates; (E) abundance of RORγt+Foxp3+ T cells in the placenta and uterus; (F) abundance of CD4+ IFN-γ+ T cells in the placenta and uterus; (G) abundance of CD8+ IFN-γ+ T cells in the placenta and uterus; (H) abundance of IL-17A+ CD4+ T cells in the placenta and uterus.

(I) Expression of H2-IAb mRNA in bone marrow MDSCs treated with I3A.

(J and K) Expression of surface MHC-II on bone marrow MDSCs treated with I3A, measured by flow cytometry; quantifications (J) and representative histograms (K) are shown.

(L) Proliferation of OT-II T cells co-cultured with OVA-pulsed MDSCs isolated from the bone marrow of E16.5 SPF or GF mice and treated with I3A.

(M–P) Female GF mice were colonized with *L. murinus* or *F. rodentium* prior to mating. (M) Resorption rates; (N) abundance of CD11b+Ly6G+ cells at E16.5; (O) abundance of RORγt+Foxp3+ T cells at E16.5; (P) abundance of IFN-γ+ T cells at E16.5. For (B), (D)–(J), (L), and (N)–(P), each dot represents one dam. For (C), each dot represents AF from a single fetus; a maximum of three AF samples were analyzed from each dam. For (D) and (M), each dot represents one litter. Error bars represent one standard deviation.

$^{*}p < 0.05$, $^{**}p < 0.01$, $^{***}p < 0.001$, $^{****}p < 0.0001$.

See also Figures S6 and S7 and Tables S1 and S2.

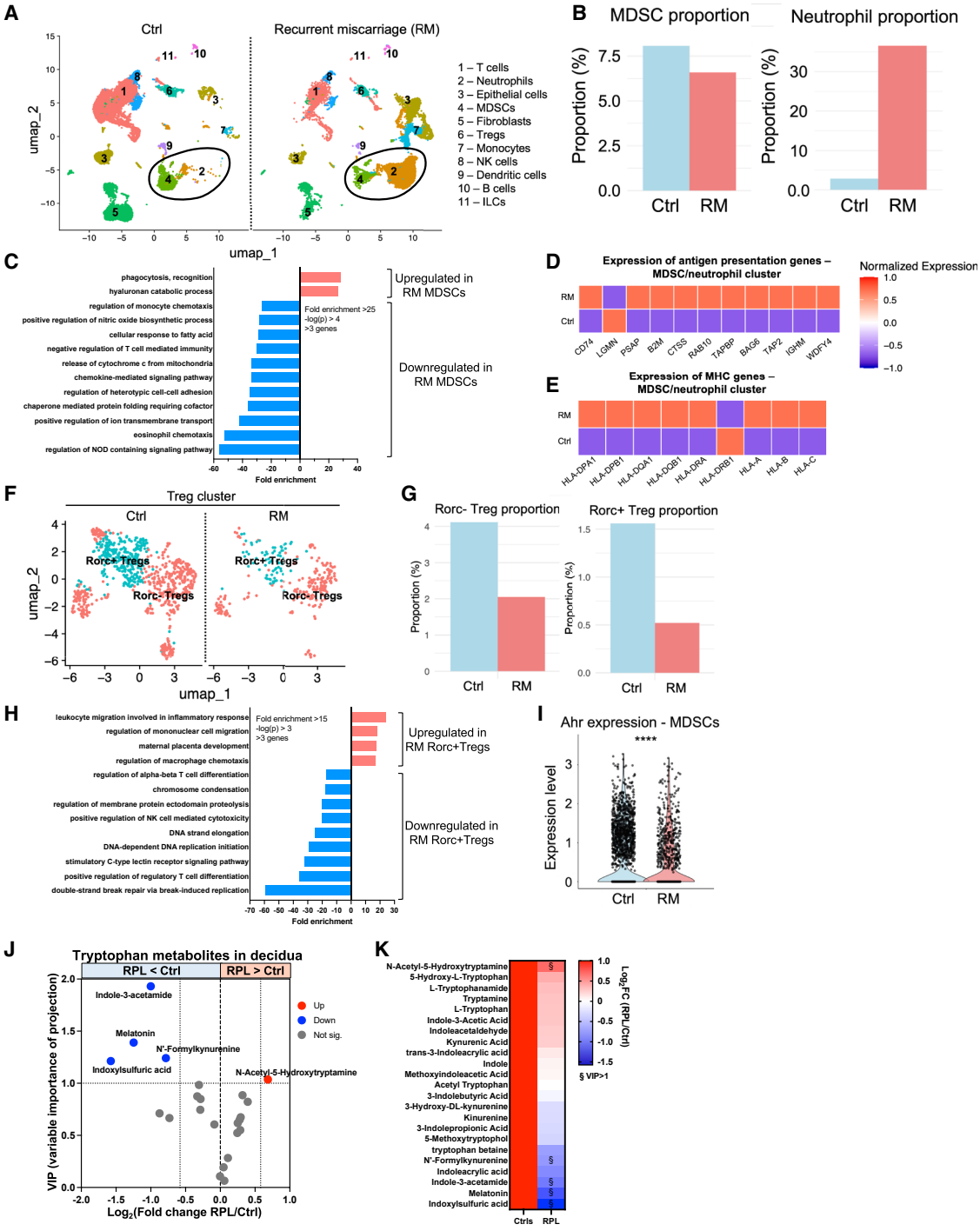

Figure 7. Dysregulation of MDSCs, RORγt+Treg cells, and microbiota-dependent tryptophan derivatives in human reccurent miscarriage

(A–I) Analysis of publicly available scRNA-seq data[66] (GEO: GSE214607), comparing first-trimester decidua from RM patients as well as healthy patients who underwent elective termination. (A) Eleven clusters were defined by gene signature. UMAP representations are shown for control and RM patients. (B) Relative abundance of the MDSC and neutrophil clusters in control and RM patients, shown as the fraction of all cells. (C) Gene Ontology terms that were significantly enriched among the genes that were significantly upregulated (red bars) or downregulated (blue bars) in MDSCs from RM patients relative to healthy controls. (D and E) Relative expression of antigen presentation genes (D) and MHC genes (E) in MDSCs and neutrophils in RM patients and healthy controls. (F–H) Analysis of decidual Tregs from RM patients or healthy controls. (F) UMAP representation of *Rorc*+ and *Rorc*− Tregs in control or RM decidua. (G) Abundance of *Rorc*+ and *Rorc*− Tregs in control or RM decidua, shown as proportion of total cells. (H) Gene Ontology terms that were significantly enriched among the genes that were

(legend continued on next page)

performed on first-trimester decidua from patients with RM as well as healthy patients who underwent elective termination. Similarly to our mouse dataset, we identified a sizeable cluster of MDSCs (Figure 7A), which was less abundant in RM patients, while neutrophils were increased (Figure 7B). In MDSCs from RM patients, genes related to phagocytosis were more highly expressed, while genes related to chemotaxis, chemokine signaling, cell adhesion, and NOD signaling were downregulated (Figure 7C). Several genes involved with antigen presentation, as well as most MHC genes, were significantly higher expressed in RM neutrophils/MDSCs (Figures 7D and 7E). We also found a cluster of Tregs that included both *Rorc*+ and *Rorc*− Tregs (Figure 7F), both of which were less abundant in RM patients (Figure7G); the *Rorc+* Tregs from RM patients exhibited an increase in genes related to immune cell migration and downregulation of genes involved in Treg differentiation (Figure 7H), suggesting that RORγt+ Tregs might be functionally impaired in RM patients. Together, these data indicate that both MDSCs and RORγt+Tregs are present at the human MFI, and both appear dysregulated in RM. Furthermore, RM was also associated with a significant reduction in MDSC *Ahr* expression (Figure 7I). In addition, reanalysis of a metabolomics dataset[67] found that many tryptophan metabolites, including microbiota-dependent indoles, were significantly reduced in the decidua of patients with RM (Figures 7J and 7K), further suggesting that dysregulation of microbiota-mediated tryptophan derivatives might play a role in human pregnancy loss.

DISCUSSION

Our results highlight a microbiota-driven immune axis between the gut and MFI, which promotes maternal-fetal tolerance via two immune pathways: restricting IFN-γ-dominant responses via MDSCs and dampening Th17 responses via RORγt+ Tregs (Figure S7M), both of which are regulated by microbiota-dependent tryptophan derivatives.

Pregnancy has been implicated to be a trigger of autoimmune responses that may manifest into autoimmune diseases.[68] IFN-γ is a major driver of autoimmune diseases that are more prevalent in women, including SLE and multiple sclerosis.[69,70] While IFN-γ signaling contributes to tissue remodeling at the site of embryo implantation, excessive IFN-γ can easily be embryotoxic.[71] Our results demonstrate a critical role for the gut microbiota to dampen maternal T cell IFN-γ responses in part via MDSCs. MDSCs have been suggested to suppress inflammation during pregnancy,[72] with reduced MDSC levels found in women experiencing RM,[73] and blood MDSC levels are positively associated with successful *in vitro* fertilization.[74] However, the crosstalk between the microbiota and MDSCs during pregnancy is not well understood. Toll-like receptor and MyD88 signaling have been found to be crucial for the induction of MDSCs[75,76]; this appears to be the case at the MFI as well, based on our data from MyD88ΔPMN mice. Our scRNA-seq dataset shows that MDSCs outnumber neutrophils in the murine MFI, suggesting they play a more critical role in regulating immune tolerance at the MFI; this appears consistent in human pregnancy as well, and RM is associated with neutrophil dominance over MDSCs in the decidua. Notably, we found significant upregulation of MHC-II and other antigen presentation-related genes in MDSCs and neutrophils from GF pregnant mice and human RM, both of which are correlated with diminished microbiota-dependent tryptophan derivatives.

Tryptophan derivatives have previously been linked with RM; for example, IDO, which converts tryptophan to kynurenine, is downregulated in the endometrium, villi, and decidua of women with RM.[77] However, the role of microbiota-dependent tryptophan derivatives—independent of IDO-mediated tryptophan derivatives—in immune regulation during pregnancy, particularly MDSC functions, is not well understood. Neutrophils express MHC-II and can present antigens to T cells[78]; although the antigen presentation capacity of MDSCs is less well studied, MDSCs have been found to express MHC-II[79,80] and to present tumor antigens to Tregs in a B cell lymphoma model.[81] IL-10, transforming growth factor β (TGF-β), and prostaglandin E2, often produced by MDSCs, downregulate MHC-II expression to maintain MDSCs' suppressive phenotype by limiting their ability to present antigens to activate T cells.[82,83] Our results suggest functional dysregulation of GF MDSCs, including upregulation of genes associated with antigen presentation, which could be reversed by microbiota-dependent tryptophan derivatives.

Tregs are critical for maintaining maternal-fetal tolerance[41]; interestingly, peripherally generated Tregs may be more important for fetal tolerance than thymically generated Tregs.[84] We have identified a population of RORγt+Tregs in the uterus and placenta that increases with gestation; the emergence of RORγt+Tregs at the MFI appears to require both the microbiota and MHC-II in RORγt-expressing cells, reminiscent of the regulatory mechanism for gut RORγt+Tregs.[50,53] Functionally, lack of RORγt+Tregs results in elevated Th17 responses in both the colon—as previously described[49,50]—and the uterus, as well as increased fetal resorption and anti-fetus IgG. IL-17 supports placentation by promoting trophoblast proliferation and invasion,[85] but overabundance of IL-17 and Th17/Treg imbalance is also associated with implantation failure, preeclampsia, and RM,[85–88] and excessive maternal Th17 responses impact offspring neurodevelopment in mouse models of MIA.[26,28] Future work is still required to delineate a mechanistic link between increased uterine Th17 responses and fetal resorption. Furthermore, our data suggest that some of the uterine RORγt+Tregs originate from the gut, supporting recent evidence of gut-derived RORγt+Tregs' ability to migrate to extraintestinal tissues.[55] Mechanistically, increased gut permeability in pregnancy, as shown in our data, likely facilitates the trafficking of T cells from the gut to the MFI; this is not unique to pregnancy,

significantly upregulated (red bars) or downregulated (blue bars) in *Rorc+* Tregs from RM patients relative to healthy controls. (I) Expression of *Ahr* on decidual MDSCs from RM patients or healthy controls.

(J and K) Fold change in concentration of tryptophan metabolites in decidua from patients with recurrent pregnancy loss (RPL) relative to healthy decidua, from a study by Wang et al.,[67] shown as a volcano plot (J) and as a heatmap (K). § VIP > 1.

however, as gut leakiness and T cell efflux are well described in autoimmune conditions, including inflammatory bowel disease (IBD).[89] Future work is needed to gain additional insights into the specificities of placental/uterine RORγt+ Tregs or the Th17 cells that they restrain.

Aberrant IFN-γ and/or IL-17A signaling are associated with autoimmune disorders, such as SLE and IBD.[90–92] Both IBD and SLE frequently flare up or worsen during pregnancy and carry significant risks for the fetus[8,93,94]; in pregnant SLE patients, plasma IFN-γ levels positively correlate with fetal death.[95] Our study suggests that microbiota perturbation may present additional risks for autoimmune patients during and after pregnancy, by upsetting the Th1/Th17/Treg balance. Our data suggest that gut microbiota-derived AhR ligands can access the AF and restore a balanced immune landscape at the MFI. In addition to the intestine, AhR is expressed throughout the placenta and uterus, and *Ahr*$^{-/-}$ mice have a high rate of fetal death,[96] indicating the importance of AhR in maintaining pregnancy; tryptophan catabolism by IDO is likewise necessary to maintain fetal tolerance.[97] However, to date, the source of the AhR ligands that drive these pathways has not been clearly identified. We have shown that the microbiota is a critical source of AhR ligands that sustain local protective AhR signaling at the MFI. It is well established that AhR signaling promotes Treg differentiation, including RORγt+Tregs,[59,60] and AhR and IDO activation can also promote MDSC differentiation and function.[98,99] Our data suggest that microbiota-dependent tryptophan derivatives might be critical to sustain the functions of RORγt+Tregs and MDSCs at the MFI.

The maternal immune system may respond differently to male fetuses owing to the presence of Y chromosome antigens, potentially increasing the risk of immune-mediated complications. Interestingly, a meta-analysis of over 30 million births across multiple countries found a male-to-female stillbirth ratio of approximately 1.1–1.2:1, with males at higher risk, particularly in preterm gestations.[100] Our observation of increased survival of female fetuses in GF pregnant mice suggests that immune dysregulation due to microbiota perturbation may pose a higher risk for male fetuses because of Y chromosome antigens; however, further investigation is needed to establish this mechanistic link. Furthermore, we found increased fetal resorption in pregnant mice orally treated with vancomycin (but not gentamycin), which were found to have lower levels of microbiota-dependent indoles in plasma and AFs and increased IFN-γ+ T cells at the MFI; these findings suggest that vancomycin-susceptible bacteria may promote maternal-fetal immune tolerance. Vancomycin is used to treat serious Gram-positive bacterial infections in pregnant women, especially those caused by methicillin-resistant *Staphylococcus aureus* (MRSA) and coagulase-negative *Staphylococci*,[32] and has been recommended for prevention of early-onset neonatal group B streptococcal infection in certain high-risk pregnancies.[101] However, controlled studies in pregnant women are lacking to determine how vancomycin treatment may affect the maternal immune response to the fetus. Our mouse study may provide insights into specific immune pathways that are perturbed due to loss of vancomycin-sensitive gut bacteria and microbiota-derived tryptophan derivatives; this, however, needs to be further validated in controlled human studies.

Limitations of the study

Our study is focused on the gut-placenta immune axis facilitated by the gut microbiota to promote maternal-fetal immune tolerance, and our data demonstrate the importance of the gut as a site for priming tolerogenic immune cells. However, this does not preclude contributions from the skin, respiratory, or reproductive microbiotas, albeit likely through mechanisms that are distinct from the gut-placenta immune axis elucidated in our study. In addition, our study uses the Th1/Th17/Treg balance at the MFI as indicative of maternal-fetal immune tolerance, and our data support that loss of this balance is associated with fetal resorption in mice; however, the downstream targets of IFN-γ and IL-17 in maternal or fetal tissues, to promote fetal growth or fetal defects when excessive, are yet to be identified and investigated. Furthermore, the specificities of the T cells that traffic from the gut to the MFI remain to be elucidated; this would provide insights into potentially beneficial gut-derived T cells that could be harnessed to promote maternal-fetal immune tolerance and to improve pregnancy outcomes.

RESOURCE AVAILABILITY

Lead contact

Further information and requests for resources and reagents should be directed to and will be fulfilled by the lead contact, Melody Zeng (myz4001@med.cornell.edu).

Materials availability

This study did not generate new unique reagents.

Data and code availability

This study used both original sequencing data and previously published sequencing and metabolomic data. Datasets original to this study include the following:

- 16S rRNA sequencing data of pregnant mice (Figures 1B and S1A), available on SRA: PRJNA1337147.
- scRNA-seq data of blood, placenta, and uterus tissue from pregnant mice (Figures 2, 4G, S2, S3I, S3M, S4F, S4H, S4I, and S5B–S5F), available on GEO: GSE310031.

Previously published datasets include the following:

- 16S rRNA sequencing data of gentamicin- and vancomycin-treated mice (Figure S2B) from a study by Brown et al.,[33] available on GEO: GSE189794.
- Bulk RNA-seq of PBMCs from 2nd- and 3rd-trimester pregnant women (Figure S4G) from a study by Munchel et al.,[40] available at 10.1126/scitranslmed.aaz0131.
- scRNA-seq data of 1st-trimester decidua from RM patients (Figures 7A–7I) from a study by Wei et al.,[66] available on GEO: GSE214607.
- Metabolomics data from 1st-trimester decidua from RM patients (Figures 7J and 7K) from a study by Wang et al.,[67] available at 10.1016/j.placenta.2021.07.001.

This study did not generate original code. Any additional information required to reanalyze the data reported in this paper is available from the lead contact upon request.

ACKNOWLEDGMENTS

We thank all members of the Zeng lab for suggestions, R. Pinedo and S. Paisner from the Weill Cornell Gnotobiotic Animal Facility for assistance with gnotobiotic animal studies, T. Miller for assistance with flow cytometry, and

Ivan Cohen for generation of the AhR luciferase reporter construct. Funding is as follows: National Institutes of Health grant R01HD110118 (M.Y.Z.), National Institutes of Health grant R01HL169989 (M.Y.Z.), National Institutes of Health grant R21CA270998 (M.Y.Z.), National Institutes of Health grant K01DK114376 (M.Y.Z.), National Institutes of Health grant R01AI123368 (G.F.S.), National Institutes of Health grant R01AI125264 (G.E.D.), National Institutes of Health grant 1F32HD112151-01A1 (J.A.B.), National Institutes of Health grant K08MH130773 (C.N.P.), National Institutes of Health grant K99CA290052 (M.L.), National Institutes of Health grant R50 CA221810 (I.S.), National Institutes of Health grant R01CA249294 (supporting M.A.B. and I.S.), Hartwell Foundation Individual Biomedical Research Award (M.Y.Z.), The Starr Cancer Consortium (M.Y.Z.), Gale and Ira Drukier Institute for Children's Health at Weill Cornell Medicine (M.Y.Z.), Children's Health Council at Weill Cornell Medicine (M.Y.Z. and J.A.B.), Center for Immunology and Office of Academic Integration of Cornell University (M.Y.Z.), Center for IBD Research at Weill Cornell Medicine (M.Y.Z.), National Center for Advancing Translational Sciences (NCATS) grant 2TL1-TR-2386 (H.C.C. and K.Z.S.) and 2KL2-TR-2385 (J.A.B.) of the Clinical and Translational Science Center at Weill Cornell Medical College, Biocodex Microbiota Foundation (J.A.B.), Hartwell Foundation Postdoc Fellowship (K.Z.S.), National Institute of Diabetes and Digestive and Kidney Diseases Multidisciplinary Research Training in Gastroenterology and Hepatology grant 3T32DK116970-05S1 of the Weill Cornell Medicine GI Division (J.A.B.), Crohn's and Colitis Foundation Research Fellowship Award #935259 (M.L.), and Brain and Behavior Research Foundation (NARSAD) Young Investigator Award (C.N.P.).

AUTHOR CONTRIBUTIONS

Conceptualization, M.Y.Z.; methodology, J.A.B., M.A., and M.Y.Z.; investigation, J.A.B., M.A., S.Y., D.S.H.W., C.N.P., L.R.H., H.C.C., M.A.B., A.A., K.Z.S., M.L., A.S., M.L.S.S., and I.S.; formal analysis, J.A.B., M.A., J.G., U.B., S.H., and N.I.; funding acquisition, M.Y.Z.; supervision, M.Y.Z.; software, S.Y., J.G., U.B., S.H., and N.I.; visualization, J.A.B., M.A., S.Y., J.G., U.B., S.H., H.C.C., and N.I.; resources, I.S., G.E.D., J.A., G.F.S., V.P., and M.Y.Z.; writing – original manuscript, J.A.B. and M.Y.Z.; and writing – review & editing, all authors.

DECLARATION OF INTERESTS

M.Y.Z. is an inventor on a patent application filed by Cornell University that relates to the subject matter discussed in this manuscript.

STAR★METHODS

Detailed methods are provided in the online version of this paper and include the following:

SUPPLEMENTAL INFORMATION

Supplemental information can be found online at https://doi.org/10.1016/j.cell.2025.11.022.

Received: July 15, 2024
Revised: June 25, 2025
Accepted: November 18, 2025
Published: December 17, 2025

REFERENCES

1. Belkaid, Y., and Harrison, O.J. (2017). Homeostatic Immunity and the Microbiota. Immunity *46*, 562–576. https://doi.org/10.1016/j.immuni.2017.04.008.
2. McDonald, B., and McCoy, K.D. (2019). Maternal microbiota in pregnancy and early life. Science *365*, 984–985. https://doi.org/10.1126/SCIENCE.AAY0618.
3. Di Simone, N., Santamaria Ortiz, A., Specchia, M., Tersigni, C., Villa, P., Gasbarrini, A., Scambia, G., and D'Ippolito, S. (2020). Recent Insights on the Maternal Microbiota: Impact on Pregnancy Outcomes. Front. Immunol. *11*, 528202. https://doi.org/10.3389/FIMMU.2020.528202.
4. Gohir, W., Whelan, F.J., Surette, M.G., Moore, C., Schertzer, J.D., and Sloboda, D.M. (2015). Pregnancy-related changes in the maternal gut microbiota are dependent upon the mother's periconceptional diet. Gut Microbes *6*, 310–320. https://doi.org/10.1080/19490976.2015.1086056.
5. Koren, O., Goodrich, J.K., Cullender, T.C., Spor, A., Laitinen, K., Bäckhed, H.K., Gonzalez, A., Werner, J.J., Angenent, L.T., Knight, R., et al. (2012). Host remodeling of the gut microbiome and metabolic changes during pregnancy. Cell *150*, 470–480. https://doi.org/10.1016/j.cell.2012.07.008.
6. Pronovost, G.N., Yu, K.B., Coley-O'Rourke, E.J.L., Telang, S.S., Chen, A.S., Vuong, H.E., Williams, D.W., Chandra, A., Rendon, T.K., Paramo, J., et al. (2023). The maternal microbiome promotes placental development in mice. Sci. Adv. *9*, eadk1887. https://doi.org/10.1126/SCIADV.ADK1887.
7. Liu, Z.Z., Sun, J.H., Wang, W.J., and Sun, J.H. (2022). Gut microbiota in gastrointestinal diseases during pregnancy. World J. Clin. Cases *10*, 2976–2989. https://doi.org/10.12998/WJCC.V10.I10.2976.
8. Brondfield, M.N., and Mahadevan, U. (2023). Inflammatory bowel disease in pregnancy and breastfeeding. Nat. Rev. Gastroenterol. Hepatol. *20*, 504–523. https://doi.org/10.1038/S41575-023-00758-3.
9. Ander, S.E., Diamond, M.S., and Coyne, C.B. (2019). Immune responses at the maternal-fetal interface. Sci. Immunol. *4*, eaat6114. https://doi.org/10.1126/sciimmunol.aat6114.
10. Mor, G., Aldo, P., and Alvero, A.B. (2017). The unique immunological and microbial aspects of pregnancy. Nat. Rev. Immunol. *17*, 469–482. https://doi.org/10.1038/nri.2017.64.
11. Mor, G., Cardenas, I., Abrahams, V., and Guller, S. (2011). Inflammation and pregnancy: the role of the immune system at the implantation site. Ann. N. Y. Acad. Sci. *1221*, 80–87. https://doi.org/10.1111/J.1749-6632.2010.05938.X.
12. Koren, O., Konnikova, L., Brodin, P., Mysorekar, I.U., and Collado, M.C. (2024). The maternal gut microbiome in pregnancy: implications for the developing immune system. Nat. Rev. Gastroenterol. Hepatol. *21*, 35–45. https://doi.org/10.1038/S41575-023-00864-2.
13. Rowe, J.H., Ertelt, J.M., Xin, L., and Way, S.S. (2012). Pregnancy imprints regulatory memory that sustains anergy to fetal antigen. Nature *490*, 102–106. https://doi.org/10.1038/NATURE11462.

14. Erlebacher, A. (2013). Mechanisms of T cell tolerance towards the allogeneic fetus. Nat. Rev. Immunol. *13*, 23–33. https://doi.org/10.1038/nri3361.

15. Deshmukh, H., and Way, S.S. (2019). Immunological Basis for Recurrent Fetal Loss and Pregnancy Complications. Annu. Rev. Pathol. *14*, 185–210. https://doi.org/10.1146/ANNUREV-PATHMECHDIS-012418-012743.

16. Arck, P.C., and Hecher, K. (2013). Fetomaternal immune cross-talk and its consequences for maternal and offspring's health. Nat. Med. *19*, 548–556. https://doi.org/10.1038/NM.3160.

17. Green, E.S., and Arck, P.C. (2020). Pathogenesis of preterm birth: bidirectional inflammation in mother and fetus. Semin. Immunopathol. *42*, 413–429. https://doi.org/10.1007/S00281-020-00807-Y.

18. Robertson, S.A., Care, A.S., and Moldenhauer, L.M. (2018). Regulatory T cells in embryo implantation and the immune response to pregnancy. J. Clin. Investig. *128*, 4224–4235. https://doi.org/10.1172/JCI122182.

19. Yockey, L.J., Lucas, C., and Iwasaki, A. (2020). Contributions of maternal and fetal antiviral immunity in congenital disease. Science *368*, 608–612. https://doi.org/10.1126/science.aaz1960.

20. Senegas, A., Villard, O., Neuville, A., Marcellin, L., Pfaff, A.W., Steinmetz, T., Mousli, M., Klein, J.P., and Candolfi, E. (2009). Toxoplasma gondii-induced foetal resorption in mice involves interferon-gamma-induced apoptosis and spiral artery dilation at the maternofoetal interface. Int. J. Parasitol. *39*, 481–487. https://doi.org/10.1016/J.IJPARA.2008.08.009.

21. Chaturvedi, V., Ertelt, J.M., Jiang, T.T., Kinder, J.M., Xin, L., Owens, K.J., Jones, H.N., and Way, S.S. (2015). CXCR3 blockade protects against Listeria monocytogenes infection-induced fetal wastage. J. Clin. Investig. *125*, 1713–1725. https://doi.org/10.1172/JCI78578.

22. Bundhun, P.K., Soogund, M.Z.S., and Huang, F. (2017). Impact of systemic lupus erythematosus on maternal and fetal outcomes following pregnancy: A meta-analysis of studies published between years 2001–2016. J. Autoimmun. *79*, 17–27. https://doi.org/10.1016/j.jaut.2017.02.009.

23. Santos, T.D.S., Ieque, A.L., de Carvalho, H.C., Sell, A.M., Lonardoni, M.V.C., Demarchi, I.G., de Lima Neto, Q.A., and Teixeira, J.J.V. (2017). Antiphospholipid syndrome and recurrent miscarriage: A systematic review and meta-analysis. J. Reprod. Immunol. *123*, 78–87. https://doi.org/10.1016/J.JRI.2017.09.007.

24. Ahn, J., Lee, J., and Kim, S. (2015). Interferon-gamma inhibits the neuronal differentiation of neural progenitor cells by inhibiting the expression of Neurogenin2 via the JAK/STAT1 pathway. Biochem. Biophys. Res. Commun. *466*, 52–59. https://doi.org/10.1016/J.BBRC.2015.08.104.

25. Wang, J., Lin, W., Popko, B., and Campbell, I.L. (2004). Inducible production of interferon-gamma in the developing brain causes cerebellar dysplasia with activation of the Sonic hedgehog pathway. Mol. Cell. Neurosci. *27*, 489–496. https://doi.org/10.1016/J.MCN.2004.08.004.

26. Choi, G.B., Yim, Y.S., Wong, H., Kim, S., Kim, H., Kim, S.V., Hoeffer, C.A., Littman, D.R., and Huh, J.R. (2016). The maternal interleukin-17a pathway in mice promotes autism-like phenotypes in offspring. Science *351*, 933–939. https://doi.org/10.1126/science.aad0314.

27. Lim, A.I., McFadden, T., Link, V.M., Han, S.J., Karlsson, R.M., Stacy, A., Farley, T.K., Lima-Junior, D.S., Harrison, O.J., Desai, J.V., et al. (2021). Prenatal maternal infection promotes tissue-specific immunity and inflammation in offspring. Science *373*, eabf3002. https://doi.org/10.1126/SCIENCE.ABF3002.

28. Kim, S., Kim, H., Yim, Y.S., Ha, S., Atarashi, K., Tan, T.G., Longman, R.S., Honda, K., Littman, D.R., Choi, G.B., et al. (2017). Maternal gut bacteria promote neurodevelopmental abnormalities in mouse offspring. Nature *549*, 528–532. https://doi.org/10.1038/NATURE23910.

29. Smith, K., McCoy, K.D., and Macpherson, A.J. (2007). Use of axenic animals in studying the adaptation of mammals to their commensal intestinal microbiota. Semin. Immunol. *19*, 59–69. https://doi.org/10.1016/J.SMIM.2006.10.002.

30. Diaz Heijtz, R.D., Wang, S., Anuar, F., Qian, Y., Björkholm, B., Samuelsson, A., Hibberd, M.L., Forssberg, H., and Pettersson, S. (2011). Normal gut microbiota modulates brain development and behavior. Proc. Natl. Acad. Sci. USA *108*, 3047–3052. https://doi.org/10.1073/PNAS.1010529108.

31. Ivanov, I.I., Atarashi, K., Manel, N., Brodie, E.L., Shima, T., Karaoz, U., Wei, D., Goldfarb, K.C., Santee, C.A., Lynch, S.V., et al. (2009). Induction of intestinal Th17 cells by segmented filamentous bacteria. Cell *139*, 485–498. https://doi.org/10.1016/J.CELL.2009.09.033.

32. Wilhelm, M.P. (1991). Vancomycin. Mayo Clin. Proc. *66*, 1165–1170. https://doi.org/10.1016/S0025-6196(12)65799-1.

33. Brown, J.A., Sanidad, K.Z., Lucotti, S., Lieber, C.M., Cox, R.M., Ananthanarayanan, A., Basu, S., Chen, J., Shan, M., Amir, M., et al. (2022). Gut microbiota-derived metabolites confer protection against SARS-CoV-2 infection. Gut Microbes *14*, 2105609. https://doi.org/10.1080/19490976.2022.2105609.

34. Perchellet, A.L., Jasti, S., and Petroff, M.G. (2013). Maternal $CD4^+$ and $CD8^+$ T cell tolerance towards a fetal minor histocompatibility antigen in T cell receptor transgenic mice. Biol. Reprod. *89*, 102. https://doi.org/10.1095/BIOLREPROD.113.110445.

35. Csepregi, J.Z., Orosz, A., Zajta, E., Kása, O., Németh, T., Simon, E., Fodor, S., Csonka, K., Barátki, B.L., Kövesdi, D., et al. (2018). Myeloid-Specific Deletion of Mcl-1 Yields Severely Neutropenic Mice That Survive and Breed in Homozygous Form. J. Immunol. *201*, 3793–3803. https://doi.org/10.4049/JIMMUNOL.1701803.

36. Gabrilovich, D.I., and Nagaraj, S. (2009). Myeloid-derived suppressor cells as regulators of the immune system. Nat. Rev. Immunol. *9*, 162–174. https://doi.org/10.1038/NRI2506.

37. Lewinsky, H., Gunes, E.G., David, K., Radomir, L., Kramer, M.P., Pellegrino, B., Perpinial, M., Chen, J., He, T.F., Mansour, A.G., et al. (2021). CD84 is a regulator of the immunosuppressive microenvironment in multiple myeloma. JCI Insight *6*, e141683. https://doi.org/10.1172/JCI.INSIGHT.141683.

38. Alshetaiwi, H., Pervolarakis, N., McIntyre, L.L., Ma, D., Nguyen, Q., Rath, J.A., Nee, K., Hernandez, G., Evans, K., Torosian, L., et al. (2020). Defining the emergence of myeloid-derived suppressor cells in breast cancer using single-cell transcriptomics. Sci. Immunol. *5*, eaay6017. https://doi.org/10.1126/SCIIMMUNOL.AAY6017.

39. Karlstetter, M., Walczak, Y., Weigelt, K., Ebert, S., Van den Brulle, J., Schwer, H., Fuchshofer, R., and Langmann, T. (2010). The novel activated microglia/macrophage WAP domain protein, AMWAP, acts as a counter-regulator of proinflammatory response. J. Immunol. *185*, 3379–3390. https://doi.org/10.4049/JIMMUNOL.0903300.

40. Munchel, S., Rohrback, S., Randise-Hinchliff, C., Kinnings, S., Deshmukh, S., Alla, N., Tan, C., Kia, A., Greene, G., Leety, L., et al. (2020). Circulating transcripts in maternal blood reflect a molecular signature of early-onset preeclampsia. Sci. Transl. Med. *12*, eaaz0131. https://doi.org/10.1126/SCITRANSLMED.AAZ0131.

41. Aluvihare, V.R., Kallikourdis, M., and Betz, A.G. (2004). Regulatory T cells mediate maternal tolerance to the fetus. Nat. Immunol. *5*, 266–271. https://doi.org/10.1038/ni1037.

42. Kahn, D.A., and Baltimore, D. (2010). Pregnancy induces a fetal antigen-specific maternal T regulatory cell response that contributes to tolerance. Proc. Natl. Acad. Sci. USA *107*, 9299–9304. https://doi.org/10.1073/PNAS.1003909107.

43. Lochner, M., Bérard, M., Sawa, S., Hauer, S., Gaboriau-Routhiau, V., Fernandez, T.D., Snel, J., Bousso, P., Cerf-Bensussan, N., and Eberl, G. (2011). Restricted microbiota and absence of cognate TCR antigen leads to an unbalanced generation of Th17 cells. J. Immunol. *186*, 1531–1537. https://doi.org/10.4049/JIMMUNOL.1001723.

44. Ohnmacht, C., Park, J.H., Cording, S., Wing, J.B., Atarashi, K., Obata, Y., Gaboriau-Routhiau, V., Marques, R., Dulauroy, S., Fedoseeva, M., et al. (2015). The microbiota regulates type 2 immunity through RORγt+ T cells. Science *349*, 989–993. https://doi.org/10.1126/science.aac4263.

45. Sefik, E., Geva-Zatorsky, N., Oh, S., Konnikova, L., Zemmour, D., McGuire, A.M., Burzyn, D., Ortiz-Lopez, A., Lobera, M., Yang, J., et al. (2015). Individual intestinal symbionts induce a distinct population of RORγ$^+$ regulatory T cells. Science *349*, 993–997. https://doi.org/10.1126/SCIENCE.AAA9420.

46. Yang, B.H., Hagemann, S., Mamareli, P., Lauer, U., Hoffmann, U., Beckstette, M., Föhse, L., Prinz, I., Pezoldt, J., Suerbaum, S., et al. (2016). Foxp3+ T cells expressing RORγt represent a stable regulatory T-cell effector lineage with enhanced suppressive capacity during intestinal inflammation. Mucosal Immunol. *9*, 444–457. https://doi.org/10.1038/MI.2015.74.

47. Britton, G.J., Contijoch, E.J., Mogno, I., Vennaro, O.H., Llewellyn, S.R., Ng, R., Li, Z., Mortha, A., Merad, M., Das, A., et al. (2019). Microbiotas from Humans with Inflammatory Bowel Disease Alter the Balance of Gut Th17 and RORγt+ Regulatory T Cells and Exacerbate Colitis in Mice. Immunity *50*, 212–224.e4. https://doi.org/10.1016/J.IMMUNI.2018.12.015.

48. Akagbosu, B., Tayyebi, Z., Shibu, G., Paucar Iza, Y.A., Deep, D., Parisotto, Y.F., Fisher, L., Pasolli, H.A., Thevin, V., Elmentaite, R., et al. (2022). Novel antigen-presenting cell imparts Treg-dependent tolerance to gut microbiota. Nature *610*, 752–760. https://doi.org/10.1038/S41586-022-05309-5.

49. Kedmi, R., Najar, T.A., Mesa, K.R., Grayson, A., Kroehling, L., Hao, Y., Hao, S., Pokrovskii, M., Xu, M., Talbot, J., et al. (2022). A RORγt+ cell instructs gut microbiota-specific Treg cell differentiation. Nature *610*, 737–743. https://doi.org/10.1038/S41586-022-05089-Y.

50. Lyu, M., Suzuki, H., Kang, L., Gaspal, F., Zhou, W., Goc, J., Zhou, L., Zhou, J., Zhang, W., and JRI; Live; Cell Bank, and et al.. (2022). ILC3s select microbiota-specific regulatory T cells to establish tolerance in the gut. Nature *610*, 744–751. https://doi.org/10.1038/S41586-022-05141-X.

51. Rodrigues, P.F., Wu, S., Trsan, T., Panda, S.K., Fachi, J.L., Liu, Y., Du, S., de Oliveira, S., Antonova, A.U., Khantakova, D., et al. (2025). Rorγt-positive dendritic cells are required for the induction of peripheral regulatory T cells in response to oral antigens. Cell *188*, 2720–2737.e22. https://doi.org/10.1016/J.CELL.2025.03.020.

52. Fu, L., Upadhyay, R., Pokrovskii, M., Chen, F.M., Romero-Meza, G., Griesemer, A., and Littman, D.R. (2025). Prdm16-dependent antigen-presenting cells induce tolerance to gut antigens. Nature *642*, 756–765. https://doi.org/10.1038/S41586-025-08982-4.

53. Hepworth, M.R., Monticelli, L.A., Fung, T.C., Ziegler, C.G.K., Grunberg, S., Sinha, R., Mantegazza, A.R., Ma, H.L., Crawford, A., Angelosanto, J.M., et al. (2013). Innate lymphoid cells regulate CD4+ T-cell responses to intestinal commensal bacteria. Nature *498*, 113–117. https://doi.org/10.1038/nature12240.

54. Hepworth, M.R., Fung, T.C., Masur, S.H., Kelsen, J.R., McConnell, F.M., Dubrot, J., Withers, D.R., Hugues, S., Farrar, M.A., Reith, W., et al. (2015). Group 3 innate lymphoid cells mediate intestinal selection of commensal bacteria-specific CD4$^+$ T cells. Science *348*, 1031–1035. https://doi.org/10.1126/SCIENCE.AAA4812.

55. Hanna, B.S., Wang, G., Galván-Peña, S., Mann, A.O., Ramirez, R.N., Muñoz-Rojas, A.R., Smith, K., Wan, M., Benoist, C., and Mathis, D. (2023). The gut microbiota promotes distal tissue regeneration via RORγ+ regulatory T cell emissaries. Immunity *56*, 829–846.e8. https://doi.org/10.1016/J.IMMUNI.2023.01.033.

56. Nowotschin, S., and Hadjantonakis, A.K. (2009). Use of KikGR a photoconvertible green-to-red fluorescent protein for cell labeling and lineage analysis in ES cells and mouse embryos. BMC Dev. Biol. *9*, 49. https://doi.org/10.1186/1471-213X-9-49.

57. Tsutsui, H., Karasawa, S., Shimizu, H., Nukina, N., and Miyawaki, A. (2005). Semi-rational engineering of a coral fluorescent protein into an efficient highlighter. EMBO Rep. *6*, 233–238. https://doi.org/10.1038/SJ.EMBOR.7400361.

58. Agus, A., Planchais, J., and Sokol, H. (2018). Gut Microbiota Regulation of Tryptophan Metabolism in Health and Disease. Cell Host Microbe *23*, 716–724. https://doi.org/10.1016/j.chom.2018.05.003.

59. Pernomian, L., Duarte-Silva, M., and de Barros Cardoso, C.R. (2020). The Aryl Hydrocarbon Receptor (AHR) as a Potential Target for the Control of Intestinal Inflammation: Insights from an Immune and Bacteria Sensor Receptor. Clin. Rev. Allergy Immunol. *59*, 382–390. https://doi.org/10.1007/s12016-020-08789-3.

60. Rankin, L.C., Kaiser, K.A., de los Santos-Alexis, K., Park, H., Uhlemann, A.C., Gray, D.H.D., and Arpaia, N. (2023). Dietary tryptophan deficiency promotes gut RORγt+ Treg cells at the expense of Gata3+ Treg cells and alters commensal microbiota metabolism. Cell Rep. *42*, 112135. https://doi.org/10.1016/J.CELREP.2023.112135.

61. Ivanov, I.I., Frutos, R. de L., Manel, N., Yoshinaga, K., Rifkin, D.B., Sartor, R.B., Finlay, B.B., and Littman, D.R. (2008). Specific Microbiota Direct the Differentiation of IL-17-Producing T-Helper Cells in the Mucosa of the Small Intestine. Cell Host Microbe *4*, 337–349. https://doi.org/10.1016/j.chom.2008.09.009.

62. Atarashi, K., Tanoue, T., Ando, M., Kamada, N., Nagano, Y., Narushima, S., Suda, W., Imaoka, A., Setoyama, H., Nagamori, T., et al. (2015). Th17 Cell Induction by Adhesion of Microbes to Intestinal Epithelial Cells. Cell *163*, 367–380. https://doi.org/10.1016/j.cell.2015.08.058.

63. Wilck, N., Matus, M.G., Kearney, S.M., Olesen, S.W., Forslund, K., Bartolomaeus, H., Haase, S., Mähler, A., Balogh, A., Markó, L., et al. (2017). Salt-responsive gut commensal modulates TH17 axis and disease. Nature *551*, 585–589. https://doi.org/10.1038/NATURE24628.

64. Wei, W., Liu, Y., Hou, Y., Cao, S., Chen, Z., Zhang, Y., Cai, X., Yan, Q., Li, Z., Yuan, Y., et al. (2024). Psychological stress-induced microbial metabolite indole-3-acetate disrupts intestinal cell lineage commitment. Cell Metab. *36*, 466–483.e7. https://doi.org/10.1016/J.CMET.2023.12.026.

65. Brawner, K.M., Yeramilli, V.A., Duck, L.W., Van Der Pol, W., Smythies, L.E., Morrow, C.D., Elson, C.O., and Martin, C.A. (2019). Depletion of dietary aryl hydrocarbon receptor ligands alters microbiota composition and function. Sci. Rep. *9*, 14724. https://doi.org/10.1038/S41598-019-51194-W.

66. Wei, P., Dong, M., Bi, Y., Chen, S., Huang, W., Li, T., Liu, B., Fu, X., and Yang, Y. (2022). Identification and validation of a signature based on macrophage cell marker genes to predict recurrent miscarriage by integrated analysis of single-cell and bulk RNA-sequencing. Front. Immunol. *13*, 1053819. https://doi.org/10.3389/FIMMU.2022.1053819.

67. Wang, L.L., Liu, H., Zhao, S.J., Shen, L., Xie, T., Luo, J., Mor, G., and Liao, A.H. (2021). The metabolic landscape of decidua in recurrent pregnancy loss using a global metabolomics approach. Placenta *112*, 45–53. https://doi.org/10.1016/J.PLACENTA.2021.07.001.

68. Piccinni, M.P., Lombardelli, L., Logiodice, F., Kullolli, O., Parronchi, P., and Romagnani, S. (2016). How pregnancy can affect autoimmune diseases progression? Clin. Mol. Allergy *14*, 11. https://doi.org/10.1186/S12948-016-0048-X.

69. Postal, M., Vivaldo, J.F., Fernandez-Ruiz, R., Paredes, J.L., Appenzeller, S., and Niewold, T.B. (2020). Type I interferon in the pathogenesis of systemic lupus erythematosus. Curr. Opin. Immunol. *67*, 87–94. https://doi.org/10.1016/J.COI.2020.10.014.

70. Lees, J.R., and Cross, A.H. (2007). A little stress is good: IFN-gamma, demyelination, and multiple sclerosis. J. Clin. Investig. *117*, 297–299. https://doi.org/10.1172/JCI31254.

71. Robertson, S.A., Chin, P.Y., Femia, J.G., and Brown, H.M. (2018). Embryotoxic cytokines-Potential roles in embryo loss and fetal programming. J. Reprod. Immunol. *125*, 80–88. https://doi.org/10.1016/J.JRI.2017.12.003.

72. Köstlin-Gille, N., and Gille, C. (2020). Myeloid-Derived Suppressor Cells in Pregnancy and the Neonatal Period. Front. Immunol. *11*, 584712. https://doi.org/10.3389/FIMMU.2020.584712.

73. Nair, R.R., Sinha, P., Khanna, A., and Singh, K. (2015). Reduced Myeloid-derived Suppressor Cells in the Blood and Endometrium is Associated with Early Miscarriage. Am. J. Reprod. Immunol. *73*, 479–486. https://doi.org/10.1111/AJI.12351.

74. Zhu, M., Huang, X., Yi, S., Sun, H., and Zhou, J. (2019). High granulocytic myeloid-derived suppressor cell levels in the peripheral blood predict a better IVF treatment outcome. J. Matern. Fetal Neonatal Med. *32*, 1092–1097. https://doi.org/10.1080/14767058.2017.1400002.

75. Delano, M.J., Scumpia, P.O., Weinstein, J.S., Coco, D., Nagaraj, S., Kelly-Scumpia, K.M., O'Malley, K.A., Wynn, J.L., Antonenko, S., Al-Quran, S.Z., et al. (2007). MyD88-dependent expansion of an immature GR-1(+)CD11b(+) population induces T cell suppression and Th2 polarization in sepsis. J. Exp. Med. *204*, 1463–1474. https://doi.org/10.1084/JEM.20062602.

76. Wang, B., Wang, L., Shang, R., and Xie, L. (2023). MDSC suppresses T cell antitumor immunity in CAC via GPNMB in a MyD88-dependent manner. Cancer Med. *13*, e6887. https://doi.org/10.1002/CAM4.6887.

77. Wei, H., Liu, S., Lian, R., Huang, C., Li, Y., Chen, L., and Zeng, Y. (2020). Abnormal Expression of Indoleamine 2, 3-Dioxygenase in Human Recurrent Miscarriage. Reprod. Sci. *27*, 1656–1664. https://doi.org/10.1007/S43032-020-00196-5.

78. Moffat, A., and Gwyer Findlay, E. (2024). Evidence for antigen presentation by human neutrophils. Blood *143*, 2455–2463. https://doi.org/10.1182/BLOOD.2023023444.

79. Bertrand, B.P., Heim, C.E., Koepsell, S.A., and Kielian, T. (2024). Elucidating granulocytic myeloid-derived suppressor cell heterogeneity during Staphylococcus aureus biofilm infection. J. Leukoc. Biol. *115*, 620–632. https://doi.org/10.1093/JLEUKO/QIAD158.

80. Kang, X., Zhang, X., Liu, Z., Xu, H., Wang, T., He, L., and Zhao, A. (2016). Granulocytic myeloid-derived suppressor cells maintain feto-maternal tolerance by inducing Foxp3 expression in CD4+CD25-T cells by activation of the TGF-β/β-catenin pathway. Mol. Hum. Reprod. *22*, 499–511. https://doi.org/10.1093/MOLEHR/GAW026.

81. Serafini, P., Mgebroff, S., Noonan, K., and Borrello, I. (2008). Myeloid-derived suppressor cells promote cross-tolerance in B-cell lymphoma by expanding regulatory T cells. Cancer Res. *68*, 5439–5449. https://doi.org/10.1158/0008-5472.CAN-07-6621.

82. Ostrand-Rosenberg, S., and Sinha, P. (2009). Myeloid-derived suppressor cells: linking inflammation and cancer. J. Immunol. *182*, 4499–4506. https://doi.org/10.4049/JIMMUNOL.0802740.

83. Bronte, V., Brandau, S., Chen, S.H., Colombo, M.P., Frey, A.B., Greten, T.F., Mandruzzato, S., Murray, P.J., Ochoa, A., Ostrand-Rosenberg, S., et al. (2016). Recommendations for myeloid-derived suppressor cell nomenclature and characterization standards. Nat. Commun. *7*, 12150. https://doi.org/10.1038/NCOMMS12150.

84. Samstein, R.M., Josefowicz, S.Z., Arvey, A., Treuting, P.M., and Rudensky, A.Y. (2012). Extrathymic generation of regulatory T cells in placental mammals mitigates maternal-fetal conflict. Cell *150*, 29–38. https://doi.org/10.1016/J.CELL.2012.05.031.

85. Piccinni, M.P., Raghupathy, R., Saito, S., and Szekeres-Bartho, J. (2021). Cytokines, Hormones and Cellular Regulatory Mechanisms Favoring Successful Reproduction. Front. Immunol. *12*, 717808. https://doi.org/10.3389/FIMMU.2021.717808.

86. Moura, G.A., Rocha, Y.M., Moura, F.L.D., Freitas, J.O., Rodrigues, J.P.V., Gonçalves, V.P., and Nicolete, R. (2024). Immune system cells modulation in patients with reproductive issues: A systematic review approach. JBRA Assist Reprod. *28*, 78–89. https://doi.org/10.5935/1518-0557.20230044.

87. Murray, E.J., Gumusoglu, S.B., Santillan, D.A., and Santillan, M.K. (2022). Manipulating CD4+ T Cell Pathways to Prevent Preeclampsia. Front. Bioeng. Biotechnol. *9*, 811417. https://doi.org/10.3389/FBIOE.2021.811417.

88. Figueiredo, A.S., and Schumacher, A. (2016). The T helper type 17/regulatory T cell paradigm in pregnancy. Immunology *148*, 13–21. https://doi.org/10.1111/IMM.12595.

89. Mu, Q., Kirby, J., Reilly, C.M., and Luo, X.M. (2017). Leaky Gut As a Danger Signal for Autoimmune Diseases. Front. Immunol. *8*, 598. https://doi.org/10.3389/FIMMU.2017.00598.

90. Caielli, S., Wan, Z., and Pascual, V. (2023). Systemic Lupus Erythematosus Pathogenesis: Interferon and Beyond. Annu. Rev. Immunol. *41*, 533–560. https://doi.org/10.1146/ANNUREV-IMMUNOL-101921-042422.

91. Pollard, K.M., Cauvi, D.M., Toomey, C.B., Morris, K.V., and Kono, D.H. (2013). Interferon-γ and Systemic Autoimmunity. Discov. Med. *16*, 123–131.

92. Friedrich, M., Pohin, M., and Powrie, F. (2019). Cytokine Networks in the Pathophysiology of Inflammatory Bowel Disease. Immunity *50*, 992–1006. https://doi.org/10.1016/J.IMMUNI.2019.03.017.

93. Mills, B.S., and Bermas, B.L. (2024). Pregnancy and the Autoimmune Patient. Curr. Allergy Asthma Rep. *24*, 261–267. https://doi.org/10.1007/S11882-024-01143-Z.

94. Clowse, M.E.B. (2007). Lupus Activity in Pregnancy. Rheum. Dis. Clin. N. Am. *33*, 237. https://doi.org/10.1016/J.RDC.2007.01.002.

95. Hong, S., Banchereau, R., Maslow, B.L., Guerra, M.M., Cardenas, J., Baisch, J., Branch, D.W., Porter, T.F., Sawitzke, A., Laskin, C.A., et al. (2019). Longitudinal profiling of human blood transcriptome in healthy and lupus pregnancy. J. Exp. Med. *216*, 1154–1169. https://doi.org/10.1084/jem.20190185.

96. Jiang, Y.Z., Wang, K., Fang, R., and Zheng, J. (2010). Expression of aryl hydrocarbon receptor in human placentas and fetal tissues. J. Histochem. Cytochem. *58*, 679–685. https://doi.org/10.1369/JHC.2010.955955.

97. Munn, D.H., Zhou, M., Attwood, J.T., Bondarev, I., Conway, S.J., Marshall, B., Brown, C., and Mellor, A.L. (1998). Prevention of allogeneic fetal rejection by tryptophan catabolism. Science *281*, 1191–1193. https://doi.org/10.1126/science.281.5380.1191.

98. Wei, Y., Peng, N., Deng, C., Zhao, F., Tian, J., Tang, Y., Yu, S., Chen, Y., Xue, Y., Xiao, F., et al. (2022). Aryl hydrocarbon receptor activation drives polymorphonuclear myeloid-derived suppressor cell response and efficiently attenuates experimental Sjögren's syndrome. Cell. Mol. Immunol. *19*, 1361–1372. https://doi.org/10.1038/S41423-022-00943-5.

99. Smith, C., Chang, M.Y., Parker, K.H., Beury, D.W., DuHadaway, J.B., Flick, H.E., Boulden, J., Sutanto-Ward, E., Soler, A.P., Laury-Kleintop, L.D., et al. (2012). IDO is a nodal pathogenic driver of lung cancer and metastasis development. Cancer Discov. *2*, 722–735. https://doi.org/10.1158/2159-8290.CD-12-0014.

100. Mondal, D., Galloway, T.S., Bailey, T.C., and Mathews, F. (2014). Elevated risk of stillbirth in males: systematic review and meta-analysis of more than 30 million births. BMC Med. *12*, 220. https://doi.org/10.1186/S12916-014-0220-4.

101. Patel, S., Preuss, C.V., and Bernice, F. (2025). Vancomycin. In StatPearls.

102. Ehst, B.D., Ingulli, E., and Jenkins, M.K. (2003). Development of a novel transgenic mouse for the study of interactions between CD4 and CD8 T cells during graft rejection. Am. J. Transplant. *3*, 1355–1362. https://doi.org/10.1046/J.1600-6135.2003.00246.X.

103. Hou, B., Reizis, B., and DeFranco, A.L. (2008). Toll-like receptors activate innate and adaptive immunity by using dendritic cell-intrinsic and -extrinsic mechanisms. Immunity *29*, 272–282. https://doi.org/10.1016/J.IMMUNI.2008.05.016.

104. Barnden, M.J., Allison, J., Heath, W.R., and Carbone, F.R. (1998). Defective TCR expression in transgenic mice constructed using cDNA-based alpha- and beta-chain genes under the control of heterologous regulatory elements. Immunol. Cell Biol. *76*, 34–40. https://doi.org/10.1046/J.1440-1711.1998.00709.X.

105. Sanidad, K.Z., Amir, M., Ananthanarayanan, A., Singaraju, A., Shiland, N.B., Hong, H.S., Kamada, N., Inohara, N., Núñez, G., and Zeng, M.Y. (2022). Maternal gut microbiome–induced IgG regulates neonatal gut microbiome and immunity. Sci. Immunol. *7*, eabh3816. https://doi.org/10.1126/SCIIMMUNOL.ABH3816.

106. Passegué, E., Wagner, E.F., and Weissman, I.L. (2004). JunB deficiency leads to a myeloproliferative disorder arising from hematopoietic stem cells. Cell *119*, 431–443. https://doi.org/10.1016/j.cell.2004.10.010.

107. Opferman, J.T., Letai, A., Beard, C., Sorcinelli, M.D., Ong, C.C., and Korsmeyer, S.J. (2003). Development and maintenance of B and T lymphocytes requires antiapoptotic MCL-1. Nature *426*, 671–676. https://doi.org/10.1038/NATURE02067.

108. Hashimoto, K., Joshi, S.K., and Koni, P.A. (2002). A conditional null allele of the major histocompatibility IA-beta chain gene. Genesis *32*, 152–153. https://doi.org/10.1002/GENE.10056.

109. Lochner, M., Peduto, L., Cherrier, M., Sawa, S., Langa, F., Varona, R., Riethmacher, D., Si-Tahar, M., Di Santo, J.P., and Eberl, G. (2008). In vivo equilibrium of proinflammatory IL-17+ and regulatory IL-10+ Foxp3+ RORgamma t+ T cells. J. Exp. Med. *205*, 1381–1393. https://doi.org/10.1084/JEM.20080034.

110. Zeng, M.Y., Cisalpino, D., Varadarajan, S., Hellman, J., Warren, H.S., Cascalho, M., Inohara, N., and Núñez, G. (2016). Gut Microbiota-Induced Immunoglobulin G Controls Systemic Infection by Symbiotic Bacteria and Pathogens. Immunity *44*, 647–658. https://doi.org/10.1016/J.IMMUNI.2016.02.006.

111. Weisburg, W.G., Barns, S.M., Pelletier, D.A., and Lane, D.J. (1991). 16S ribosomal DNA amplification for phylogenetic study. J. Bacteriol. *173*, 697–703. https://doi.org/10.1128/JB.173.2.697-703.1991.

112. Kozich, J.J., Westcott, S.L., Baxter, N.T., Highlander, S.K., and Schloss, P.D. (2013). Development of a Dual-Index Sequencing Strategy and Curation Pipeline for Analyzing Amplicon Sequence Data on the MiSeq Illumina Sequencing Platform. Appl. Environ. Microbiol. *79*, 5112–5120. https://doi.org/10.1128/AEM.01043-13.

113. Schloss, P.D., Westcott, S.L., Ryabin, T., Hall, J.R., Hartmann, M., Hollister, E.B., Lesniewski, R.A., Oakley, B.B., Parks, D.H., Robinson, C.J., et al. (2009). Introducing mothur: Open-source, platform-independent, community-supported software for describing and comparing microbial communities. Appl. Environ. Microbiol. *75*, 7537–7541. https://doi.org/10.1128/AEM.01541-09.

114. Quast, C., Pruesse, E., Yilmaz, P., Gerken, J., Schweer, T., Yarza, P., Peplies, J., and Glöckner, F.O. (2013). The SILVA ribosomal RNA gene database project: improved data processing and web-based tools. Nucleic Acids Res. *41*, D590–D596. https://doi.org/10.1093/NAR/GKS1219.

115. Wang, Q., Garrity, G.M., Tiedje, J.M., and Cole, J.R. (2007). Naïve Bayesian classifier for rapid assignment of rRNA sequences into the new bacterial taxonomy. Appl. Environ. Microbiol. *73*, 5261–5267. https://doi.org/10.1128/AEM.00062-07.

116. Tunster, S.J. (2017). Genetic sex determination of mice by simplex PCR. Biol. Sex Differ. *8*, 31. https://doi.org/10.1186/S13293-017-0154-6.

117. Hao, Y., Hao, S., Andersen-Nissen, E., Mauck, W.M., Zheng, S., Butler, A., Lee, M.J., Wilk, A.J., Darby, C., Zager, M., et al. (2021). Integrated analysis of multimodal single-cell data. Cell *184*, 3573–3587.e29. https://doi.org/10.1016/J.CELL.2021.04.048.

118. Wolock, S.L., Lopez, R., and Klein, A.M. (2019). Scrublet: Computational Identification of Cell Doublets in Single-Cell Transcriptomic Data. Cell Syst. *8*, 281–291.e9. https://doi.org/10.1016/J.CELS.2018.11.005.

119. Korsunsky, I., Millard, N., Fan, J., Slowikowski, K., Zhang, F., Wei, K., Baglaenko, Y., Brenner, M., Loh, P.R., and Raychaudhuri, S. (2019). Fast, sensitive and accurate integration of single-cell data with Harmony. Nat. Methods *16*, 1289–1296. https://doi.org/10.1038/S41592-019-0619-0.

120. Becht, E., McInnes, L., Healy, J., Dutertre, C.A., Kwok, I.W.H., Ng, L.G., Ginhoux, F., and Newell, E.W. (2018). Dimensionality reduction for visualizing single-cell data using UMAP. Nat. Biotechnol. *37*, 38–44. https://doi.org/10.1038/nbt.4314.

121. R Core Team (2018). R: a Language and Environment for Statistical Computing (R Foundation for Statistical Computing).

122. Wickham, H., Navarro, D., and Pedersen, T.L. (2016). ggplot2: Elegant Graphics for Data Analysis (Springer-Verlag).

123. Maere, S., Heymans, K., and Kuiper, M. (2005). BiNGO: a Cytoscape plugin to assess overrepresentation of Gene Ontology categories in Biological Networks. Bioinformatics *21*, 3448–3449. https://doi.org/10.1093/BIOINFORMATICS/BTI551.

124. Shannon, P., Markiel, A., Ozier, O., Baliga, N.S., Wang, J.T., Ramage, D., Amin, N., Schwikowski, B., and Ideker, T. (2003). Cytoscape: a software environment for integrated models of biomolecular interaction networks. Genome Res. *13*, 2498–2504. https://doi.org/10.1101/GR.1239303.

125. Ashburner, M., Ball, C.A., Blake, J.A., Botstein, D., Butler, H., Cherry, J.M., Davis, A.P., Dolinski, K., Dwight, S.S., Eppig, J.T., et al. (2000). Gene Ontology: tool for the unification of biology. The Gene Ontology Consortium. Nat. Genet. *25*, 25–29. https://doi.org/10.1038/75556.

126. Gene Ontology Consortium, Aleksander, S.A., Balhoff, J., Carbon, S., Cherry, J.M., Drabkin, H.J., Ebert, D., Feuermann, M., Gaudet, P., Harris, N.L., et al. (2023). The Gene Ontology knowledgebase in 2023. Genetics *224*, iyad031. https://doi.org/10.1093/GENETICS/IYAD031.

127. Ramanan, D., Sefik, E., Galván-Peña, S., Wu, M., Yang, L., Yang, Z., Kostic, A., Golovkina, T.V., Kasper, D.L., Mathis, D., et al. (2020). An Immunologic Mode of Multigenerational Transmission Governs a Gut Treg Setpoint. Cell *181*, 1276–1290.e13. https://doi.org/10.1016/j.cell.2020.04.030.

128. Brader, P., Riedl, C.C., Woo, Y., Ponomarev, V., Zanzonico, P., Wen, B., Cai, S., Hricak, H., Fong, Y., Blasberg, R., et al. (2007). Imaging of hypoxia-driven gene expression in an orthotopic liver tumor model. Mol. Cancer Ther. *6*, 2900–2908. https://doi.org/10.1158/1535-7163.MCT-07-0432.

129. Fisher, J.M., Wu, L., Denison, M.S., and Whitlock, J.P., Jr. (1990). Organization and function of a dioxin-responsive enhancer. J. Biol. Chem. *265*, 9676–9681. https://doi.org/10.1016/S0021-9258(19)38723-X.

130. Ory, D.S., Neugeboren, B.A., and Mulligan, R.C. (1996). A stable human-derived packaging cell line for production of high titer retrovirus/vesicular stomatitis virus G pseudotypes. Proc. Natl. Acad. Sci. USA *93*, 11400–11406. https://doi.org/10.1073/PNAS.93.21.11400.

131. Lu, W., Meng, Z., Hernandez, R., and Zhou, C. (2021). Fibroblast-specific IKK-β deficiency ameliorates angiotensin II-induced adverse cardiac remodeling in mice. JCI Insight *6*, e150161. https://doi.org/10.1172/JCI.INSIGHT.150161.

132. Xia, J., Zhang, Y., Zhao, H., Wang, J., Gao, X., Chen, J., Fu, B., Shen, Y., Miao, F., Zhang, J., et al. (2017). Non-Invasive Monitoring of CNS MHC-I Molecules in Ischemic Stroke Mice. Theranostics *7*, 2837–2848. https://doi.org/10.7150/THNO.18968.

133. Zhao, Z., Wang, Y., Zhou, R., Li, Y., Gao, Y., Tu, D., Wilson, B., Song, S., Feng, J., Hong, J.S., et al. (2020). A novel role of NLRP3-generated IL-1β in the acute-chronic transition of peripheral lipopolysaccharide-elicited neuroinflammation: implications for sepsis-associated neurodegeneration. J. Neuroinflamm. *17*, 64. https://doi.org/10.1186/S12974-020-1728-5.

134. Hohenstein, P., Slight, J., Ozdemir, D.D., Burn, S.F., Berry, R., and Hastie, N.D. (2008). High-efficiency Rosa26 knock-in vector construction for Cre-regulated overexpression and RNAi. PathoGenetics *1*, 3. https://doi.org/10.1186/1755-8417-1-3.

STAR★METHODS

KEY RESOURCES TABLE

REAGENT or RESOURCE	SOURCE	IDENTIFIER
Antibodies		
Anti-Ly6G (clone 1A8)	BioXCell	BE0075-1; RRID: AB_1107721
Anti-Ly6G isotype control (clone 2A3)	BioXCell	BE0089; RRID: AB_1107769
Anti-IFNγ (clone XMG1.2)	BioXCell	BE0055; RRID: AB_1107694
Anti-IFNγ isotype control (clone HRPN)	BioXCell	BE0088; RRID: AB_1107775
Anti-mouse CD16/32 (Fc Block); clone 93	BioLegend	101301; RRID: AB_312800
Anti-mouse CD3e (clone 145-2C11)	Thermo Scientific	16-0031-82; RRID: AB_468847
Anti-mouse CD28 (clone 37.51)	Thermo Scientific	16-0281-82; RRID: AB_468921
Sheep anti-bovine IgG heavy chain (polyclonal)	Bethyl Laboratories	A10-118A; RRID: AB_67626
Goat anti-mouse IgG1 (polyclonal)	Bethyl Laboratories	A90-205A; RRID: AB_10634645
Goat anti-mouse IgG3 (polyclonal)	Bethyl Laboratories	A90-111A; RRID: AB_67167
Goat anti-mouse IgG-Fc fragment HRP (polyclonal)	Bethyl Laboratories	A90-131P; RRID: AB_67175
Anti-mouse CD3 – APC (clone 17A2)	BioLegend	100236; RRID: AB_2561456
Anti-mouse CD3 – BV711 (clone 145-2C11)	BioLegend	100349; RRID: AB_2565841
Anti-mouse CD3 – Super Bright 780 (clone 17A2)	Invitrogen	78-0032-82; RRID: AB_2762806
Anti-mouse CD4 – BV510 (clone RM4-4)	BioLegend	116025; RRID: AB_2800580
Anti-mouse CD4 – eFluor 506 (clone RM4-5)	Invitrogen	69-0042-80; RRID: AB_2637458
Anti-mouse CD4 – PerCP/Cy5.5 (clone RM4-5)	BD Biosciences	550954; RRID: AB_393977
Anti-mouse CD8a – PerCP/eFluor710 (clone 53-6.7)	Invitrogen	46-0081-82; RRID: AB_1834433
Anti-mouse CD8a – FITC (clone 5H10-1)	BioLegend	100803; RRID: AB_312764
Anti-mouse CD11b – APC (clone M1/70)	BioLegend	101212; RRID: AB_312795
Anti-mouse CD11b – Pacific Blue (clone M1/70)	BioLegend	101224; RRID: AB_755986
Anti-mouse CD11b – PerCP/Cy5.5 (clone M1/70)	BD Biosciences	550993; RRID: AB_394002
Anti-mouse CD11b – PE (clone M1/70)	BioLegend	101207; RRID: AB_312790
Anti-mouse CD11c – FITC (clone N418)	BioLegend	117305; RRID: AB_313774
Anti-mouse CD11c – PE/Cy5 (clone N418)	eBioscience	15-0114-82; RRID: AB_468717
Anti-mouse CD19 – Pacific Blue (clone 1D3/CD19)	BioLegend	152415; RRID: AB_2927869
Anti-mouse CD25 – PE (clone PC61)	BioLegend	102007; RRID: AB_312856
Anti-mouse CD44 – Pacific Blue (clone IM7)	BioLegend	103019; RRID: AB_493682
Anti-mouse CD45 – Alexa Fluor 700 (clone 30-F11)	BioLegend	103128; RRID: AB_493715
Anti-mouse CD45 – APC (clone 30-F11)	BioLegend	103112; RRID: AB_312977
Anti-mouse CD45 – FITC (clone 30-F11)	BioLegend	103107; RRID: AB_312972
Anti-mouse CD45 – BB700 (clone 30-F11)	BD Biosciences	566440; RRID: AB_2744406
Anti-mouse CD45.1 – Alexa Fluor 700 (clone A20)	BioLegend	110723; RRID: AB_493732
Anti-mouse CD45R/B220 – APC (clone RA3-6B2)	BioLegend	103212; RRID: AB_312997
Anti-mouse CD45R/B220 – Pacific Blue (clone RA3-6B2)	BioLegend	103227; RRID: AB_492876
Anti-mouse CD62L – PerCP (clone MEL-17)	BioLegend	104429; RRID: AB_893397
Anti-mouse CD86 – BUV395 (clone GL1)	BD Biosciences	564199; RRID: AB_2738664
Anti-mouse CD90/Thy1.1 – eFluor 450 (clone HIS51)	eBioscience	48-0900-80; RRID: AB_1272257
Anti-mouse CD90/Thy1.1 – PerCP/Cy5.5 (clone HIS51)	Life Technologies	A14798; RRID: AB_2534313
Anti-mouse CD127 – BV605 (clone A7R34)	BioLegend	135025; RRID: AB_2562114
Anti-mouse CD127 – PerCP/Cy5.5 (clone A7R34)	Invitrogen	45-1271-80; RRID: AB_906212
Anti-mouse Foxp3 – PE/Cy5.5 (clone FJK-16s)	Invitrogen	35-5773-82; RRID: AB_11218094

(*Continued on next page*)

Continued

REAGENT or RESOURCE	SOURCE	IDENTIFIER
Anti-mouse γδTCR – eFluor 450 (clone eBioGL3)	eBioscience	48-5711-80; RRID: AB_2574070
Anti-mouse GzmB – FITC (clone QA18A28)	BioLegend	396404; RRID: AB_2801073
Anti-mouse IFNγ – BV650 (clone XMG1.2)	BioLegend	505832; RRID: AB_2734492
Anti-mouse IL-4 – PE/Cy7 (clone 11B11)	BD Biosciences	560699; RRID: AB_1727548
Anti-mouse IL-17A – BV421 (clone TC11-18H10.1)	BioLegend	506926; RRID: AB_2632611
Anti-mouse IL-22 – APC (clone IL22JOP)	Invitrogen	17-7222-80; RRID: AB_10597584
Anti-mouse Ly-6G – PE/Cy7 (clone RB6-8C5)	BioLegend	127618; RRID: AB_1877261
Anti-mouse MHC-I (H2-Kb) – BV421 (clone AF6-88.5)	BioLegend	116525; RRID: AB_2876430
Anti-mouse MHC-II (I-A/I-E) – PerCP/Cy5.5 (clone M5/114.15.2)	BioLegend	107625; RRID: AB_2191072
Anti-mouse MHC-II (I-A/I-E) – APC (clone M5/114.15.2)	BioLegend	107614; RRID: AB_313329
Anti-mouse MHC-II (I-A/I-E) – BV650 (clone M5/114.15.2)	BioLegend	107641; RRID: AB_2565975
Anti-mouse Rorγt – PE-CF594 (clone Q31-378)	BD Biosciences	562684; RRID: AB_2651150
Anti-mouse TNFα – PE/Cy7 (clone MP6-XT22)	BioLegend	506323; RRID: AB_2204356
Bacterial and virus strains		
Lactobacillus murinus	Zeng et al.[110]	N/A
Faecalibaculum rodentium	Gregory Sonnenberg, Weill Cornell Medicine	N/A
Chemicals, peptides, and recombinant proteins		
Ampicillin	Sigma	A0166
Neomycin	Millipore	4801
Metronidazole	Sigma	M3761
Vancomycin	Sigma	V2002
Gentamicin	Millipore	345814
Tryptic soy agar	BD Biosciences	236950
Sheep blood	Thermo Fisher	R54016
Brucella broth	Remel	R452662
Phosphate-buffered saline	Gibco	20012-027
Glycerol	Sigma	G5516
FITC-Dextran	Sigma	46944
RPMI-1640	Sigma	R0883
Fetal bovine serum	Gibco	10437-028
DNAse I	Sigma	DN25
Dispase	Gibco	17105-041
Collagenase type 3	Worthington Biochemical	LS004183
ACK lysis buffer	Quality Biological	118-156-101
Percoll	Cytiva	17089101
Hank's balanced salt solution	Gibco	14170–112
Ethylenediaminetetraacetic acid (EDTA)	Invitrogen	AM9261
Dithiothreitol (DTT)	Thermo Scientific	R0861
Dulbecco's modified Eagle's medium (DMEM)	Gibco	11965-092
Phorbol 12-myristate 13-acetate (PMA)	Sigma	P8139
Ionomycin	Sigma	I0634
GolgiPlug Protein Transport Inhibitor	BD Biosciences	51-2301KZ
Bovine serum albumin	Sigma	A2153
Fixable Viability Dye eFluor™ 780	eBioscience	65-0865-14
Transcription Factor Staining Buffer Set	eBioscience	00-5523-00
OVA MHCI tetramer (chicken ova 257-264; peptide sequence: SIINFEKL)	NIH Tetramer Core	N/A

(*Continued on next page*)

Continued

REAGENT or RESOURCE	SOURCE	IDENTIFIER
OVA MHCII tetramer (chicken ova 323-339; peptide sequence: QAVHAAHAEIN)	NIH Tetramer Core	N/A
Control tetramer (human CLIP 87-101, peptide sequence: PVSKMRMATPLLMQA)	NIH Tetramer Core	N/A
Tween-20	Thermo Scientific	85113
TMB substrate	Thermo Scientific	34028
ELISA stop solution	Invitrogen	SS04
cOmplete™ EDTA-free Protease Inhibitor Cocktail	Sigma	11873580001
Carboxyfluorescein succinimidyl ester (CFSE)	Invitrogen	C34570
Murine IL-2	Stemcell Technologies	78081
Isoflurane	Covetrus	11695067771
Paraformaldehyde	Sigma	158127
Indole-3-carbinol	Sigma	I7256
Dimethylsulfoxide (DMSO)	Sigma	D8418
Corn oil	Mazola	N/A
Trizol	Invitrogen	15596026
Indole-3-acetaldehyde/sodium bisulfite addition compound	Sigma	I1000
Sodium bisulfite	Sigma	243973
Ovalbumin	Sigma	A5503
Lipopolysaccharide	VWR	MSPP-TLRL3PELP
CH-223191 (AhR inhibitor)	Sigma	C8124
L-kynurenine	Sigma	K8625
Critical commercial assays		
E.Z.N.A. stool DNA kit	Omega Bio-tek	D4015-02
Miltenyi Biotec anti-APC beads	Miltenyi Biotec	130-090-855
Miltenyi Biotec MS columns	Miltenyi Biotec	130-042-201
LegendPlex™ IFNγ capture beads	BioLegend	740153
LegendPlex™ Immunoassay standard	BioLegend	740371
LegendPlex™ Immunoassay detection antibodies	BioLegend	740165
LegendPlex™ Immunoassay buffer set	BioLegend	740373
High-Capacity cDNA Reverse Transcription Kit	Applied Biosystems	4368814
ig SYBR Green 2x Master Mix	Intact Genomics	3354
RNEasy Micro Kit	Qiagen	74004
Promega Luciferase Assay Reagent	Promega	E1483
Deposited data		
16S rRNA sequencing of gentamicin- and vancomycin-treated mice	Brown et al.[33]	GEO: GSE189794
Bulk RNA-seq of PBMCs from pregnant women	Munchel et al.[40]	10.1126/scitranslmed.aaz0131
scRNA-seq of decidua from recurrent miscarriage patients	Wei et al.[66]	GEO: GSE214607
Metabolomics analysis of decidua from patients with recurrent pregnancy loss	Wang et al.[67]	10.1016/j.placenta.2021.07.001
16S rRNA sequencing of pregnant and nonpregnant mice	This study	SRA: PRJNA1337147
Single-cell RNA-seq of immune cells from blood, placenta, and uterus of SPF and GF mice	This study	GEO: GSE310031
Experimental models: Cell lines		
B16F10 cells	ATCC	CRL-6475
GPG293 cells	Ory et al.[130]	N/A

(*Continued on next page*)

Continued

REAGENT or RESOURCE	SOURCE	IDENTIFIER
Experimental models: Organisms/strains		
C57BL/6J mice	Jackson Laboratories	Strain # 000664; RRID:IMSR_JAX:000664
IgG-/- mice (C57BL/6J-Del(12Ighg3-Ighg2b)1Mzeng/J)	Sanidad et al.[105]	Strain # 038643; RRID:IMSR_JAX:038643
OVA mice (C57BL/6-Tg(CAG-OVA)916Jen/J)	Jackson Laboratories	Strain # 005145; RRID:IMSR_JAX:005145
Mrp8-Cre mice (B6.Cg-Tg(S100A8-cre,-EGFP)1Ilw/J)	Jackson Laboratories	Strain # 021614; RRID:IMSR_JAX:021614
Mcl-flox mice (B6;129-Mcl1^{tm3Sjk}/J)	Jackson Laboratories	Strain # 006088; RRID:IMSR_JAX:006088
MyD88-flox mice (B6.129P2(SJL)-Myd88tm1Defr/J)	Jackson Laboratories	Strain #008888; RRID:IMSR_JAX:008888
MHCII-flox mice (B6.129X1-*H2-Ab1*^{tm1Koni}/J)	Jackson Laboratories	Strain # 037709; RRID:IMSR_JAX:037709
Rorc-Cre mice	Gérard Eberl,[109] Institut Pasteur	n/a
OT-II mice (B6.Cg-Tg(TcraTcrb)425Cbn/J)	Jackson Laboratories	Strain # 004194; RRID: IMSR_JAX:004194
KikGR mice (Tg(CAG-KikGR)33Hadj/J)	Gretchen Diehl, Memorial Sloan Kettering Cancer Center; and Josef Anrather, Weill Cornell Medicine	Strain # 013753; RRID:IMSR_JAX:013753
Recombinant DNA		
dxHRE-tknes/GFP/FLuc-Neo plasmid	Brader et al.[128]	N/A
Dioxin Responsive Element 482 bp fragment	Fisher et al.[129]	N/A
Oligonucleotides		
16S 1492F (5'- CGGTTACCTTGTTACGACTT-3')	Weisburg et al.[111]	N/A
16S 8F (5'- AGAGTTTGATCCTGGCTCAG-3')	Weisburg et al.[111]	N/A
Rbm31x/Rbm31y F (5'- CACCTTAAGAAC AAGCCAATACA-3')	Tunster[116]	N/A
Rbm31x/Rbm31y R (5'- GGCTTGTCCTGA AAACATTTGG-3')	Tunster[116]	N/A
Tgfb1 F (5'- CAAGGGCTACCATGCCAACT -3')	Lu et al.[131]	N/A
Tgfb1 R (5'- GTACTGTGTGTCCAGGCTCCAA -3')	Lu et al.[131]	N/A
H2-Kb F (5'- GCTGGTGAAGCAGAGAGACTCAG -3')	Xia et al.[132]	N/A
H2-Kb R (5'- GGTGACTTTATCTTCAGGTCTGCT -3')	Xia et al.[132]	N/A
H2-IAβ F (5'- CCG TCA CAG GAG TCA GAA AGG -3')	Zhao et al.[133]	N/A
H2-IAβ R (5'- CGG AGC AGA GAC ATT CAG GTC -3')	Zhao et al.[133]	N/A
β-actin F (5'- AAGGCCAACCGTGAAAAGAT -3')	Hohenstein et al.[134]	N/A
β-actin R (5'- GTGGTACGACCAGAGGCATAC -3')	Hohenstein et al.[134]	N/A
Software and algorithms		
Mothur v1.40.5	Kozich et al.,[112] Schloss et al.[113]	https://github.com/mothur/mothur/releases/tag/v1.40.5
SILVA 16S rRNA reference file release 132	Quast et al.[114]	https://www.arb-silva.de/documentation/release-132/
Ribosomal Database Project (RDP) training set v16 – 86	Wang et al.[115]	https://mothur.org/wiki/rdp_reference_files/#version-16
LegendPlex™ Data Analysis Software Suite (version 2023-02-15)	BioLegend	https://www.biolegend.com/de-de/immunoassays/legendplex/support/software
CellRanger v3.1.0	10X Genomics	https://www.10xgenomics.com/support/software/cell-ranger/latest
Seurat v4.1.0	Hao et al.[117]	https://github.com/satijalab/seurat/releases/tag/v4.1.0
Scrublet v0.2.2	Wolock et al.[118]	https://pypi.org/project/scrublet/0.2.2/
Harmony v1.0	Korsunsky et al.[119]	https://github.com/immunogenomics/harmony

(*Continued on next page*)

Continued

REAGENT or RESOURCE	SOURCE	IDENTIFIER
R v4.1.2	R Core Team[121]	https://cran.r-project.org/bin/windows/base/old/4.1.2/
ggplot2 v3.2.0	Wickham et al.[122]	https://www.tidyverse.org/blog/2019/06/ggplot2-3-2-0/
Cytoscape v3.9.1	Shannon et al.[124]	https://github.com/cytoscape/cytoscape/releases/3.9.1/
BiNGO Cytoscape plugin (v3.0.5).	Maere et al.[123]	https://apps.cytoscape.org/apps/bingo
Mus musculus gene ontology reference annotation (May 16, 2022 release)	Gene Ontology Consortium[125,126]	https://release.geneontology.org/2022-05-16/annotations/index.html
Homo sapiens gene ontology reference annotation (March 16, 2025 release)	Gene Ontology Consortium[125,126]	https://release.geneontology.org/2025-03-16/annotations/index.html
Mus musculus reference genome GRCm38.p6	GenBank	https://www.ncbi.nlm.nih.gov/datasets/genome/GCA_000001635.8/
Prism 10.1.0	GraphPad Software	https://www.graphpad.com/scientific-software/prism/
FlowJo 10.9.0	Beckton Dickinson	https://www.flowjo.com/
Other		
SpectraMax M5 microplate reader	Molecular Devices	M5
SpectraMax iD3 microplate reader	Molecular Devices	iD3
Illumina MiSeq	Illumina	N/A
Cytek Aurora flow cytometer	Cytek	N/A
Cytek AuroraCS cell sorter	Cytek	N/A
BD FACSMelody cell sorter	Becton, Dickinson	N/A
Invitrogen Countess 3 automated cell counter	Invitrogen	AMQAX2000
405nm laser (Laserland 22*70mm Fat Beam 405nm 250mW Dot Laser Module, 16mm diameter)	Laserland	N/A
Q Exactive Orbitrap mass spectrometer	Thermo Scientific	IQLAAEGAAPFALGMBDK
Vanquish Flex UHPLC system	Thermo Scientific	N/A

EXPERIMENTAL MODEL AND STUDY PARTICIPANT DETAILS

Mice

Wild-type C57BL/6 mice, ovalbumin-overexpressing (OVA) mice (C57BL/6-Tg(CAG-OVA)916Jen/J),[102] *MyD88*$^{fl/fl}$ mice (B6.129P2(SJL)-Myd88tm1Defr/J),[103] and OT-II mice (B6.Cg-Tg(TcraTcrb)425Cbn/J)[104] were originally purchased from the Jackson Laboratory and maintained and expanded in-house by the Zeng laboratory. IgG KO (C57BL/6J-Del(12Ighg3-Ighg2b)1Mzeng/J) mice were generated by the Zeng laboratory.[105] *Mcl1*$^{fl/fl}$*Mrp8-Cre* neutrophil-deficient mice were generated by breeding *Mrp8-Cre* mice (B6.Cg-Tg(S100A8-cre,-EGFP)1Ilw/J)[106] obtained from Jackson Laboratories with *Mcl*$^{fl/fl}$ mice (B6;129-Mcl1^{tm3Sjk}/J)[107] obtained from Dr. You-Wen He's laboratory at Duke University. *MHCII*$^{fl/fl}$ (B6.129X1-*H2-Ab1*^{tm1Koni}/J)[108] mice were provided by Gregory Sonnenberg. *Rorc*-cre[109] mice were originally from Gérard Eberl. KikGR mice (Tg(CAG-KikGR)33Hadj/J)[56] were provided by Gretchen Diehl and Josef Anrather. Littermate controls were used and animals were cohoused after weaning. SPF animals were housed in microisolator cages in the barrier facility of Weill Cornell Medicine. Germ-free mice were bred and maintained in semi-rigid gnotobiotic isolators and transferred into individually ventilated isocages for experimentation. To generate pregnant mice for in vivo studies, breeding pairs were formed from 8-10-week-old nulliparous females and >8-week old non-virgin males. Each female was paired with the same male for all her pregnancies, and up to 4 females were included in each breeding cage with the same male. Due to limitations on the mouse number per cage, not all experiments used the same male breeder; instead, males from same litters (same genetic background and same parents) were used as breeders to reduce variability. E0.5 was defined as the date of detection of the copulation plug and pregnant females were sacrificed on E16.5 except where otherwise indicated. For comparisons of pregnant and nonpregnant mice, nonpregnant mice were housed separately to avoid estrous cycle synchronization. For all in vivo experiments, the pregnancies of mice from all groups were timed and synchronized, and immune cell isolation and analysis were

performed at the same time in order to accurately compare all groups; all in vivo experiments were performed independently at least twice. All animal experiments were approved by the Institutional Animal Care and Use Committee at Weill Cornell Medicine.

Bacteria

Lactobacillus murinus was isolated from fecal pellets of adult WT SPF mice in a previous study.[110] *Faecalibaculum rodentium* was originally isolated from mice and obtained from G. Sonnenberg. Bacterial identities were confirmed by Sanger sequencing using the universal 16S primers 1492R (5' – CGGTTACCTTGTTACGACTT – 3') and 8F (5' – AGAGTTTGATCCTGGCTCAG – 3').[111] The bacteria were cultured anaerobically at 37°C on tryptic soy agar (BD Biosciences 236950) supplemented with 5% sheep blood (Thermo Fisher R54016) or in Brucella broth (Remel R452662) supplemented with 5% sheep blood. For oral inoculation, fresh liquid cultures were inoculated and allowed to grow overnight, after which the concentration was measured by OD600 reading, the bacteria were washed once in sterile PBS, resuspended in sterile PBS at a concentration of $2x10^8$ CFU/mL, and administered to mice via oral gavage (100μL/mouse). For long-term storage, aliquots were stored in Brucella broth with 25% glycerol (Sigma G5516) and frozen at −80°C.

METHOD DETAILS

Mouse treatments

The broad-spectrum antibiotic cocktail consisted of ampicillin (2.5mg/mL; Sigma A0166), neomycin (2.5mg/mL; Millipore 4801), vancomycin (1.25mg/mL; Sigma V2002), and metronidazole (1.25mg/mL; Sigma M3761), dissolved in autoclaved water and sterile filtered; 100μL was administered to pregnant mice by oral gavage daily from E7.5 to E16.5 (after placentation). For gentamicin and vancomycin treatments, 0.1g/L gentamicin (Millipore 345814) or 1g/L vancomycin was dissolved in mouse drinking water and sterile filtered, and given to mice from E7.5 to E16.5. For anti-Ly6G antibody treatment, starting at E7.5 and every two days thereafter until E16.5, pregnant wild-type mice were injected intraperitoneally with 500μg anti-Ly6G antibody (clone 1A8, Bio X Cell BE0075-1) or isotype control (clone 2A3, Bio X Cell BE0089). For anti-IFNg antibody treatment, starting at E5.5 and every two days thereafter until E16.5, pregnant mice were injected intraperitoneally with 500μg anti-IFNg antibody (clone XMG1.2, Bio X Cell BE0055) or isotype control (clone HRPN, BioXCell BE0088). Indole-3-carbinol (I3C, Sigma I7256) was prepared by dissolving 15mg I3C in 50μL DMSO (Sigma D8418), which was then suspended in 950μL corn oil (Mazola). Female mice were treated via oral gavage with either 100mg/kg I3C or an equivalent volume of vehicle (DMSO diluted 1:20 in corn oil), or via intraperitoneal injection of 50mg/kg I3C or equivalent volume of vehicle. I3C was administered on alternate days starting with commencement of breeding until E16.5.

FITC-Dextran gut permeability assay

To measure gut permeability, FITC-Dextran (Sigma 46944) was dissolved in sterile PBS to a concentration of 37.5mg/mL and administered to SPF pregnant mice and age-matched nonpregnant females via oral gavage (500mg/kg). Mice were deprived of food for four hours before administration of FITC-Dextran. Blood was collected immediately before and one hour following FITC-Dextran administration. Plasma was separated and diluted 1:10 in PBS, and 50μL per well added to a 96-well plate. A standard curve was generated using the remaining FITC-Dextran solution. Endpoint fluorescence intensity was measured on a SpectraMax M5 microplate reader (excitation, 485 nm; emission, 525 nm).

16S rRNA sequencing analysis

Fecal samples were freshly collected, and DNA was extracted using the E.Z.N.A. stool DNA kit (Omega Bio-tek D4015-02). The V4 region of the 16S rRNA gene was amplified using universal primers and sequenced using an Illumina MiSeq apparatus as previously described.[112] Paired-end reads were analyzed and classified into operational taxonomic units (OTUs) at > 97% identity level using Mothur v.1.40.5.[113] Taxonomic assignments were determined using the SILVA 16S rRNA reference file release 132[114] and the Ribosomal Database Project (RDP) training set version 16.[115] A total of 46,380 OTUs were identified, encompassing 102 genera, 45 families, 23 orders, 17 classes, and 7 phyla. NMDS analysis and LEfSe linear discriminant analysis was performed by the mothur nmds and lefse commands using all OTU reads. The OTUs shown in the LEfSe panels are those whose abundance was statistically different with $p < 0.05$.

Immune cell isolation for flow cytometry

Placenta and uterus

Uterine horns and placenta tissues were harvested from E16.5 pregnant mice. Decidua was separated from the placenta and combined with uterus tissue for subsequent steps. All placentas from a single dam were pooled together. Tissues were minced using sterile scissors, and incubated at 37°C for 15 minutes (placenta) or 30 minutes (uterus) in RPMI-1640 (Sigma R0883) containing 10% fetal bovine serum (FBS; Gibco 10437-028), 100 μg/mL DNase I (Sigma DN25), 800 μg/mL dispase (Gibco 17105-041), and 0.8mg/mL collagenase type 3 (Worthington Biochemical LS004183). Digested tissues were pushed through a 70μm filter to create a single-cell suspension. For placenta, cells were centrifuged at 2000rpm for 4 minutes, then resuspended in ACK lysis buffer (Quality Biological 118-156-101) and incubated for 3 minutes at room temperature to lyse red blood cells. After 3 minutes, 25mL phosphate-buffered saline (PBS) was added and cells were centrifuged at 2000rpm for 4 minutes. Placental and uterine cells were then washed twice with PBS and resuspended in 40% Percoll (Cytiva 17089101), overlayed on 75% Percoll, and centrifuged at 700g for 20 min without brakes to enrich the lymphocytes.

Intestinal lamina propria cells

Mouse intestines were removed, cleaned of remaining fat tissue, and washed in ice-cold PBS. Intestines were opened longitudinally, washed in ice-cold PBS, and cut into small pieces (~2mm). Dissociation of epithelial cells was performed by incubation on a shaker in Hanks' balanced salt solution (no calcium or magnesium; Gibco 14170-112) containing 2.5 mM ethylenediaminetetraacetic acid (EDTA; Invitrogen AM9261), 0.5 mM dithiothreitol (DTT; Thermo Scientific R0861), and 2% heat-inactivated FBS (heat-inactivated by incubating at 56°C for 30 minutes) for 10 min at 37°C in a glass beaker with stirring. The tissue was washed once in PBS prior to enzymatic digestion in digestion buffer containing dispase (800 μg/ml; Gibco 17105-041), collagenase type 3 (1 mg/ml; Worthington Biochemical LS004183), and DNase I (100 μg/ml; Sigma DN25) in Dulbecco's modified Eagle's medium (DMEM; Gibco 11965-092) with 10% FBS for 20 minutes (small intestine) or 30 minutes (colon) at 37°C. Digested tissues were pushed through a 70μm filter to create a single-cell suspension. The cell suspension was washed twice with phosphate-buffered saline (PBS) and resuspended in 40% Percoll (Cytiva 17089101), overlayed on 75% Percoll, and centrifuged at 700g for 20 min without brakes to enrich the lymphocytes.

Blood immune cells

To isolate immune cells from blood, 1mL ACK lysis buffer (Quality Biological 118-156-101) was added to 0.1mL blood and incubated at room temperature for 3 minutes to lyse the red blood cells, after which the cells were washed twice in PBS.

Spleen and mesenteric lymph node (mLN)

Spleens and mLNs were pushed through a 70μm filter to create a single-cell suspension. For spleens, cells were centrifuged at 2000rpm for 4 minutes, then resuspended in ACK lysis buffer (Quality Biological 118-156-101) and incubated for 3 minutes at room temperature to lyse red blood cells. After 3 minutes, 25mL phosphate-buffered saline (PBS) was added and cells were centrifuged at 2000rpm for 4 minutes. Splenocytes and mLN cells were then washed twice in PBS.

Bone marrow

Femurs and tibias were removed, cleaned of skin and muscle, and placed in a 0.5 mL tube with a hole punched in the bottom, which was then placed in a 1.5 mL tube. 50 μL of sterile PBS was added to the upper tube and the tubes were centrifuged at 1000 rpm for 1 minute to flush the bone marrow into the bottom tube. All bone marrow from a single mouse was then pooled, resuspended in 1mL ACK lysis buffer (Quality Biological 118-156-101), and incubated for 1 minute at room temperature. After 1 minute, 10mL PBS was added and cells were centrifuged at 1500rpm for 5 minutes to remove lysis buffer.

Immune cell flow cytometry analysis

Immune cells were isolated as described above, resuspended in RPMI-1640 (Sigma R0883) with 10% FBS and stimulated for four hours with phorbol 12-myristate 13-acetate (PMA, 50ng/mL; Sigma P8139) and ionomycin (1μg/mL; Sigma I0634) at 37°C. GolgiPlug Protein Transport Inhibitor (1:1000, BD Biosciences 51-2301KZ) was added two hours into the stimulation period. Cells were then washed twice in FACS buffer (PBS with 1% bovine serum albumin; Sigma A2153), blocked for 15 minutes in FACS buffer containing anti-mouse CD16/32 antibody (1:200), and incubated with Fixable Viability Dye eFluor™ 780 (1:3000; eBioscience 65-0865-14) and surface antibodies (all antibodies used at 1:200) at 4°C for 30 minutes in the dark. Cells were then washed twice in FACS buffer and incubated in Fix/Perm solution (eBioscience 00-5523-00) for 30 minutes at 4°C in the dark. Cells were then washed twice in permeabilization buffer (eBioscience 00-5523-00) and incubated with intracellular antibodies (all antibodies used at 1:200) for 30 minutes at 4°C in the dark. For panels that included only surface markers, the PMA/ionomycin stimulation and fixation/permeabilization steps were omitted. Cells were then washed twice in permeabilization buffer, resuspended in FACS buffer, and analyzed on a Cytek Aurora flow cytometer. APC-labeled OVA-specific MHCI tetramer (H-2K(b) chicken ova 257-264; peptide sequence: SIINFEKL), PE-labeled OVA-specific MHCII tetramer (chicken ova 323-339; peptide sequence: QAVHAAHAEIN) and control (human CLIP 87-101, peptide sequence: PVSKMRMATPLLMQA) MHCI/II tetramers were obtained from the NIH Tetramer Core Facility. Tetramers were diluted in FACS buffer (OVA MHCI tetramer, 1:1000; OVA MHCII tetramer, 1:200) and cells were incubated with the tetramer for 1 hour at room temperature, mixing periodically, after Fc Block but before staining with surface antibodies.

B cell coculture assay

Single cell suspensions from uterine horns and placenta tissues from GF or SPF E16.5 pregnant mice were generated as described above, stained with anti-B220 APC antibody (clone RA3-6B2, BioLegend 103212) diluted 1:200 in FACS buffer (PBS + 1% bovine serum albumin) and enriched via magnetic-activated cell sorting (MACS) using Miltenyi Biotec anti-APC beads (Miltenyi Biotec 130-090-855) diluted 1:10 in FACS buffer following the manufacturer's instructions. The purified B cells were resuspended in RPMI-1640 with 10% FBS and 50,000 cells/well were plated in 96 well plate coated with fetal antigens (100μg/well). To prepare the fetal antigens, approximately 100mg of fetal tissues (skin, liver, and brain) were sonicated in 1mL PBS. The purified B cells were cocultured with fetal antigens for 48 hrs, after which the culture supernatants were centrifuged briefly to clarify and IgG concentrations were measured via ELISA.

ELISA quantification of IgG

To measure the concentrations of total IgG, IgG1, or IgG3, 96-well plates were coated in capture antibody (total IgG: sheep anti-bovine IgG heavy chain, 1:500; IgG1: goat anti-mouse IgG1, 1:250; IgG3: goat anti-mouse IgG3, 1:1000) diluted in PBS and incubated

at 4°C overnight. For detection of fetal specific IgG in the plasma of GF and SPF mice, 96-well plates were coated with sonicated fetal antigens (prepared as described for the B cell coculture assay; 100μg/well) and incubated at 4°C overnight. For analysis of IgG reactivity against male or female fetal antigens, fetal sex was determined by PCR for *Rbm31x/Rbm31y* as previously described,[116] and lysates were generated from exclusively male or exclusively female fetuses. For analysis of OVA-specific IgG, plates were coated with 100μL/well OVA (2μg/mL in PBS; Sigma A5503) and incubated at 4°C overnight.

After coating, plates were washed 5 times in 200μL wash buffer (PBS + 0.05% Tween-20; Thermo Scientific 85113), then blocked for 2 hours at room temperature using blocking buffer (PBS + 1% BSA), and washed 5 times in 200μL wash buffer. Plasma, amniotic fluid, or culture supernatants were diluted 1:10 in blocking buffer and 100 μL added to the plate, then incubated overnight at 4°C. Plates were washed 5 times in 200μL wash buffer, then 100μL detection antibody (HRP conjugated goat anti-mouse IgG Fc fragment, diluted 1:5000 in blocking buffer) was added and plates were incubated 1 hour at room temperature. Plates were then washed 5 times in 200μL wash buffer and 100μL TMB substrate (Thermo Scientific 34028) was added per well. The colorimetric reaction was allowed to develop for 10 minutes before quenching with 50uL/well of ELISA stop solution (Invitrogen SS04), and absorbance was measured at 450nm.

Multiplex cytokine analysis

Abundance of IFNγ and IL-17A was measured using the LegendPlex™ assay system (BioLegend 740153) following the manufacturer's instructions, adapted for measurement of amniotic fluid and placenta/uterus homogenates. Placenta and uterus samples were sonicated in PBS containing protease inhbitors (Sigma 11873580001; 500μL buffer per 10mg tissue), centrifuged at 10000rpm for 5 minutes to clarify, then supernatants were stored at -80°C. Immediately before mixing with capture beads, placenta lysates and amniotic fluid samples were diluted 1:4 in LegendPlex assay buffer, while uterus lysates were used undiluted. The manufacturer's protocol was followed for subsequent steps. Samples were read on a Cytek Aurora flow cytometer and data analysis performed using BioLegend's LegendPlex™ Data Analysis Software Suite (version 2023-02-15).

qPCR

Total RNA was extracted from tissue samples using Trizol (Invitrogen 15596026) following the manufacturer's instructions. RNA extraction from MDSC/neutrophil cell pellets was performed using the RNeasy Micro Kit (Qiagen 74004). 2000ng RNA per sample was used to generate cDNA using Applied Biosystems High-Capacity cDNA Reverse Transcription Kit (Applied Biosystems 4368814) following the manufacturer's instructions. cDNA was diluted to 1:5 in water before performing qPCR using Intact Genomics ig SYBR Green 2x Master Mix (Intact Genomics 3354). qPCR was carried out with the CFX384 Real-Time Systems C1000 Touch Thermal Cycler (Bio-Rad Laboratories). Cycling conditions were as follows: Initial denaturation 95°C for 2 minutes, 40 cycles of denaturation at 95°C for 5 seconds followed by annealing/extension at 60°C for 30 seconds. Relative expression was calculated using the ΔΔCt method, using β-actin as the reference gene.

Single-cell RNA-seq

Sample preparation

Single cell suspensions from blood, uterine horns and placenta tissues from GF or SPF E16.5 pregnant mice were generated as described above. Five placentas were pooled from each dam, and three dams were used per group. Blood, placenta, and uterine single-cell suspensions were stained with anti-CD45 APC antibody (clone 30-F11, BioLegend 103112) diluted 1:200 in FACS buffer (PBS + 1% bovine serum albumin; Sigma A2153) and enriched via MACS sorting using Miltenyi Biotec anti-APC beads (Miltenyi Biotec 130-090-855) diluted 1:10 in FACS buffer following the manufacturer's instructions. The purified cells were resuspended at 750 cells/μL and viability was verified using an Invitrogen Countess automated cell counter. >10,000 live CD45+ cells from each tissue (blood, uterine horns or placenta) from each mouse, 3 mice per group, were FACS sorted and subjected to the 10x Genomics pipeline.

Quality filtering and doublets removal

Filtered barcode matrices generated by CellRanger v3.1.0 for each sample were first merged using Seurat[117] merge function and then assessed for nFeature_RNA, nCount_RNA, and percentage of mitochondrial gene expression (%mito). To remove low-quality/dying cells from the data, only cells with 500 < nFeaure RNA < 4000, and %mito > 7.8 (90% quantile of %mito in all cells) were retained. Scrublet[118] v0.2.2 was used to systematically remove doublets/multiplets in the data with a Scrublet score > 0.2. Additionally, we also removed cells with Ppbp expression that may be derived from platelet cells or platelet-related doublets that weren't detected by Scrublet. Finally, 44,754 singlets were used for downstream analysis.

Global cluster analysis workflow

We followed the Seurat guided clustering tutorial (https://satijalab.org/seurat/articles/pbmc3k_tutorial.html) for single cell data analysis with a few key modifications. Briefly, quality-filtered cells were first normalized and scaled (regress out nCount-RNA) followed by principal component analysis (PCA) on highly variable features. To account for sample-sample variation and improve cell cluster identification, single-cell batch integration that simultaneously integrated across samples (θ=1) and tissues (θ=0.5) was performed using Harmony[119] v1.0. Top 20 harmony embeddings were used to run UMAP[120] and to perform clustering analysis (resolution = 0.3). Clusters with low CD45 (Ptprc) expression or with less than 100 cells were excluded from downstream analysis. Fourteen final clusters from 43,682 cells were defined and annotated. The FindAllMarkers function with Wilcox method was used to identify cell-

type-specific markers comparing every cluster against the rest of the clusters. Similar analysis was also performed to identify differentially expressed genes between SPF and GF mice for clusters of interest. Markers that likely originated from ambient RNAs (e.g., Igkc in Tregs) were manually removed from the top differentially expressed gene list.

Sub-cluster analysis of T cells

To better understand the molecular heterogeneity of the T cell compartment, we performed sub-cluster analysis of T cells. Briefly, 6159 T cells from the global cluster analysis were extracted and analyzed from scratch by re-performing variable feature selection, scaling, PCA, harmony integration and clustering analysis (resolution = 0.5). Clusters with very low cell counts as well as doublet-like clusters were removed from further analysis. Based on expression of marker genes (Cd4, Cd8a, S100a4, Ccr7, Foxp3), total T cells were further classified into naïve, memory, and regulatory Cd4/Cd8 T cells. All analysis were performed on R.[121] R packages Seurat and ggplot2[122] was used to generate figures.

Pathway analysis

Pathway analysis was performed using the BiNGO[123] plugin (v3.0.5) in Cytoscape[124] (v3.9.1). Reference annotations were obtained from the Gene Ontology Consortium[125,126] (mouse annotation: May 16, 2022 release; human annotation: March 16, 2025 release). Differentially expressed genes with a fold change >1.5 and adjusted p value <0.05 were used for the analysis.

Adoptive transfer of CD8+ or CD11b+Ly6G+ cells

Pregnant GF females were sacrificed at E16.5 and cells were isolated from uterus and placenta as described above. Cells were washed twice in PBS, then blocked for 15 minutes in FACS buffer containing anti-mouse CD16/32 antibody (1:200). Cells were washed twice in FACS buffer and resuspended in 200μL of FACS buffer containing anti-CD45, CD3, and CD8 antibodies diluted 1:200, incubated for 20 minutes on ice, and washed twice in FACS buffer. Live CD45+CD3+CD8+ or CD45+CD11b+Ly6G+ cells were then purified using a BD FACSMelody cell sorter. 25,000 cells/mouse were injected retro-orbitally into E7.5 SPF females; at E16.5 mice were sacrificed and cells isolated from placenta and uterus for flow cytometry analysis as described above.

Sorting of MDSCs/neutrophils

Single cell suspensions from uterus, placenta, or bone marrow from GF or SPF E16.5 pregnant mice were generated as described above, stained with anti-CD11b APC antibody (clone M1/70, BioLegend 101212) diluted 1:200 in FACS buffer (PBS + 1% bovine serum albumin) and enriched via MACS sorting using Miltenyi Biotec anti-APC beads (Miltenyi Biotec 130-090-855) diluted 1:10 in FACS buffer following the manufacturer's instructions. The enriched cells were then stained with anti-Ly6G, and MDSCs (CD11b+Ly-6G^{mid}) or neutrophils (CD11b+Ly-6G^{hi}) cells were isolated using a BD FACSMelody or Cytek AuroraCS cell sorter.

T cell coculture assays

To obtain T cells, spleens from 6-8 week old non-pregnant SPF WT or OT-II mice were harvested and single-cell suspensions were generated as described above. Cells were washed twice in PBS, then blocked for 15 minutes in FACS buffer containing anti-mouse CD16/32 antibody (1:200). Cells were washed twice in FACS buffer and resuspended in 200μL of FACS buffer containing Fixable Viability Dye eFluor™ 780 (1:3000; eBioscience 65-0865-14) and surface antibodies (1:400), incubated for 20 minutes on ice, and washed twice in FACS buffer. Live CD45+CD62L+CD44-CD19-CD11b- cells were then purified using a BD FACSMelody or Cytek AuroraCS cell sorter.

T cells were incubated in 1 mL PBS with carboxyfluorescein succinimidyl ester (CFSE; 1:1000 dilution; Invitrogen C34570) at 37°C for 20 minutes, after which unbound CFSE was quenched by adding 10mL of RPMI-1640 with 10% FBS and incubating at 37°C for a further 10 minutes. T cells were then washed twice in PBS and resuspended in RPMI with 10% FBS, 0.5μg/mL anti-CD28 antibody (clone 37.51, Thermo Scientific 16-0281-82), and 50ng/mL IL-2 (Stemcell Technologies 78081).

For cocultures with WT T cells, T cells were plated at a density of $2x10^5$ cells/well in U-bottom 96-well plates coated in anti-CD3e antibody (prepared by adding 100uL/well of antibody at 1mg/mL and incubating at 4°C overnight; clone 145-2C11, Thermo Scientific 16-0031-82), and the purified MDSCs were then added at a 1:4 ratio (MDSCs:T cells). Anti-CD3e and anti-CD28 antibodies were added to the culture media at a final concentration of 1μg/mL. The cocultured cells were incubated at 37°C for 3 days before the CFSE dilution in T cells was measured via flow cytometry.

For cocultures with OT-II T cells, MDSCs/neutrophils were plated at a density of $5x10^4$ cells/well in U-bottom 96-well plates in RPMI-1640 containing 10% FBS, 40ng/mL ovalbumin (Sigma A5503), and 50ng/mL lipopolysaccharide (VWR MSPP-TLRL3PELP). MDSCs/neutrophils were incubated at 37°C for 18 hours, irradiated at 5000 rads, then media was removed and replaced with fresh RPMI with 10% FBS, after which the CFSE-labeled T cells were added. The cocultured cells were incubated at 37°C for 48 hours before the CFSE dilution in T cells was measured via flow cytometry.

Intestinal immune cell trafficking analysis

Photoconversion of intestinal cells was performed via laparotomy, as described previously.[127] Briefly, 8 week old nonpregnant female KikGR[56] mice were anesthetized with isoflurane, after which the abdomen was shaved and disinfected with betadine and 70% ethanol. A longitudinal 2cm incision was made in the skin and peritoneum, and the intestines were gently removed and placed on a sterile gauze soaked in saline. 405nm light (Laserland 22*70mm Fat Beam 405nm 250mW Dot Laser Module, 16mm diameter)

was shone onto the small intestine for 10 minutes, then onto the upper colon for 20 minutes, after which the intestines were replaced into the abdomen and the incision closed with 6-0 monofilament nylon sutures. 24 hours later, mice were euthanized and immune cells isolated as described above. Intracellular staining was performed as described above, with one modification in order to preserve the KikG/KikR signal: prior to incubating in Fix/Perm buffer, cells were first incubated in 4% paraformaldehyde (Sigma 158127; diluted in PBS) for 60 seconds, then washed once in FACS buffer and resuspended in Fix/Perm buffer, after which staining proceeded as described above.

Metabolomics analysis

Plasma and amniotic fluid were harvested from WT SPF and GF mice (3 per group) at E16.5 for metabolomic profiling. Metabolites were measured on a Q Exactive Orbitrap mass spectrometer (Thermo Scientific), coupled to a Vanquish UHPLC system (Thermo Scientific), and targeted identification was performed based on an in-house library using known chemical standards. Metabolomic analyses were performed by the Weill Cornell Medicine Proteomics and Metabolomics Core Facility.

AhR reporter assay

To develop the dxDRE-HSV1-tknes/Green Fluorescent Protein/FLuc-Neo retroviral vector, the dxHRE-tknes/GFP/FLuc-Neo plasmid[128] was used as a backbone. The HRE enhancer was replaced by the 482 bp fragment of the Dioxin Responsive Domain (DRE), containing 4 AhR-responsive elements[129]; this fragment was amplified using the mouse CYP1A1 gene. Transfection of the GPG293 cell line[130] for transient retroviral vector production and transduction of B16F10 cells (ATCC CRL-6475) with the resultant vector was performed as previously described.[128] Cells were maintained in RPMI supplemented with 10% FBS and penicillin/streptomycin. Transduced reporter cells were selected in neomycin antibiotic at 1mg/mL for 5 to 7 days. Cells were confirmed for transduction by assessment of GFP via flow cytometry and fluorescence microscopy. Functional reporter validation was assessed by treating cells with the AhR inhibitor CH-223191 (Sigma C8124) and L-kynurenine (Sigma K8625) at 10μM in cell culture and measuring luciferase expression using the Promega luciferase Assay Reagent (Promega E1483). To measure abundance of AhR-activating ligands, transduced cells were cultured in the presence of plasma or amniotic fluid (diluted 1:10 in culture media) for 18 hours at 37°C; 10μM kynurenine was used as a positive control. After 18 hours media was removed and the cells were incubated in PBS + 0.1% Tween-20 at room temperature for 10 minutes. 50μL cell lysate was mixed with 100μL Luciferase Assay Reagent and endpoint luminescence was read immediately using a SpectraMax M5 microplate reader.

In vitro indole-3-acetaldehyde treatment

MDSCs and neutrophils were isolated from bone marrow of E16.5 SPF and GF dams as described above, resuspended in RPMI with 10% FBS, and plated in U-bottom 96-well plates at a density of $5x10^4$ cells/well. Indole-3-acetaldehyde (I3A) with sodium bisulfite addition compound (Sigma I1000) was added to a final concentration of 40μM. 40μM sodium bisulfite (Sigma 243973) was used as a vehicle control. The cells were incubated for 24 hours at 37°C, after which MHC expression was measured by flow cytometry, or cells were pelleted for RNA extraction. For coculture experiments, OVA treatment was initiated at the same time as I3A or vehicle, and coculture proceeded as described above after 24 hours.

QUANTIFICATION AND STATISTICAL ANALYSIS

All statistical analyses were performed using Prism 10 (GraphPad Software, San Diego, CA). Normality was determined using the Shapiro–Wilk normality test. Differences between two groups were evaluated using the unpaired t-test (for parametric data) or Mann–Whitney test (for nonparametric data), and comparisons of more than 3 groups were evaluated using ordinary one-way ANOVA followed by Tukey's correction for multiple comparisons (for parametric data) or Kruskal–Wallis test followed by Dunn's correction for multiple comparisons (for nonparametric data). Differences of $p<0.05$ were considered significant in all statistical analyses. Statistically significant differences are shown with asterisks as follows: *$p<0.05$, **$p<0.01$, ***$p<0.001$ and ****$p<0.0001$; comparisons which were nonsignificant are unmarked. Each figure shows data for individual animals or biological replicates; where individual data is not shown, sample sizes are listed in the figure legends.

Supplemental figures

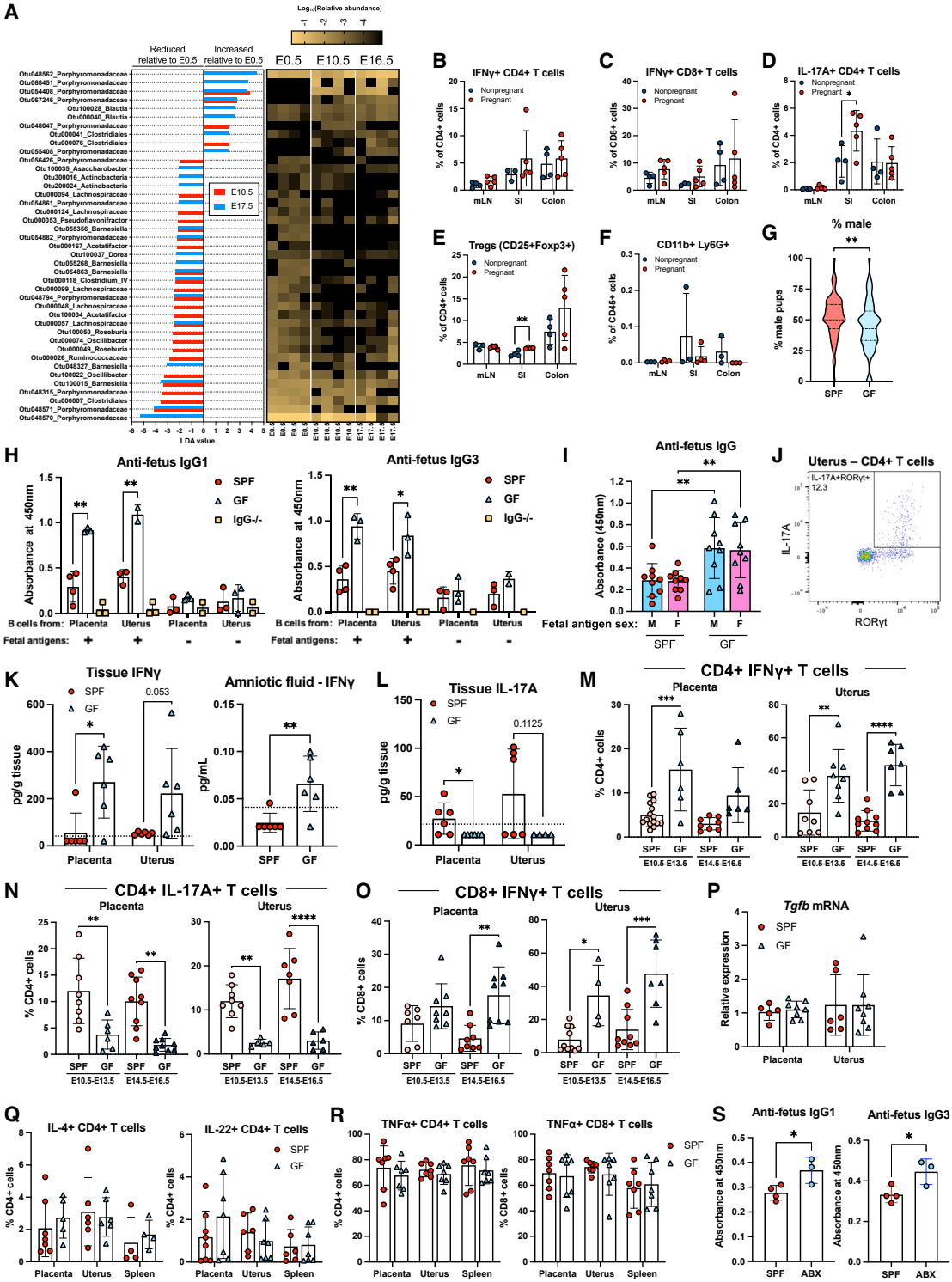

(legend on next page)

Figure S1. The maternal gut microbiota changes dynamically during pregnancy and shapes immune responses at the MFI, related to Figure 1

(A) 16S rRNA sequencing of fecal pellets collected at E0.5, E10.5, and E16.5. Linear discriminant analysis and differential abundance of operational taxonomic units (OTUs) are shown; $n = 4$ for each group.

(B–F) Frequency and number of IFN-γ+ CD4+ T cells (B), IFN-γ+ CD8+ T cells (C), IL-17A+ CD4+ T cells (D), Tregs (E), and CD11b+Ly6G+ cells (F) in the mLN, small intestine, and colon of nonpregnant and pregnant SPF mice (E16.5).

(G) Percentage of male pups per litter in SPF ($n = 105$ litters) and GF ($n = 149$ litters) mice; litters of only one pup were excluded.

(H) MACS-sorted B cells were isolated from the placenta and uterus of SPF or GF mice at E16.5 and cultured on plates coated with fetal antigens for 48 h before measuring production of IgG1 or IgG3 by ELISA. B cells from $IgG^{-/-}$ mice were included as a negative control.

(I) Plasma was collected from SPF and GF dams at E16.5 and measured for IgG reactivity against fetal antigens from either male or female fetuses.

(J) Gating strategy for defining IL-17A+ T cells.

(K) Concentration of IFN-γ in AF, uterus, and placenta from E16.5 SPF and GF dams; dotted line indicates limit of detection.

(L) Concentration of IL-17A in placenta and uterus homogenates from E16.5 SPF and GF dams; dotted line indicates limit of detection.

(M–O) Frequency of CD4+ IFN-γ+ T cells (M), CD4+ IL-17A+ T cells (N), and CD8+ IFN-γ+ T cells (O) in placenta and uterus of SPF and GF mice during mid-gestation (E10.5–E13.5) or late gestation (E14.5–E16.5).

(P) Relative expression of *Tgfb* mRNA in placenta and uterus homogenates from E16.5 SPF and GF mice, measured by qPCR.

(Q) Abundance of IL-4+ and IL-22+ CD4+ T cells from placenta and uterus of E16.5 SPF and GF mice.

(R) Abundance of TNF-α+ T cells from placenta and uterus of E16.5 SPF and GF mice.

(S) SPF mice were treated with PBS or Abx from E7.5 to E16.5, at which point plasma was collected and anti-fetus IgG1 and IgG3 was measured via ELISA. For (B)–(F) and (I)–(S), each dot represents one dam. For the AF data in (K), each dot represents AF from a single fetus; a maximum of three AF samples were analyzed from each dam. Error bars represent one standard deviation. $^{*}p < 0.05$, $^{**}p < 0.01$, $^{***}p < 0.001$, $^{****}p < 0.0001$.

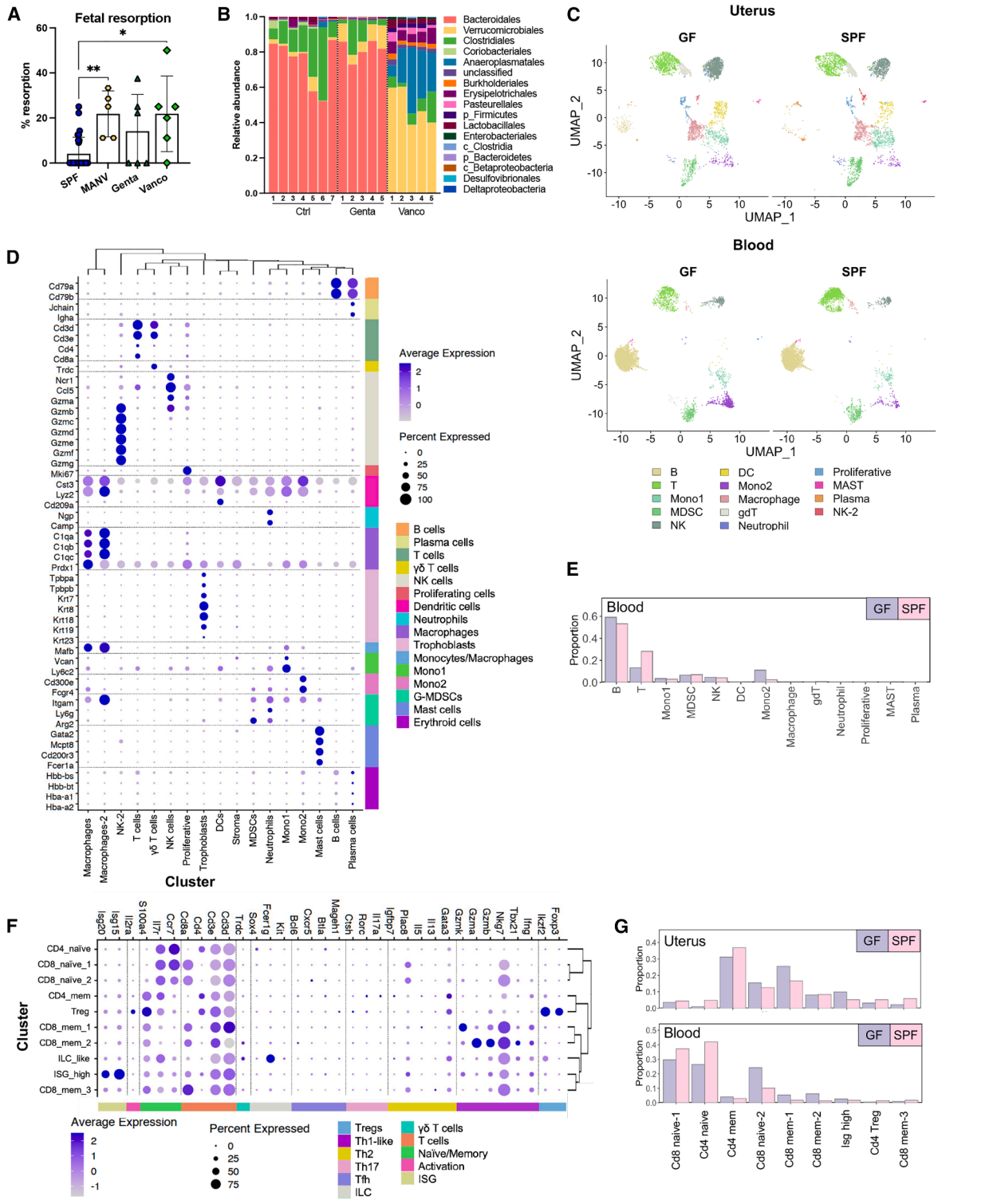

Figure S2. Altered immune cell landscape at the MFI in female mice lacking microbiota, related to Figures 1 and 2

(A) Fetal resorption rates in SPF dams treated with PBS, broad-spectrum Abx (MANV: metronidazole, ampicillin, neomycin, vancomycin), gentamicin, or vancomycin from E7.5 to E16.5.

(B) 16S rRNA sequencing of fecal pellets from adult gentamicin- or vancomycin-treated mice, from a previously published dataset (GSE189794). Relative abundance of OTUs with abundance > 0.05% is shown at the order level.

(legend continued on next page)

(C–G) scRNA-seq was performed on CD45+ cells from the blood, placenta, and uterus of pregnant SPF and GF mice. (C–E) Fourteen clusters were defined by gene signature. (C) UMAP representations are shown for blood and uterus. (D) Expression of the marker genes used to define each cluster. (E) Relative abundance of each cluster within the blood, shown as the fraction of all blood immune cells. (F and G) Within the T cell cluster (6,159 cells total), nine sub-clusters were defined. (F) Expression of the marker genes used to define each sub-cluster. (G) The relative abundance of each T cell sub-cluster is shown as the fraction of all T cells from the indicated tissue. For (A), each dot represents one litter; for (B), each column represents one mouse. Error bars represent one standard deviation. $^{*}p < 0.05$, $^{**}p < 0.01$.

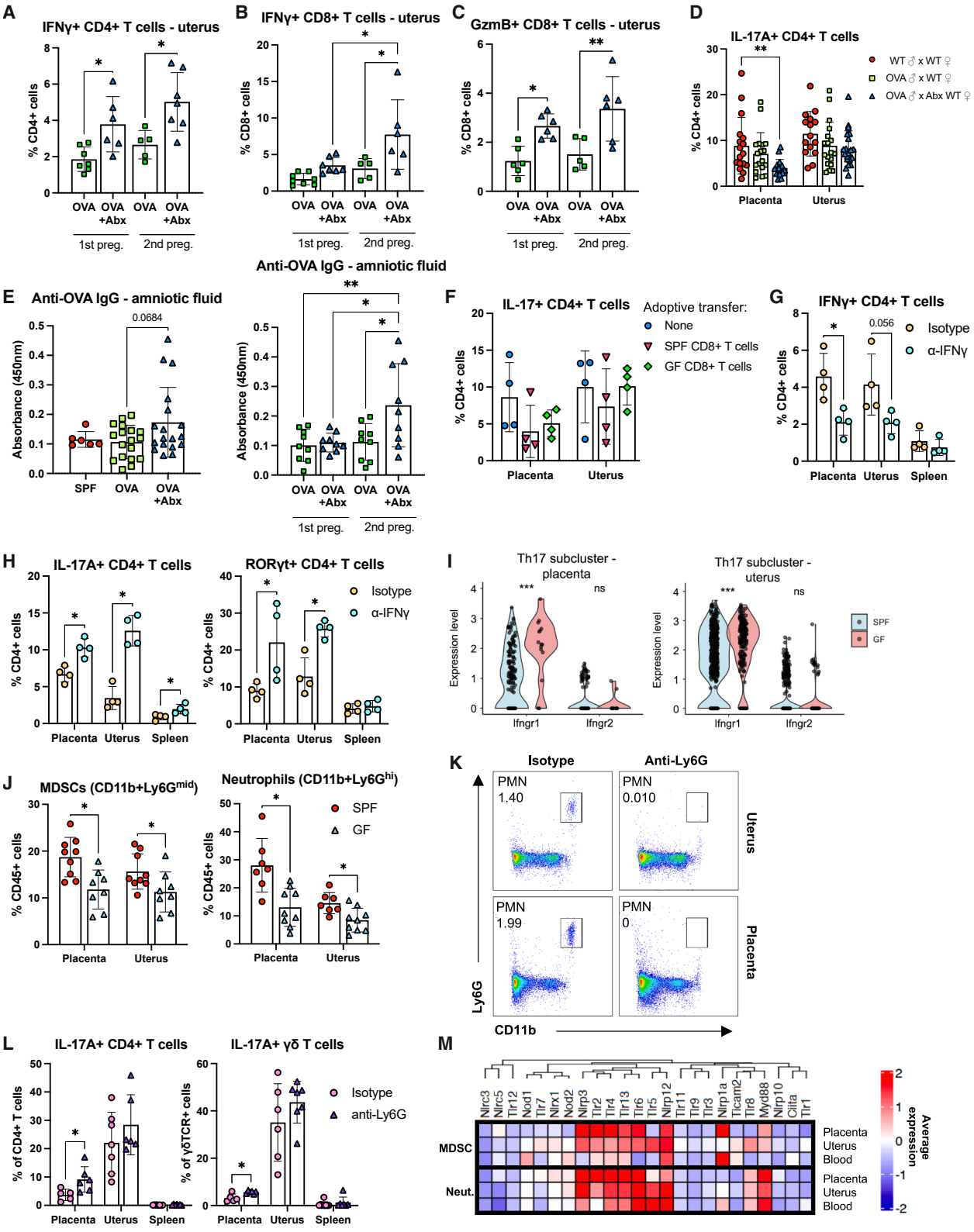

(legend on next page)

Figure S3. The absence of gut microbiota affects T cells and MDSCs at the MFI, related to Figures 3 and 4

(A–E) Female WT mice were mated with male OVA-expressing mice and treated with Abx or PBS from E7.5 to E16.5. (A) Abundance of uterine IFN-γ+ CD4+ T cells during the 1st and 2nd pregnancy. (B) Abundance of uterine IFN-γ+ CD8+ T cells during the 1st and 2nd pregnancy. (C) Abundance of placental GzmB+ CD8+ T cells during the 1st and 2nd pregnancy. (D) Abundance of IL-17A+ CD4+ T cells in the placenta and uterus. (E) Anti-OVA IgG in AF, shown in aggregate and separated into 1st and 2nd pregnancy.

(F) CD8+ T cells were isolated from the uterus and placenta of E16.5 SPF and GF females and adoptively transferred into E7.5 SPF females. At E16.5, the abundance of IL-17A+ CD4+ T cells was assessed by flow cytometry.

(G and H) SPF mice were treated with α-IFN-γ or isotype control antibody from E7.5 to E16.5. (G) Abundance of IFN-γ+ CD4+ T cells in the placenta and uterus; (H) abundance of IL-17A+ and RORγt+ CD4+ T cells in the placenta and uterus.

(I) *Ifngr1* and *Ifngr2* expression in the Th17 sub-cluster defined in Figure 2.

(J) Frequency of MDSCs (CD11b+Ly-6G^{mid}) and neutrophils (CD11b+Ly-6G^{hi}) in placenta, decidua, and uterus of E16.5 SPF and GF mice.

(K and L) In SPF mice, Ly-6G+ cells were depleted by the administration of anti-Ly6G antibody, starting at E5.5. (K) Representative flow plots of CD11b+Ly-6G+ cells in pregnant SPF mice injected with anti-Ly6G or isotype control antibody, gated on live CD45+ cells. (L) Frequency of IL-17A+ γδ T cells and CD4+ T cells in the placenta, uterus, and spleen of anti-Ly6G- or isotype-treated dams at E16.5.

(M) scRNA-seq analysis of the MDSC and neutrophil clusters defined in Figure 2; average expression of genes associated with microbe sensing is shown. For (A)–(D), (F)–(H), (J), and (L), each dot represents one dam. For (E), each dot represents AF from a single fetus; a maximum of three AF samples were analyzed from each dam. Error bars represent one standard deviation. *$p < 0.05$, **$p < 0.01$.

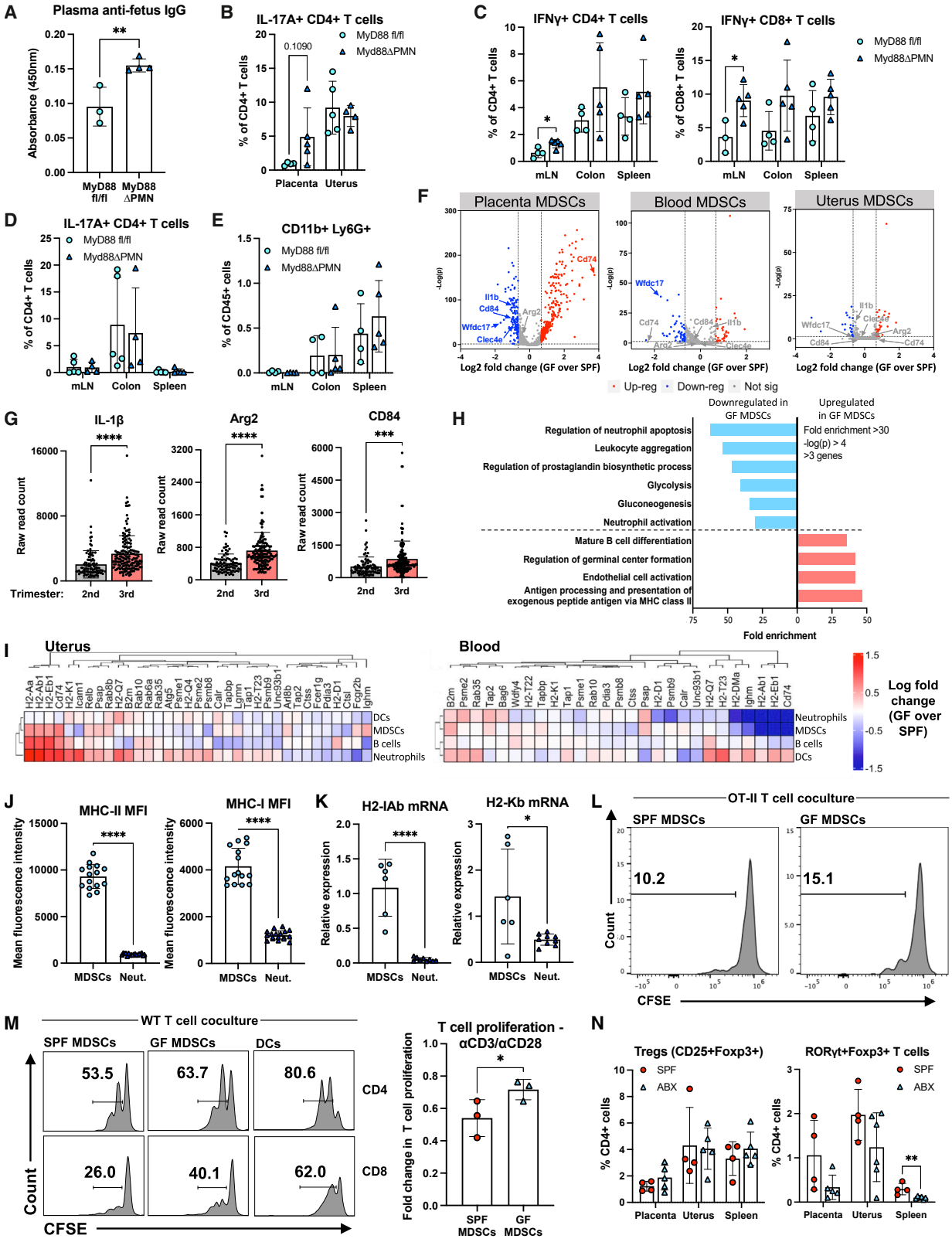

(legend on next page)

Figure S4. The absence of gut microbiota affects T cells and MDSCs at the MFI, related to Figures 4 and 5

(A–E) PMN-specific knockout of MyD88 (MyD88ΔPMN) was achieved by crossing MyD88-fl/fl mice with Mcl1-Cre mice. Pregnant MyD88ΔPMN mice and Cre− littermate controls were sacrificed at E16.5. (A) The level of anti-fetal IgG in the plasma was measured via ELISA, (B) the frequency of placental and uterine IL-17A+ CD4+ T cells was measured via flow cytometry, and the frequencies of IFN-γ+ T cells (C), IL-17A+ CD4+ T cells (D), and CD11b+Ly6G+ cells (E) were measured in the mLN, colon, and spleen.

(F–I) scRNA-seq analysis of the MDSC cluster defined in Figure 2. (F) volcano plot of differentially regulated genes within the placental MDSCs, showing fold change in expression within GF MDSCs over SPF. (G) Relative abundance of the MDSC-associated genes *Il1β*, *Arg2*, and *CD84* in circulating RNA from plasma of healthy pregnant individuals collected during the 2nd or 3rd trimester, taken from a publicly available transcriptomic dataset generated by Munchel et al.

(H) Gene Ontology terms that were significantly enriched among the genes that were significantly upregulated (red bars) or downregulated (blue bars) in GF MDSCs relative to SPF.

(I) Fold change in expression of genes associated with antigen presentation within the indicated cell clusters, measured by scRNA-seq.

(J and K) Expression of MHC-I and MHC-II in MDSCs and neutrophils isolated from bone marrow, measured by flow cytometry (J) and qPCR (K).

(L) MDSCs were isolated from placentas of E16.5 SPF or GF mice, pulsed with OVA for 18 h, and co-cultured with CFSE-labeled splenic T cells from OT-II mice. After 48 h, T cell proliferation was assessed by CFSE dilution. Representative flow plots are shown.

(M) MDSCs were isolated from placentas of E16.5 SPF or GF mice and co-cultured with CFSE-labeled α-CD3/α-CD28-stimulated T cells from age-matched nulliparous WT mice. After 72 h, T cell proliferation was assessed by CFSE dilution.

(N) Frequency of conventional Tregs (CD25+Foxp3+) and RORγt+Foxp3+ T cells isolated from placenta, uterus, and spleen of E16.5 SPF mice gavaged with PBS or Abx from E7.5 to E16.5. For (A)–(E) and (J)–(N), each dot represents one dam. Error bars represent one standard deviation. *$p < 0.05$, **$p < 0.01$, ***$p < 0.001$, ****$p < 0.0001$.

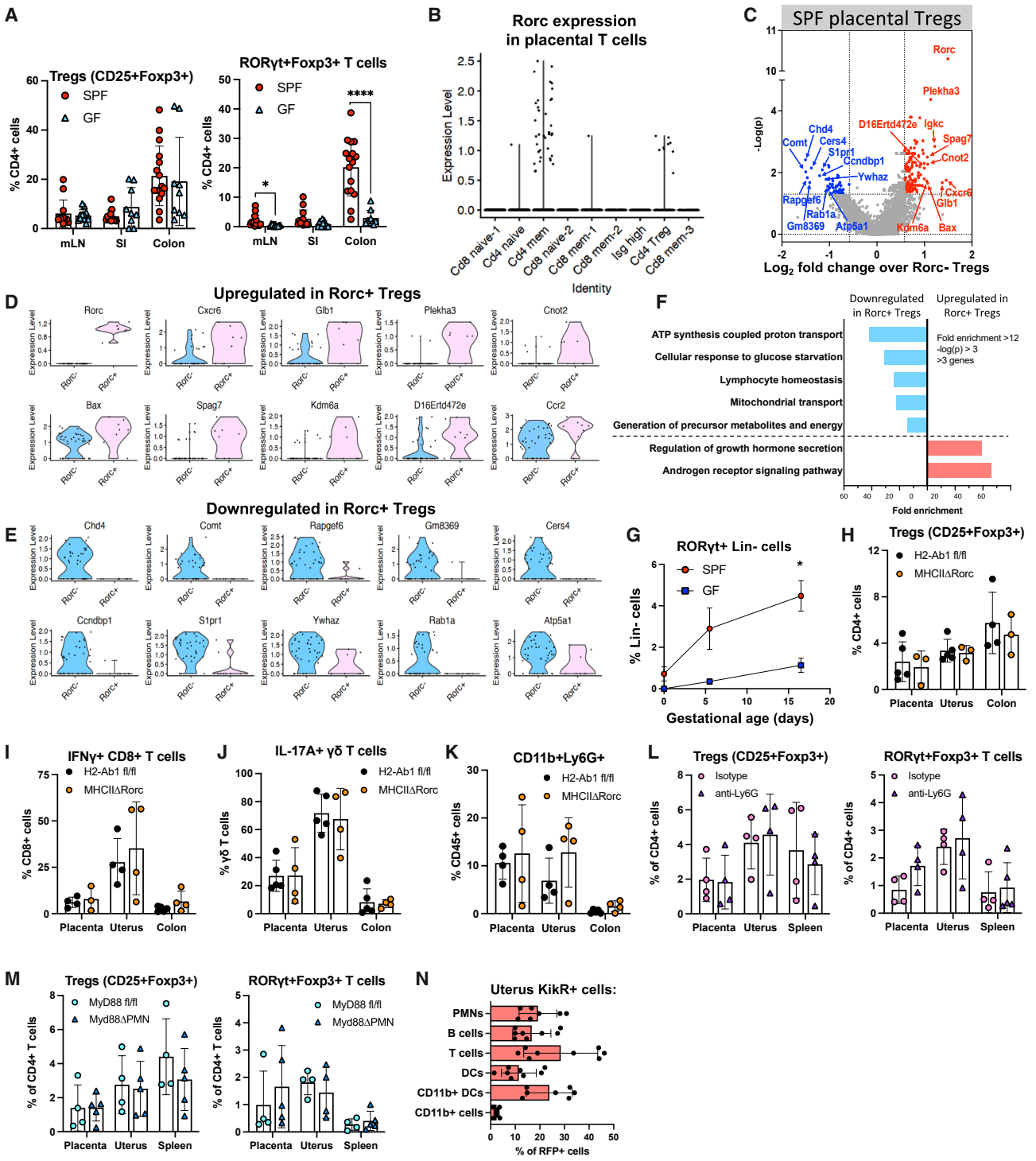

Figure S5. The absence of gut microbiota affects RORγt+FoxP3+ cells at the MFI, related to Figure 5

(A) Abundance of conventional Tregs (CD25+Foxp3+) and RORγt+Foxp3+ T cells in mLN, SI, and colon of E16.5 SPF and GF mice.

(B–F) Analysis of the T cell sub-clusters defined in Figure 2. (B) Relative expression of *Rorc* in the indicated sub-clusters of placental T cells. (C) Volcano plot of differentially regulated genes among placental Tregs, showing the fold change in expression within *Rorc+* Tregs over *Rorc−* Tregs. (D and E) Relative abundance of the 10 most significantly upregulated (D) or downregulated (E) genes in *Rorc+* Tregs relative to *Rorc−* Tregs from placentas of SPF mice. (F) Gene Ontology terms that were significantly enriched among the genes that were significantly upregulated (red bars) or downregulated (blue bars) in the *Rorc+* Tregs relative to *Rorc−*.

(legend continued on next page)

(G) Abundance of RORγt+ Lin− cells (lineage markers = CD3, CD4, CD8, CD11b) in the uterus of SPF and GF mice at E0.5 (n = 3 per group), E5.5 (n = 5 SPF and 6 GF), and E16.5 (n = 4 SPF and 3 GF).

(H–K) Percentage of Tregs (CD25+Foxp3+) (H), IFN-γ+ CD8+ T cells (I), IL-17A+ γδ T cells (J), and CD11b+Ly6G+ cells (K) in the placenta, uterus, and colon of E16.5 MHCIIΔRorc and littermate control *H2-Ab1*$^{fl/fl}$ mice.

(L) Abundance of Tregs (CD25+Foxp3+) and RORγt+Foxp3+ T cells in SPF dams treated with anti-Ly6G antibody or isotype control from E7.5 to E16.5.

(M) Abundance of Tregs (CD25+Foxp3+) and RORγt+Foxp3+ T cells in E16.5 MyD88ΔPMN mice and Cre− littermate controls.

(N) The intestines of adult female KikGR mice were exposed to 405 nm light via laparotomy, and photoconverted cells in the uterus were analyzed 24 h later. The composition of the KikR+ cell population is shown as proportion of uterine KikR+ cells. For (A) and (H)–(N), each dot represents one dam. Error bars represent one standard deviation. *$p < 0.05$, ****$p < 0.0001$.

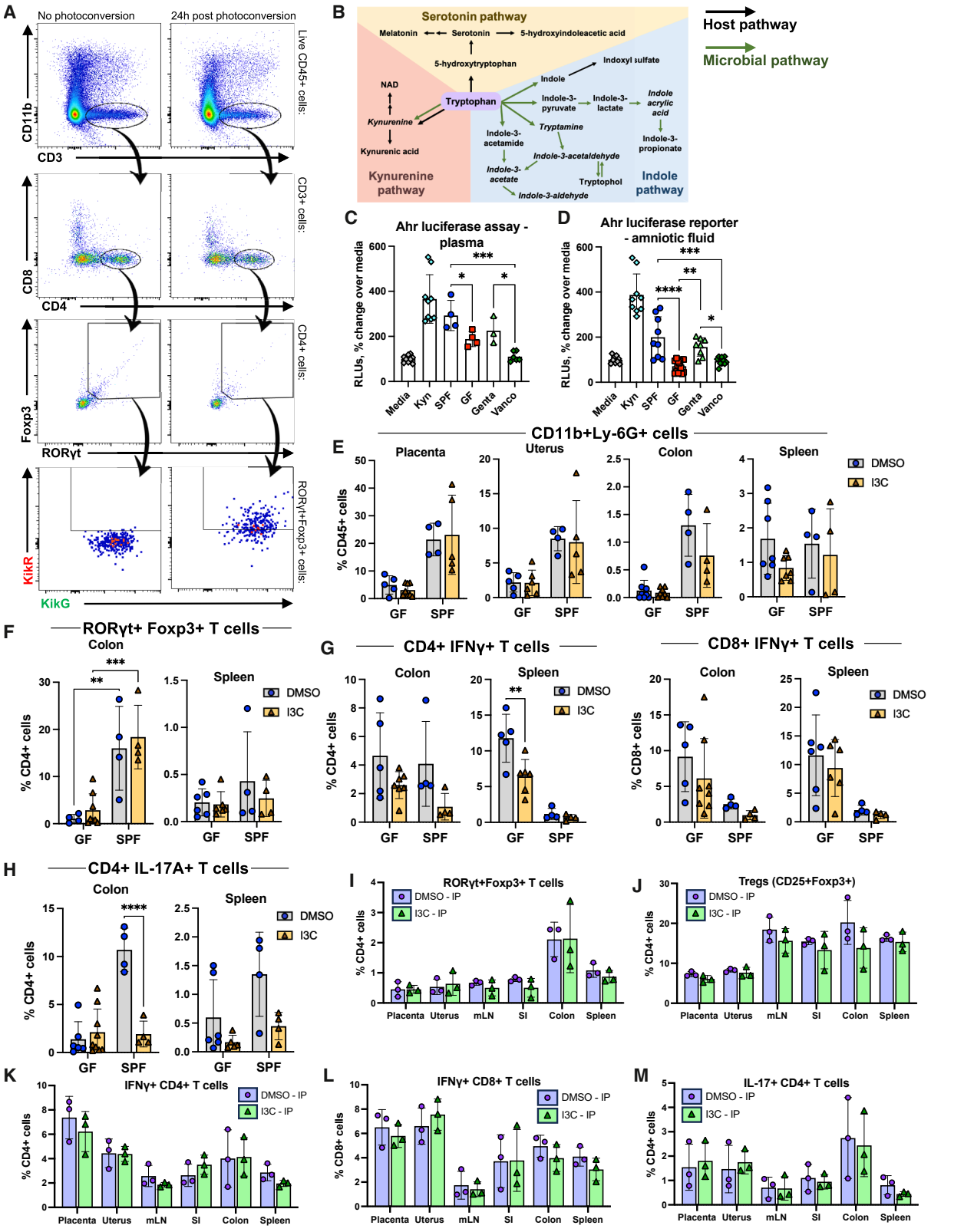

(legend on next page)

Figure S6. Tryptophan metabolites restore a balanced T cell response at the MFI, related to Figures 5 and 6

(A) The intestines of adult female KikGR mice were exposed to 405 nm light via laparotomy, and photoconverted cells in the uterus were analyzed 24 h later. The gating strategy for KikR+ RORγt+Foxp3+ cells is shown.

(B) Tryptophan metabolic pathways and their intermediary metabolites. Black arrows indicate host metabolic pathways; green arrows indicate microbial metabolic pathways; italics indicate known AhR ligands.

(C and D) AhR reporter cells (expressing firefly luciferase under the control of an AhR-activated promoter) were cultured with plasma (C) or AF (D) from E16.5 SPF, GF, gentamicin-treated, or vancomycin-treated dams, and endpoint luminescence was measured as a readout of the level of AhR-activating ligands. Media alone or 10 μM L-Kyn was used as control.

(E–H) Female SPF and GF mice were treated orally with I3C or vehicle (DMSO) prior to mating and continuing every 48 h until E16.5, at which point the abundance of CD11b+Ly6G+ cells (E), RORγt+Foxp3+ T cells (F), IFN-γ+ T cells (G), and IL-17A+ CD4+ T cells (H) was measured in the indicated tissues via flow cytometry.

(I–M) Female GF mice were treated intraperitoneally with I3C or vehicle (DMSO) prior to mating and continuing every 48 h until E16.5, at which point the abundance of RORγt+Foxp3+ T cells (I), conventional Tregs (J), IFN-γ+ CD4+ T cells (K), IFN-γ+ CD8+ T cells (L), and IL-17A+ CD4+ T cells (M) was measured in the indicated tissues via flow cytometry. For (C) and (E)–(M), each dot represents one dam. For (D), each dot represents AF from a single fetus; a maximum of three AF samples were analyzed from each dam. Error bars represent one standard deviation. $^{*}p < 0.05$, $^{**}p < 0.01$, $^{***}p < 0.001$, $^{****}p < 0.0001$.

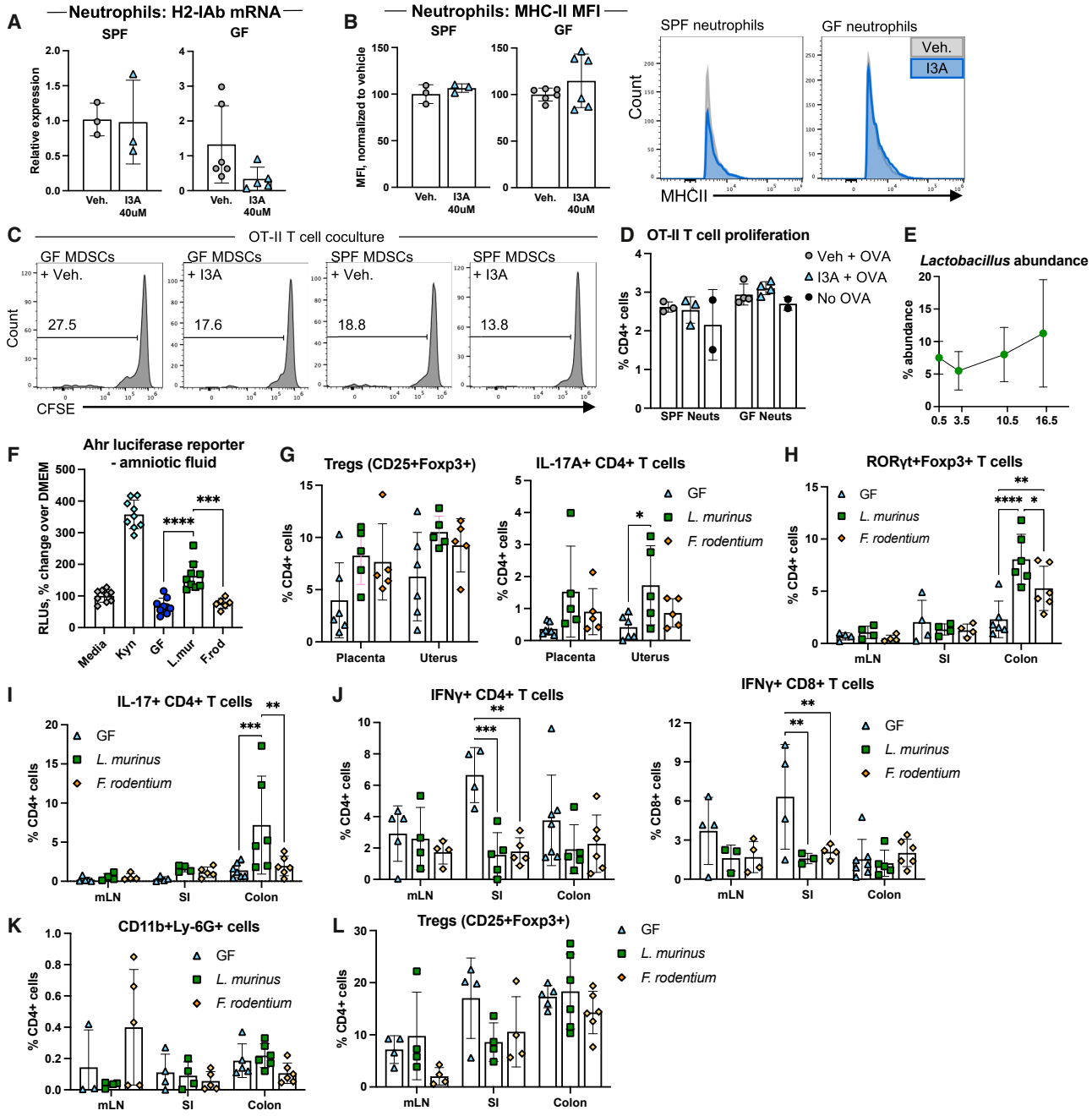

Figure S7. Tryptophan metabolites restore a balanced T cell response at the MFI, related to Figure 6

(A) Expression of H2-IAb mRNA in bone marrow neutrophils treated with I3A.

(B) Expression of MHC-II on bone marrow neutrophils treated with I3A, measured by flow cytometry.

(C and D) MDSCs (C) and neutrophils (D) were isolated from the bone marrow of E16.5 SPF or GF mice, treated with I3A and pulsed with OVA for 18 h, then co-cultured with CFSE-labeled splenic T cells from OT-II mice. After 48 h, T cell proliferation was assessed by CFSE dilution.

(E) Abundance of *Lactobacillus* in fecal pellets collected at E0.5, E3.5, E10.5, and E16.5, measured by 16S rRNA sequencing; $n = 4$ for each group.

(F–L) Female GF mice were colonized with *L. murinus* or *F. rodentium* prior to mating. (F) AhR reporter cells (expressing firefly luciferase under the control of an AhR-activated promoter) were cultured with AF from E16.5 GF, *L. murinus*, and *F. rodentium* dams, and endpoint luminescence was measured as a readout of the level of AhR-activating ligands. Media alone or 10 μM L-Kyn was used as control. (G–L) The abundance of conventional Tregs and IL-17A+ CD4+ T cells in the

(legend continued on next page)

placenta and uterus (G) and the abundance of RORγt+Foxp3+ T cells (H); IL-17A+ CD4+ T cells (I); IFN-γ+ T cells (J); CD11b+Ly-6G+ cells (K); and conventional Tregs (L) in the mLN, SI, and colon were measured at E16.5 by flow cytometry.

(M) Model of microbiota-dependent gut-placenta immune crosstalk. For (A)–(D) and (G)–(L), each dot represents one dam. For (F), each dot represents AF from a single fetus; a maximum of three AF samples were analyzed from each dam. Error bars represent one standard deviation. *$p < 0.05$, **$p < 0.01$, ***$p < 0.001$, ****$p < 0.0001$.